NUREG-0105
NRC-2,4

HEAT TRANSFER AND CARRYOVER OF LOW PRESSURE WATER IN A HEATED VERTICAL TUBE

Thomas A. Smith

Manuscript Completed: January 1976
Date Published: August 1976

Massachusetts Institute of Technology
Cambridge, Massachusetts 02139

Prepared for the U.S. Nuclear Regulatory Commission
Under Contract No: AT(49-24)-0230

HEAT TRANSFER AND CARRYOVER OF LOW PRESSURE WATER IN A HEATED VERTICAL TUBE

by

THOMAS A. SMITH

B.S., United States Military Academy
(1969)

SUBMITTED IN PARTIAL FULFILLMENT
OF THE REQUIREMENTS FOR THE
DEGREE OF

MASTER OF SCIENCE

at the

MASSACHUSETTS INSTITUTE OF TECHNOLOGY

January 1976

Signature of Author: Thomas A. Smith
Department of Mechanical Engineering, January 21, 1976

Certified by: Peter Griffith
Thesis Supervisor

Accepted by: .....
Chairman, Department Committee on Graduate Students

HEAT TRANSFER AND CARRYOVER OF LOW PRESSURE WATER IN A HEATED VERTICAL TUBE

by

THOMAS A. SMITH

Submitted to the Department of Mechanical Engineering
on January 21, 1976 in partial fulfillment of the
requirements for the Degree of Master of Science

ABSTRACT

Local heat transfer coefficients in the stable film boiling and dispersed flow regimes were studied for the upward flow of low pressure water in a heated vertical tube. Wall temperatures were maintained constant with time and along the tube so that both axial and time temperature gradients approached zero. Heat flux along the tube was not constant but was applied so as to maintain a steady state temperature profile. A preheater was used to bring the liquid to saturation before it entered the main portion of the test section and in some cases the equilibrium quality was greater than zero at the entrance to the main test section.

The test section was made of stainless steel, and the lower portion, the preheater, was heated directly by DC current. Copper block heat spikes were clamped to the upper test section and were used to apply the heat flux to maintain the wall temperature constant with time.

The range of system parameters was very extensive. Pressure was varied from 20 to 67 psia. Coolant mass fluxes were varied from 18,720 to 112,320 lb_m/ft^2-hr, representing flooding rates from 1 to 6 inches/sec. Inlet coolant temperature was between 75 and 188°F. The maximum wall temperature along the test section was between 1260 and 1905°F, and the heat transfer coefficient at locations other than the ends of the tube was a maximum of 207 and a minimum of 3BTU/ft^2-hr°F. Net heat fluxes at the heat spikes were between 7,800 and 160,000 BTU/ft^2-hr.

Several theories for the different possible types of flow (laminar or turbulent, tube or film) were compared with the experimental data. The carryover point for low flooding rates (1 inch/sec or less) was inferred from these comparisons and gave good agreement with the Plummer critical mass criterion for liquid carry over.

Thesis Supervisor: Peter Griffith
Title: Professor of Mechanical Engineering

ACKNOWLEDGEMENTS

Financial support for this research project was provided by a research assistantship funded by the NRC (Nuclear Regulatory Commission).

The author is indebted to Professor Peter Griffith for his many suggestions, in particular for that which became the final experimental design concept. He would also like to recognize Professor Griffith's optimism, wit, and unending patience.

The author received much constructive advice and support from his fellow research assistant, Walter Kirchner. He also thanks another research assistant, Jill Kaufman, for her computer program which calculated the theoretical heat transfer coefficients.

Finally, the author would like to thank the technicians in M.I.T.'s Engineering Projects Lab., especially J. A. Caloggero and F. Johnson, for their advice and technical assistance.

TABLE OF CONTENTS

LIST OF FIGURES

1. INTRODUCTION

The concern for the safe operation of nuclear reactors has increased with the growth of the nuclear power industry over the past several years. Receiving considerable attention in the field of reactor safety is the LOCA (Loss of Coolant Accident), a hypothetical loss of reactor coolant causing excessive temperature gradients in the heater fuel rods. A detailed description of the LOCA will not be presented here but may be found in a topical report prepared for the Electrical Power Research Institute [1].* However, the present experimental program did investigate some heat transfer effects of the post-LOCA reflood phase, and a brief summary of the accident will be helpful in understanding this report. Following this summary, there will be a cursory review of the Westinghouse FLECHT (Full Length Emergency Cooling Heat Transfer) tests with a short discussion of their contribution to the study of liquid carry-over. The last section of this introduction will highlight a previous experimental program that provided guidance for the design of the apparatus featured in this report.

1.1 The Loss of Coolant Accident (LOCA).

Concerning reactor safety, the policy of the NRC (Nuclear Regulatory Commission) has been to direct that in areas of uncertainty the most conservative approach, that providing the greatest margin of safety, must be the one taken. Therefore, as improbable as it is, the LOCA is assumed to be the result of an instantaneous double-ended guillotine break of the largest primary coolant system pipe. This rupture of the coolant system is followed by a decompression or blowdown phase, at the end of which the

---

*Numbers in brackets designate references.

amount of coolant in the core is negligible. The core is filled with stagnant vapor whose heat transfer capabilities are ineffectual. At this time the system pressure is usually less than 60 psia. Although the reactor is automatically shut down as soon as possible after the accident is detected, decay heat from the fissionable materials exacerbates the problem. Given this poor heat transfer environment, the fuel rod temperature transients could become critical.

However, there is an Emergency Core Coolant System (ECCS) which is designed to cool the core to prevent degradation of reactor heater rods caused by extreme temperatures and cladding oxidation. In the PWR (Pressurized Water Reactor) the ECCS is employed through bottom flooding. The coolant fills the lower plenum and the water level rises until it reaches the bottom of the core. The fuel rods are too hot to allow contact with the water and boiling takes place. Eventually the quench front (defined as the location below which the rods have rewet and above which they can not) rises and the heater rods are cooled to a safe temperature. In the interim between the water level reaching the bottom of the core and the quenching of the top of the heater rods, a series of complex heat transfer phenomena occur, the study of one of which is the subject of this experimental program.

1.2 FLECHT

Beginning in the late 1960's, Westinghouse began a program of research called FLECHT (Full Length Emergency Cooling Heat Transfer) whose objective was to obtain experimental reflooding heat transfer data under simulated LOCA conditions for use in evaluating the heat transfer capabilities of PWR ECCS's [2]. The scope of these tests is vast and the procedures, data

and results are contained in several volumes. Obviously, a comprehensive review of FLECHT cannot be given here and the reader is referred to reference 2 for an outline of the FLECHT reports and their relation to the overall program. However, on a smaller scale the work detailed in this report is an extension of FLECHT and an attempt to summarize FLECHT will be made to better introduce the material presented herein.

1.2.1 Test Program

The FLECHT test program investigated the effects of initial clad temperature, flooding rate, power, inlet coolant subcooling, and pressure on transient heat transfer coefficients. Westinghouse, with a simulated "core" of a 10 x 10 or 7 x 7 rod bundle, studied the above parameters and also collected data on entrained liquid. The "fuel rods" were either stainless steel clad or Zircaloy-4 clad heater rods with either Nichrome or Kanthal heating elements. Axial and radial power distributions were typical of those in actual PWR assemblies, as were all other parameters. The heater rods were well instrumented with thermocouples to provide temperature information at several elevations along the 12 ft. heated length.

a. Test Procedure

The temperature of the heater rods was raised by applying power to the Nichrome or Kanthal heating elements. When the rods were at the desired initial clad temperature, the coolant was automatically injected into the "core." Power to the heater rods was decreased exponentially to simulate the reactor decay heat. Heater rod thermocouples were read and recorded as a function of time, and the local coolant temperature and pressure transducer readings were continuously monitored. Once the upper elevation thermocouples quenched, the test was terminated.

b. Test Results

The FLECHT results illustrated the effects of the system parameters on post-LOCA reflooding heat transfer. The most useful form of presenting the data is graphically, showing clad temperature and heat transfer coefficients versus time as functions of initial clad temperature, flooding rate, inlet coolant subcooling, pressure, and peak power. The conclusions of this program are too extensive to enumerate here, but the demonstrated effectiveness of liquid entrainment as a heat transfer mechanism will be discussed in detail below because of its direct bearing to the subject of the present report.

1.2.2 FLECHT Movie Observations

High speed movies were made of the phenomena occuring within the rod bundle, and the author had the opportunity to view the films of several runs. A rather detailed analysis of the author's observations of entrainment as illustrated by the movies will be presented because of the movies' relation to his own experimental program. There are, however, two general inferences which will be discussed first.

The movies confirmed that a spectrum of flow regimes exists, although all of them are not usually present simultaneously (See Fig. 1. The quench front is defined as the boundary between the film boiling and transition boiling regimes [2]). FLECHT was a transient experiment, and these regimes were observed moving up the bundle. However, the emphasis on the present experiment is steady state in the stable film boiling regime where appropriate heat transfer data may be taken. Thus, all regimes were quantitatively experienced, and Fig. 1 is also representative of what occured in

this program's test section, with all regimes often occuring simultaneously.

The regime between film boiling and dispersed flow, the flow pattern transition regime, was seen to be highly turbulent, with either swirls of liquid or entrained water droplets intermixed with vapor generated at the heated rod surfaces. This observation has led to a "Turbulent Thin Film Theory" in the theoretical portion of this report to try to explain some of the experimental results. The analysis of the movies will now be presented.

a. Procedure

Several of the Westinghouse FLECHT movies (Runs #0085, 0487, 0538, 0690, 3440, and 9983) were viewed using a projector with single-framing and stop-action capabilities. Most movies showed a clock in the lower left corner which gave the time after inception of flooding. The particular interest of this analysis was the liquid droplets entrained by the vapor and carried up the bundle. The window through which the movies were filmed was at the 6 ft. elevation and the time on the clock indicated that the quench front (inferred from temperature-time plots for each run [2]) was several feet below this height. Thus the observed droplets had indeed been "carried over" and were not near the continuous liquid. (See Figs. 2 and 3 for photographs of entrained droplets for low pressure-low flooding rate and for high pressure-high flooding rate runs, respectively).

As the movies were shown, several individual droplets were observed for each run. The diameters of these droplets and their velocities were measured (the single-frame feature of the projector established the time interval, and the distances were physically measured on a screen and related to actual dimensions by the known heater pitch of 0.563 inches).

All reported runs were made at 500 frames per second, except Run #3440 at 1000 frames per second. The parameters for each run are given in Table I below, and all pertinent data is contained in Appendix A to this report.

TABLE I

Run #	P(psia)	FR(in/sec)	V_f^*(ft/sec)	V_v^* (ft/sec)	W_e^*
0085	25	2.0	11.1	43	5.7
0487	18	0.8	5.7	35	2.3
0588	15	0.6	7.0	40	2.5
0690	15	0.6	7.2	40	2.3
3440	55	5.9	11.3	29	2.6
9983	19	1.0	6.6	38	3.4

As mentioned above, the liquid droplet velocities, V_f, and droplet diameters, D_d, were inferred from real time and distance measurements. As can be seen in Appendix A, they did not show much variance for any one run, especially considering the crudeness of the procedure. The vapor velocities were computed from a force balance in the following way. The drops were assumed to be moving at constant velocity so that their acceleration was zero. Then Newton's second Law yields

$$\Sigma F_z = \text{droplet mass} \times \text{droplet acceleration} = 0 \qquad (1\text{-}1)$$

This is equivalent to saying that the drag force equals the force of gravity,

$$F_{drag} = F_g \qquad (1\text{-}2)$$

or

$$\frac{\rho_v (V_v - V_f)^2}{2g_o} C_d \left[\frac{\pi D_d^2}{4}\right] = \left[\frac{\pi D_d^3}{6}\right] \frac{\rho_f g}{g_o} \qquad (1\text{-}3)$$

*These are average quantities.

where C_d, the drag coefficient is taken to be 0.45 [3]. Then after rearranging, an expression for the vapor velocity is

$$V_v = V_f + \left[\frac{4D_d \rho_f g}{3\rho_v C_d}\right]^{1/2} \qquad (1\text{-}4)$$

Weber Numbers (We) were then computed for each drop, based on the relative velocity of vapor to liquid,

$$We = \frac{\rho_v (V_v - V_f)^2 D_d}{\sigma g_o} \qquad (1\text{-}5)$$

b. Conclusions

Several inferences were drawn from the movies that either substantiated previous theories or generated new ideas or assumptions for this program. The average vapor velocities usually showed the effect of pressure one would expect, and as predicted by Plummer [3]. As pressure is increased, the vapor velocity required for carry over is decreased. However, at the elevation at which the drop measurements were taken (several feet above the carry-over point), the drops were assumed to be at zero acceleration. The vapor velocity at the carry-over point itself may have been less than calculated by eqn. (1-4) above, if the drops actually were accelerating. In any case, most of the vapor velocities inferred by this procedure are lower than predicted by reference 3, and this may imply that the minimum vapor velocity necessary for carry-over is in fact less than previously thought (see Fig. 4).

Another factor that was considered in questioning the predicted carry-over velocity is the effect of Weber Number. Reference 3 predicts the mass flux necessary for carry-over, the "C-Critical Criterion":

$$G_{crit} = \frac{\rho_g \rho_v}{\rho_f - \rho_v} \left[\frac{4\, We_{crit}}{3 C_d} \right]^{1/4} \left[\frac{\sigma(\rho_f - \rho_v) g}{\rho_v^2} \right]^{1/4} \quad (1\text{-}6)$$

and

$$V_{co} = G_{crit}/\rho_v \quad (1\text{-}7)$$

The above reference assumed a critical We of 7.5, whereas the We's calculated from the FLECHT movies were generally much lower. The effect of pressure and flooding rate on droplet We is not clear, but it is reasonable to infer that the previous assumption for the critical We is too great. Of course, the carry-over velocity is only a function of $(We)^{1/4}$, and this mitigates the effect of We on the prediction. However, reducing the critical We by half still decreases the predicted carry-over velocity by almost 10%.

The movies also assisted in generating or limiting assumptions to help explain the data from the present experimental program. The thin film assumptions of the next chapter are consistent with the thin vapor annuli surrounding each heater rod observed in the movies. Another assumption made in the analytical section of this report is that the vapor-liquid interfacial shear stress is approximately equal to that at the wall, allowing the further assumption of a parabolic velocity profile for the vapor in the thin film, symmetrical about the centerline. The velocity of the continuous liquid within the vapor annulus is expected to be only slightly greater than the flooding rate, only a few inches per second. This is indeed negligible when compared to the estimated vapor velocities of 30 to 40 ft/sec. So, it is reasonable to assume the vapor velocity at the vapor-liquid interface is approximately zero, and that the two

shear stresses are equal. Further assumptions of a smooth vapor-liquid interface are not in consonance with the movies, as they show the liquid wave motion typical of film boiling. However, the wave velocity was 5 to 10 times the flooding rate [2] and this would tend to dampen the effects of wave motion on the smooth interface assumption. The final section of this introduction will briefly describe the procedure and results of a somewhat similar program that inspired the method used by the experimenter to maintain steady state stable film boiling.

1.3 Previous Experimentation

At Canada's Chalk River Nuclear Laboratories in 1973, D.C. Groeneveld [4] investigated stable film boiling heat transfer using Freon-12 coolant. His program will be briefly outlined because of its influence on the author's experiment discussed later in this report. Groeneveld used an Inconel test section, uniformly heated by a DC power supply, except at a "hot patch" clamp where the tube was short circuited. This hot patch clamp was a copper cylinder with cartridge heaters powered by a variable transformer. Dryout at the hot patch was achieved by raising its temperature, and thus the tube temperature, so the tube wall was too hot to support liquid contact. Groeneveld found that if he first achieved dryout at the hot patch, he could promulgate dryout in the downstream direction simply by increasing the DC power to the rest of the test section.

There were several interesting results that are worth mentioning. Groeneveld found that the hot patch surface heat flux at which dryout occurred was 2 to 4 times the critical CHF with uniform heating, although the hot patch power was much less than the test section power. Also, after dryout had been first achieved at the hot patch, dryout started to spread

downstream from the hot patch at power levels well below the power required to achieve dryout with uniform heating.

The procedure described above and inferences derived from Groeneveld's observations were at first applied to the author's own experimental apparatus. Subsequent problems demanded revision of the original approach and redesign of the test section, but Groeneveld's basic idea was applied throughout this program: use a heat spike to produce a heat flux greater than that required for CHF to prevent liquid contact with the heated surface. The author wishes to acknowledge that Groeneveld's technique (although originally applied elsewhere, but not for the same purpose) and observations were the initial guidelines for his own experimental program.

2. THEORETICAL PROGRAM

2.1 General

There are many reliable correlations in the literature to predict heat transfer coefficients as a function of system parameters. Ongoing research programs are also attempting to refine traditional methods or to innovate new techniques to better estimate heat transfer behavior. However, all existing correlations (and most certainly any future developments) are dependent upon well-defined flow conditions, i.e., laminar or turbulent, film or tube flow. It stands to reason that a specific correlation may not be utilized unless the flow is defined, and so a criterion is necessary for deciding which correlation is appropriate.

The objective of this research project has been to establish such a criterion for selecting the appropriate correlation to predict heat transfer behavior during the post-LOCA reflood phase of a PWR. The carry over point, the location at which liquid droplets are literally carried up the rod bundle by the vapor, is a logical criterion for deciding which heat transfer correlation to use. Before defending this assertion, it would be helpful to first describe the two principal flow regimes of interest.

Inverted annular flow, or stable film boiling, is the inverse of traditional annular flow. An annulus of superheated vapor surrounds the heater rods, and the channels of the core are filled with saturated liquid. The dispersed flow regime consists of liquid droplets dispersed throughout a vapor mist. Fig. 1 shows how these two and other regimes might occur simultaneously in the FLECHT test section, or in a PWR. In this present program, an interior channel of a PWR was modeled by a standard

stainless steel tube whose inner diameter was approximately equal to the hydraulic diameter of a PWR interior channel. The wall of the tube simulated the heated surfaces of the fuel rods, and the tube flow area the interior channel. In the test section, inverted annular film boiling consisted of an annulus of superheated vapor surrounding a central core of saturated liquid, and in dispersed tube flow liquid droplets were dispersed in vapor.

Heat transfer behavior in the different regimes has been examined by a considerable number of investigators, and the general trend inferred from their reports may be found in any standard reference. In the nucleate boiling regime, the liquid wets the wall and heat transfer coefficients are very high. In the inverted annular regime a film of vapor separates the liquid from the wall and offers resistance to transfer of heat from the wall to the liquid. Heat transfer coefficients in this regime are expected to be very low. However, in the dispersed flow regime the heat transfer improves because of the increased velocity of the vapor and the presence of liquid droplets near the heated surface. The carry over point is also the location at which heat transfer improves with quality because it is where the vapor velocity is high enough to entrain the liquid droplets. The carry over point is thus the best criterion for deciding which heat transfer correlation to use because it is where the flow regimes change from film to tube and where the heat transfer coefficient reaches its minimum.

The remainder of this chapter describes the development of several theories which try to explain the experimental data from the test section. The purpose of these theories is not the development of an empirical correlation for predicting heat transfer, but rather it is to show how

closely the data fits the possible types of flow found during the post-LOCA reflood phase, e.g., laminar film or turbulent tube. When the data can be so categorized, the carry over point may be inferred based on its previous definition. That is to say, the behavior of the heat transfer coefficient and the type of flow may be used to experimentally determine the carry over point.

2.2 Development of Theories

The FLECHT movies indicated that the flow pattern around the heater rods may be laminar or turbulent, and it is to be expected that the heat transfer coefficient is influenced by the Reynolds Number (Re). Also, a vapor film around the heater rods was occasionally observed, and this was described as the film boiling or inverted annular regime [2]. Any explanation of heat transfer behavior should then consider the Re and the film thickness (in the inverted annular regime).

2.2.1 Film Thickness

Film thickness is of great importance below the carry over point, in the film boiling regime. It is the vapor film that offers resistance to the transfer of heat from the heater rods to the saturated liquid in the channels. Unfortunately there is not much material in the literature on inverted annular flow, but there is a wealth of information on traditional annular flow and on film condensation on vertical walls. Film condensation theories may be applied to vapor as well as if appropriate force, mass, and momentum balances are used. There is an excellent method [5] for calculating film thicknesses as a function of Re, but the particular problem at hand does not readily lend itself to such a solution. Different methods

for determining film thickness must be used for laminar and for turbulent flow, but no clear transition Re is available for deciding which to use.

Instead of deciding if the flow was laminar or turbulent, the film theories presented in this chapter are applied throughout the test section, regardless of Re. Film thickness will then be inferred from the film theories and utilized as explained later in this chapter.

2.2.2 Reynolds Number

One would naturally assume that in the inverted annular film boiling regime a Re based on film thickness must be used, and in the dispersed flow regime the Re should be a function of the tube diameter. This presents another dilemma because the carry over point would also be the criterion for selecting the appropriate form of Re, but the carry over point is not known a priori. Fortunately, this issue may be conveniently sidestepped because in this case the tube Re and film Re are equal, as explained below.

a. Film Re

If the curvature of the tube is negligible (i.e., the film thickness is small compared with the tube diameter), the tube may be approximated by a vertical flat plate. The vapor film Re may then be found from analogous film condensation theories,

$$Re_v = \frac{4\Gamma_v}{\mu_v} \qquad (2\text{-}1)$$

and Γ_v is vapor mass flow rate per unit width, and for a thin vapor film,

$$\Gamma_v = \frac{w_v}{\pi D} \qquad (2\text{-}2)$$

b. Tube Re

If the regime is dispersed flow, the vapor is no longer a thin film but instead it fills the entire tube. The Re must then be based on tube diameter, and assuming a zero shear interface,

$$Re_v = \frac{G_v D}{\mu_v} = \frac{(\frac{w_v}{2})D}{\pi D^2/4} = \frac{4\Gamma_v}{\mu_v} \qquad (2\text{-}3)$$

From Eqs. (2-1) to (2-3) it can be seen that the tube and film Re are equal and a decision as to which to use is fortuitously unnecessary.

c. Film Properties

All film properties are to be evaluated at system pressure and film temperature, assumed to be the average of wall and saturation temperatures,

$$T_v = \frac{1}{2}(T_w + T_{sat}) \qquad (2\text{-}4)$$

2.3 Tube Theories

The tube theories are based on the premise that the vapor fills the entire tube, and it discounts the contribution of the liquid droplets to the heat transfer mechanisms. These theories were developed as a limit to the experimental data in the higher quality range, generally at the upper elevations of the test section. There the regime might be expected to be dispersed flow and tube theories would be more appropriate.

2.3.1 Laminar Tube

With variations of approximately 100°F from a mean tube temperature, the temperature profile is not constant along the experimental test section. But, considering the high temperatures at which it was operated, an assumption of a constant axial temperature profile would not be too unreasonable.

For such an assumption, Rohsenow and Choi [6] have derived an asymptotic value for the Nusselt Number (Nu) for laminar flow in circular tubes with a parabolic velocity profile,

$$Nu = 3.66 \qquad (2\text{-}5)$$

From this equation, with the vapor thermal conductivity and tube diameter, the heat transfer coefficient may be found for laminar flow of vapor in the dispersed flow regime.

2.3.2 Turbulent Tube

For turbulent flow, there are several correlations which predict Nu as function of other dimensionless parameters. One of these, the McAdams Equation, gives

$$Nu = 0.023(Re)^{.8}(Pr)^{.4} \qquad (2\text{-}6)$$

The heat transfer coefficient may again be found, knowing the vapor conductivity and the tube diameter. As discussed before, the Re for tube flow is the same as that for film flow, with the vapor mass flow rate based on the equilibrium quality,

$$m_v = Xm \qquad (2\text{-}7)$$

2.3.3 Modified Turbulent Tube

If the Re is based on the total mass flow rate rather than on the vapor flow rate, an upper limit for the heat transfer coefficient, independent of quality, for turbulent flow in tubes may be established. Because of its independence of quality, the Re may be calculated by

$$Re = \frac{GD}{\mu_v} \qquad (2\text{-}8)$$

Since film properties are relatively constant along the tube, given the slight axial temperature gradient, the heat transfer coefficient may be derived from the McAdams Equation (2-6) as a function of the flooding rate only. The purpose of this theory is to place an upper limit on the heat transfer data much as the turbulent tube theory of sec. 2.3.2 is a lower limit. That is, heat transfer coefficients above this theory are definitely turbulent film and those below the turbulent tube theory are definitely laminar film. However, this modified theory is applicable only for higher flooding rates, those 4 in/sec or greater. At flooding rates of 3 in/sec, this modified theory approximates the data well, but its results are meaningless because the experimental heat transfer coefficients indicate the data was taken in the film boiling regime and not in tube flow. But, at the higher flooding rates it does reliably present an upper limit to the data for tube flow.

2.4 Film Theories

In the inverted annular film boiling regime, below the carry over point, heat transfer is greatly influenced by the film thickness. It is this vapor film that resists the transfer of heat from the tube wall to the liquid. The following two theories investigated the effect of laminar and turbulent films on heat transfer coefficients.

2.4.1 Laminar Film

Heat transfer through films is a rather complex phenomenon and several simplifying assumptions must first be made to arrive at a solution. These assumptions are:

a. Axial heat conduction is negligible. This is reasonable except at the ends of the heated section.

b. All the heat passes from the wall to the liquid through the film. This is not quite correct because of superheating of the vapor, but it should not induce too great an error.

c. Curvature of the tube may be neglected and the film may be considered thin. This allows us to consider the film as flow between a vertical flat plate and a parallel liquid-vapor interface.

d. The velocity distribution in the film is the universal velocity distribution. This will be discussed in more detail later in this section.

e. Momentum terms are negligible compared to viscous and pressure forces. This assumption is within reason.

At fig. 5 is representation of the thin vapor film in the experimental test section, showing the universal velocity distribution and a control volume. A force balance on the control volume yields:

$$-\frac{\partial \tau}{\partial y} = g(\rho_\ell - \rho_v) \tag{2-9}$$

Substituting into Eqn. (2-9) the definition of the shear stress,

$$\tau = \mu_v \frac{\partial V_z}{\partial y} \tag{2-10}$$

gives

$$-\mu_v \frac{\partial^2 V_z}{\partial y^2} = g(\rho_\ell - \rho_v) \tag{2-11}$$

We further assume that the shear stress at the wall and the shear stress at the vapor-liquid interface are equal. This is tantamount to assuming the universal velocity distribution, with the vapor velocity at the wall and vapor-liquid interface equal to zero. These assumptions establish the boundary conditions for the differential equation above,

$$\begin{aligned} &1) \quad \text{at } y = 0, \ \frac{\partial V_z}{\partial y} = 0 \\ &2) \quad \text{at } y = \pm \ \delta/2, \ V_z = 0 \end{aligned} \tag{2-12}$$

Integrating eq. (2-11) with eq. (2-12) yields the vapor velocity profile as a function of film thickness,

$$V_z = \frac{g(\rho_\ell - \rho_v)}{\mu_v}\left[\frac{(\delta/2)^2}{2} - \frac{y^2}{2}\right] \qquad (2\text{-}13)$$

The vapor flow rate per unit width, Γ_v, is then calculated as follows:

$$\Gamma_v = \rho_v \int_{-\delta/2}^{\delta/2} V_z \, dy = \frac{g\rho_v(\rho_\ell - \rho_v)}{4\mu_v} \frac{\delta^3}{3} \qquad (2\text{-}14)$$

From the definition of the vapor film Reynolds Number, eq. (2-1), the film thickness may be found as a function of Re,

$$Re_v = \frac{g\rho_v(\rho_\ell - \rho_v)}{\mu_v^2} \frac{\delta^3}{3} \qquad (2\text{-}15)$$

For a thin laminar film, the film thickness is equal to the ratio of vapor thermal conductivity to the heat transfer coefficient. Eq. (2-16) is the expression for heat transfer coefficients in a thin laminar vapor film,

$$\frac{h}{k_v} = \frac{1}{\delta} \qquad (2\text{-}16)$$

2.4.2 Turbulent Film

This is again a very complex situation, and several assumptions must be made to simplify the mathematics required. These assumptions, the same as in Sec. 2.4, and this particular problem are very similar to that solved by Dougall [7], and his solution will be adopted as the turbulent film theory. The specific details of his method will not be repeated here, but the general procedure will be presented for a better understanding of how this experiment's theoretical turbulent film heat transfer coefficients were derived.

Given the film Re, Dougall integrated the universal velocity distribution to obtain a dimensionless film thickness:

$$\text{for } 5 \leq \frac{\delta^*}{2} \leq 30,\ Re_v = 100.4 - 64.4\left(\frac{\delta^*}{2}\right) + 40\left(\frac{\delta^*}{2}\right)\ln\left(\frac{\delta^*}{2}\right)$$

$$\text{for } 30 \leq \frac{\delta^*}{2},\ Re_v = -512 + 24\left(\frac{\delta^*}{2}\right) + 20\left(\frac{\delta^*}{2}\right)\ln\left(\frac{\delta^*}{2}\right) \qquad (2\text{-}17)$$

For the problem at hand, film Re were calculated as in section 2.2.2 and used in the above equation. Then, with the further assumption that the shear stresses at the liquid vapor interface and at the wall were equal, and with the definition of the dimensionless film thickness,

$$\delta^* \equiv \frac{\delta}{\nu_v}\sqrt{\frac{\tau_w g_o}{\rho_v}} \qquad (2\text{-}17a)$$

Dougall was able to relate the film thickness to the dimensionless film thickness as a function of film properties rather than of shear stress,

$$\left[\frac{\rho_v(\rho_\ell - \rho_v)gD^3}{\mu_v^2}\right]\left(\frac{\delta}{D}\right)^3 = 2(\delta^*)^2 \qquad (2\text{-}18)$$

The assumption of equal shear stress at the wall and at the vapor-liquid interface in essence means that the vapor velocity at the wall and at the vapor-liquid interface are both zero, and the velocity distribution is parabolic, symmetric about the vapor film centerline. This is the assumption of the universal velocity distribution presented earlier, and it appears to be quite reasonable. The vapor velocity, on the average, is much greater than that of the liquid, which is only slightly greater than the flooding rate, i.e., a few inches per second. The vapor velocity at the vapor-liquid interface is the same as the liquid, a few inches per second, which indeed is negligible compared to the average vapor velocity.

Dougall divided the vapor film into several regions in order to determine their individual thermal resistances. He then utilized eqn. (2-18) above to express the Nu as

$$Nu_v = \frac{0.794 \left(\frac{\rho_v(\rho_\ell - \rho_v) g D^3}{\mu_v^2} \right)^{1/3} (\delta^*)^{1/3}}{\int_0^{\delta^*} \frac{dy^+}{1 + Pr\, \varepsilon/\nu_v}} \qquad (2\text{-}19)$$

where $\int_0^{\delta^*} \frac{dy^+}{1 + Pr\, \varepsilon/\nu_v}$ is defined as the thermal resistance of the vapor film (see Reference 7 for evaluation of these thermal resistances).

Once the Nu and the film thickness have been calculated by Eqs. (2-19) and (2-18) respectively, the theoretical turbulent film heat transfer coefficient may be found from

$$Nu = h\delta/k \qquad (2\text{-}20)$$

This turbulent film theory as well as the other four theories will be presented in Chapter 4 with the experimental data. The form of presentation will be graphical, with h/k_v plotted on the ordinate and equilibrium quality on the abscissa. h/k_v will be plotted instead of just the heat transfer coefficient because the former decreases the influence of temperature on the experimental data.

The next chapter describes the test apparatus, procedure, and method of arriving at the experimental heat transfer coefficients.

3. EXPERIMENTAL PROGRAM

3.1 Description of Apparatus

The experimental apparatus basically consisted of a test section and control and instrumentation devices. A different configuration and procedure were used for the first two data points, and this is briefly discussed in Appendix B. The objective of all experiments was to obtain steady state heat transfer data in the stable film boiling regime. At Fig. 6 is a schematic drawing of the apparatus and at Fig. 7 is a photograph of the test section and associated equipment. Reference to both figures will assist in understanding the apparatus and the concept of operation. For all but the first two data points, the remainder of this section is applicable.

3.1.1 Control and Instrumentation

System parameters such as pressure, coolant flooding rate, coolant subcooling, and tube wall temperature were representative of the post-LOCA reflood phase. System pressurizing was achieved by nitrogen gas and read at a calibrated pressure gauge, 0 to 100 psig. The accuracy of the pressure readings was within 3 psi. Coolant circulation was provided by a commercially procured centrifugal pump, 10 GPM capacity (a bypass line decreased this flow to approximately 2 GPM), and flow to the test section was monitored by a rotometer and controlled by a standard globe valve. The rotometer had been calibrated and subsequent checks of flow rate indicated its accuracy was within 4%. Coolant inlet temperature was varied by using a shell and tube water-steam heat exchanger and was monitored by two thermocouples, one in the fluid stream and one on the tube wall just upstream of the test section. All thermocouples (except the one in the

fluid) were chromel-alumel duplex wire with glass-on-glass insulation. The temperatures were read in millivolts on a digital DC voltmeter accurate to 0.02mv. Calibration tables supplied by the manufacturer were used to convert thermocouple millivolts to °F. The temperature readings were assumed accurate to at least 5°F. The thermocouples were placed on the outside wall of the test section, but because the tube wall was thin (0.091 in), the temperature gradient was negligible, and the inside wall temperature was assumed to be the same as the outside.

Heat to the test section was supplied by two different means. The lower 4 ft. of the tube, called the preheater, were heated uniformly by resistance heat induction. The current through the preheater was controlled at the DC generator console and could be varied as high as 3000 amps. The voltage drop across the preheater was read with the digital DC voltmeter and used with the calculated tube resistance [8] to compute the heat flux. A separate ohmmeter with adequate accuracy was not available to read tube resistance, but Mantell reliably predicts resistance as a function of temperature. The voltage drop across the preheater was considered accurate to 0.003 volts. The main portion of the test section was heated by heat spikes powered by Variacs (variable transformers). The variacs were calibrated, but as there were six (6) individual cartridge heaters powered by each variac, and the voltage across each heater was critical in determining the heat provided by each heat spike, the voltage across each heater was also checked. This voltage was found to be 1 volt (on the average) less than the calibrated variac reading.

3.1.2 Test Section

The test section itself was a type 304 stainless steel tube, 0.493 in

ID, 0.675 in, OD, 8 ft. long. The lower 4 ft. of the tube, the preheater, was heated separately and was used to raise the coolant temperature as close to saturation as possible so that tube wall dryout could be achieved at the first heat spike. Also, the effect of total heat added was to be considered, and this could be easily varied with the preheater. Thermocouples were placed at several locations along the preheater to monitor temperature.

The remainder of the test section was heated by the heat spikes, small concentrations of very high heat flux (the maximum flux for each spike was approximately 2×10^5 BTU/hr-ft^2). These heat spikes were copper blocks with six (6) each Chromalox cartridge heaters, 250 watts each. These blocks were cut into sections and clamped tightly to the tube. (At. Fig. 8 is a schematic drawing of the copper block heat spikes and their arrangement on the test section. At Fig. 9 is a photograph of several copper blocks without insulation). There were ten (10) blocks total, 2.5 in. long, 2.5 in. in diameter, spaced 1/8 in apart. At this interval, the tube wall between the blocks did not quench because of axial conduction between the blocks. One thermocouple was placed between each block and the tube wall to monitor tube temperature. Contact resistance between the copper block and the tube wall was neglected and it was assumed that the wall and the copper were at the same temperature. (This assumption was reasonable since, in some places, the tube wall could be viewed through the insulation, and its color was approximately that of the copper). The entire test section was insulated with commercially procured tubes of magnesium oxide.

3.1.3 Additional Components

The apparatus had a recirculation line whose purpose was to allow the coolant to reach the desired inlet temperature while the tube was being

heated. A condenser was used to condense the vapor to liquid before it reentered the reservoir (30 Gal. supply of distilled water). There was also a bleeder valve to make coarse adjustments to system pressure and a drain at the bottom of the test section to purge the system. On several occasions during the experimental program, all coolant was drained and the system replenished with fresh distilled water to eliminate impurities.

3.2 Procedure of Operation

The system was first pressurized to approximately 5 psi below desired operating pressure (the subsequent generation of steam would increase the pressure and the bleeder valve would then be used to lower the pressure as close as possible to the desired level). The variac voltage (for all ten heat spikes) was increased and the tube temperature allowed to rise to at least 1000°F above saturation temperature (the test section had previously been drained of water and the tube wall was dry before heat was applied). While the tube temperature was increasing, the coolant was circulating through the heat exchanger and the recirculation line and was raised to the desired inlet temperature. As the tube temperature approached T_{sat} + 1000°F, the main generator DC current was applied to the pre-heater.

When T_w, T_i, and G all were approximately at desired levels, the coolant was diverted from the recirculation line into the test section. As necessary or desired, the following refinements were made: T_w was raised or lowered by adjusting variac voltage; pressure was lowered by the bleeder valve; coolant flow was monitored and held constant; T_i was controlled by the heat exchanger; and heat flux to the preheater was varied at the main generator console.

3.3 Recording the Data

Since this was a series of steady state experiments, emphasis was on insuring that all parameters were relatively constant over time (a correction for heat losses due to changes in wall temperature was applied- see paragraph 3.4 below). The pertinent quantities measured and recorded were as follows: T_w, T_i, P, G, E, and e. All parameters except T_w could be held relatively constant for the duration of any data point. T_w was recorded over a convenient, arbitrary time interval (dt) of 12 minutes. However, recording of data did not begin until T_w appeared to settle to a reasonably constant level. (Although a data point required only 12 minutes to record, it sometimes required over 4 hours of adjustments to hold the system at steady state for any one data point). Once recording began, however, no adjustments were made, other than insuring the flow rate and inlet temperature remained constant.

3.4 Data Reduction

The objective of this experiment was steady state heat transfer data. The heat transfer coefficients were computed from

$$h = \frac{q_{net}}{A_{HT}\,(T_w - T_{sat})} \qquad (3\text{-}1)$$

where T_w was the average wall temperature over 12 minutes, and q_{net} was the net amount of heat added to an incremental section of the tube by one copper block heat spike. Then

$$q_{net} = q - q_l - q_L \qquad (3\text{-}2)$$

where

$$q = \left(\frac{E}{120}\right)^2 \times 6W \qquad (3\text{-}3)$$

Each individual cartridge heater was nominally rated by the manufacturer at 250 Watts at 120 volts. However, the resistance of each heater varied, and the actual wattage per heater was used in the computations. (The heaters contained high resistance wire which, when current was applied, transferred heat to the stainless steel clad. The variance of each heater's resistance with temperature was negligible and was not considered). q_ℓ, the heat losses through the insulation to the ambient, were taken from heat loss curves as a function of T_w prepared by the author for these experiments. q_L, the heat losses due to raising the wall temperature over time (or heat gains if T_w decreased) were calculated by

$$q_L = [(wc_p)_{ss} + (wc_p)_{cu}] \frac{dT_w}{dt} \qquad (3\text{-}4)$$

Also, equilibrium quality (X) for each heat spike was calculated by first computing the enthalpy, H(z), of the coolant as a function of length from a heat balance

$$\int_{z_1}^{z_2} q'' \pi D dz = \int_{H_1}^{H_2} \dot{m}\, dH \qquad (3\text{-}5)$$

where $z_1 = 0$, the bottom of the test section, z_2 is the height at any level (e.g., the carry-over point) and H_1 and H_2 are the enthalpies at these locations. Next, calculate the quality,

$$X(z) = \frac{H(z) - H_f}{H_{fg}} \qquad (3\text{-}6)$$

Then relate quality to vapor flow rate by

$$V_g = \frac{G_v}{\rho_v} \qquad (3\text{-}7)$$

(3-8)

where $G_v = XG$

In order to verify the validity of the above procedure, a heat balance check was performed. At a low system pressure and flooding rate, coolant was circulated through the test section. Thermocouples were mounted on the outside wall of the test section immediately upstream and downstream of the bottom and top copper block heat spikes, respectively, to monitor the temperature of the liquid. The bulk temperature of the liquid was assumed to be the same as the outside temperature of the wall (the following procedure would validate this assumption, within reason). Heat was applied to the main test section by the copper block heat spikes. The system was then allowed to achieve steady state at wall temperatures below saturation.

Given the heat input, the coolant flow rate, and the inlet temperature (and enthalpy), eqn. (3-5) was used to calculate the outlet temperature (enthalpy). The results agreed with the measured outlet temperature within 7%. The above test was repeated for just the preheater and for both the preheater and the main test section with similar percent error. It is believed the above check validates the experimental procedure described in this chapter.

The results of the experimental program, compared with the theories derived in Chapter 2, are presented in Chapter 4. The experimental heat transfer coefficients calculated by eqn. (3-1) will be plotted versus the equilibrium quality calculated by eqn. (3-6). Carryover velocities, when appropriate, will be calculated by eqn. (3-7).

4. RESULTS

Experimental heat transfer coefficients, calculated as shown in Chapter 3, were corrected for the influence of temperature by dividing by the thermal conductivity of the vapor film, k_v. The theoretical heat transfer coefficients derived in Chapter 2 also were divided by k_v to compare all heat transfer coefficients on the same scale. Both experimental and theoretical results, except the laminar tube theory, are tabulated in Appendix C. The laminar tube theory was not calculated for each point because it is constant for all system parameters [see eqn. (2-1)],

$$(h/k_v)\ \text{laminar tube} = 89.1 \qquad (4\text{-}1)$$

This theory, as well as the others, are compared with several data points to determine how well the data agree with the various theories. The purpose of this type of presentation is not to derive a new empirical correlation. Instead, by plotting the theories with the data, a better appreciation of the type of flow represented by the data may be gained, and the criterion for liquid carry over may be inferred from heat transfer behavior.

In addition to the tabulation of data in Appendix C, the agreement of the data with the theories will be described and shown graphically. Next, several data points will be presented to show the effect of pressure, flooding rate, and wall temperature on heat transfer and carry over. Then all runs with carry over discernible (flooding rates of 1 in/sec or less), will be plotted separately, with the carry over points indicated for each. Finally, the carry over velocities deduced from these data

points will be compared with Plummer's Critical Mass Criterion which predicts carry over velocities as a function of pressure.

Before the data is presented, a few general comments would be helpful. The first heat transfer coefficient for each run, at the axial point corresponding to the bottom of the main test section, is not plotted. Axial conduction effects are too great at this location and the wall temperature and heat transfer coefficients are not representative of the film boiling regime. Also, at this position, experimental heat transfer coefficients are very large (h/k_v is of the order of 10^4) and a scale of axes that includes this point would distort the trend shown by the remaining points. All individual coordinates $(X, h/k_v)$ for each data point are connected with straight lines to more clearly indicate the change of heat transfer coefficient with quality. Finally, all theories are plotted as straight lines, approximating a slope for the individual values calculated by the theories of Chapter 2.

4.1 Agreement of Data with Theory

Heat transfer coefficients (h/k_v) for all data points were plotted versus equilibrium quality to show the agreement with the theories derived in Chapter 2. When the plots for all data points were compared, some general trends were evident. These comparisons of data with theory will be discussed in this section, and several data points will be presented as illustration.

4.1.1 Low Pressure, Low Flooding Rate

When the pressure and flooding rate are low, the heat transfer coefficient steadily decreases with quality. At low qualities, the heat

transfer coefficients are very high, indicating the data falls in the nucleate boiling regime. In the higher quality range, the heat transfer coefficients are lower and approach the values expected of transition to dispersed flow. Most of the data falls in the area of decreasing heat transfer coefficients and indicates the flow regime is turbulent film boiling. As the vapor film thickens, the tube wall encounters more resistance to transferring heat to the liquid core, and the heat transfer decreases.

At Fig. 10 is a plot of the heat transfer coefficient of Data Point 3 (20 psia, 1 in/sec) versus equilibrium quality. The data points indicate that most of the lower quality region corresponds to the turbulent film prediction, but at higher qualities, the turbulent tube theory is approached. On Fig. 10, as on all figures comparing theory with data, the full range of the theory over quality is shown. Although DP 3 may not have quite reached carry over, its carry over velocity will be computed based on its maximum quality attained. This will be compared later in this chapter with the carry over velocity prediction.

4.1.2 Low Pressure, High Flooding Rate

When the flooding rate is increased at low pressure, the heat transfer coefficients remain relatively constant with quality. Data Point 13 (25 psia, 6 in/sec) is plotted at Fig. 11 to compare data with theory. As can be seen in the figure, the heat transfer coefficients correspond very closely to the turbulent tube theory and are remote from the other theories. This means that the entire test section is in stable film boiling and that the film resisting heat transfer is turbulent. The

implications of this are obvious: at low pressure and high flooding rates, with the quality range examined, carry over does not occur. The heat transfer has not deteriorated to that of the dispersed flow regime and the vapor film does not offer much resistance to heat transfer because of the increased vapor velocity. High flooding rates result in inverted annular flow and carry over is not an important consideration.

Data Point 4 (not plotted here but listed in Appendix C) indicates that this phenomenon occurs at flooding rates as low as 2 in/sec. This would mean that given the range of parameters specified in the report (pressure, quality, wall temperature, heat flux, etc.) carry over will not occur at flooding rates of 2 in/sec of greater. The influence of flooding rate on carry over will be further examined later in this report.

4.1.3 High Pressure, Low Flooding Rate

There is basically no difference between the respective agreement of high pressure, low flooding rate data and low pressure, low flooding rate data with the theories. The heat transfer coefficient decreases through film boiling to turbulent tube dispersed flow. However, as shown in Fig. 12, for DP 32 (67 psia, 1 in/sec), there are differences at the higher quality range. The heat transfer coefficients of DP 32 decrease through the film boiling regime to a minimum that is definitely turbulent tube flow, but approaching laminar film. The change of heat transfer coefficient with quality and the change of regime definitely indicate carry over has occurred. Looking back at Section 4.1.1, it is

reasonable to speculate that as the higher qualities are approached, DP 3 might have shown the same increase of heat transfer coefficient with quality, and possibly the same incursion into the laminar film theory.

For both low flooding rate cases shown (20 psia and 67 psia) the theories give a good indication of what the data represent. The heat transfer behavior of low flooding rates show a progression with quality through a deteriorating heat transfer environment to a minimum heat transfer coefficient. At this point, the flow becomes dispersed and carry over occurs, and the heat transfer again improves because of the increased vapor velocity and the presence of entrained liquid droplets in the vapor.

4.1.4 High Pressure, High Flooding Rate

DP 37 (67 psia, 6 in/sec) at Fig. 13 indicate that the theories again bound the data. The heat transfer coefficients lie between the turbulent film and turbulent tube predictions, and although no clear decision may be made as to which regime the data belong, it appears that the data tend more to turbulent film. The heat transfer coefficients are representative of values expected in the film boiling regime.

Because the heat transfer data are definitely not turbulent tube, and because the heat transfer coefficients have not decreased to a low enough minimum for us to define the carry over point, we must assume that carry over has not occurred. From the trend established by the data shown, it might be inferred that a well-defined carry over point

cannot be observed and the tube will remain in turbulent film boiling. Comparing DP 37 with DP 13, no significant difference as relates to heat transfer behavior or carry over can be seen. Therefore it is reasonable to assume that at higher flooding rates, within the range of parameters given, a distinct carry over point will not be found and the test section (or flow channel) will remain in inverted annular film boiling.

4.2 System Effects on Carry Over

For those points for which carry over is possible, the effect of pressure and wall temperature will now be shown. Also, the effects of flooding rate on carry over will be presented in this section.

4.2.1 Effect of Pressure

For a low flooding rate the effect of pressure on carry over was examined by comparing the plots of h/k_v versus quality for several data point, all at 1 in/sec. (see Fig. 14). As was stated in Sec. 4.1.1 and 4.1.3, at low flooding rates the heat transfer coefficient decreases through the film boiling regime to a minimum at the transition to dispersed flow. All points but DP 3 then increase, but it is not known if this is an effect of pressure or due to inadequate quality range for DP 3. However, the former should not be accepted because only one data point was taken at that pressure (20 psia). As the pressure increases, the carry over points occur at decreasing qualities, which is to be expected. Also, the effect of pressure on heat transfer can be seen. At a constant quality, as the pressure increases, the heat transfer coefficient de-

creases in the film boiling regime.

4.2.2 Effect of Wall Temperature

Three data points, at the same pressure and flooding rate (67 psia and 1 in/sec) were compared to observe the effect of wall temperature (or heat added) on carry over (see Fig. 15). The three points chosen (DP 30, 31, and 32) had an increasing amount of heat added to both the preheater and to all copper block heat spikes, and thus the temperature of each point along the tube was greater. That is T_w(DP 30) < T_w(DP 31) < T_w(DP 32). As T increases, the carry over quality, and thus the carry over velocity, increases. The implications of this are that, for the same quality at higher wall temperatures, the vapor film velocity is the same but the heat transfer coefficient is higher. This would further imply that since vapor film velocity and pressure are the same, the film thickness decreases at higher wall temperatures.

4.2.3 Effect of Flooding Rate

Three data points at the same pressure (67 psia) and approximately the same wall temperatures were compared (see Fig. 16) to observe the effects of flooding rate on carry over. The three points, DP 31, 35, and 37, had flooding rates of 1, 3, and 6 in/sec respectively. The effects is obvious: at low flooding rates of 1 in/sec a distinct carry over point can be observed while at flooding rates of greater than 1 in/sec a carry over point cannot be defined and the regime appears to remain inverted annular film boiling. The heat transfer for higher flooding rates remains good in the film boiling regime because the vapor

film velocity is sufficiently high to compensate for the thickening vapor film as the quality increases.

4.3 Comparison of Experimental Carry over Velocities with Plummer's Critical Mass Criterion

In Fig. 17 through 24 are plotted the data points for which carry over can be defined (DP 3, 20, 21, 22, 23, 30, 31, and 32). The carry over point is indicated along the abscissa by an asterisk (*) and was inferred in the following way. The carry over point, as explained earlier, is the location at which the flow regime changes from a film configuration to a dispersed flow tube configuration. Ideally, it would indicate the transition from turbulent or laminar inverted annular film flow to turbulent (or laminar, perhaps) tube flow. As such, it should also be the location where the heat transfer coefficient reaches a minimum. The heat transfer coefficient decreases with increasing quality through the inverted annular film boiling regime, until the vapor velocity increases sufficiently to carry over liquid droplets. The heat transfer coefficient then increases with quality primarily because of the increased vapor velocity. The carry over point should correspond to a turbulent tube theory because of the definition of dispersed flow and the high vapor velocity (a laminar tube flow theory makes little sense in this context because the low vapor velocity at the wall would let the liquid droplets fall back). Therefore, the carry over point is the location at which the heat transfer coefficient reach a minimum low enough so that transition from inverted annular film boiling to turbulent tube flow can be defined.

These experimental carry over velocities are compared in Fig. 25 with the Plummer Critical Mass Velocity Criterion [3]. The curve represents the predicted carry over velocities as a function of pressure, and the experimental carry over velocities are plotted as points as shown. DP 3 is plotted with an arrow to indicate that the actual carry over velocity is probably greater than indicated because of the inadequate quality range as explained in Sec. 4.1.1). Table I below lists the experimental carry over velocities for each data point and the predicted carry over velocity. As can be seen, the prediction agrees quite well with the experimental data.

TABLE I

DP	Pressure (psia)	V_{co} (Predicted) (ft/sec)	V_{co} (Experimental) (ft/sec)
3	20	38.5	60
20	31	30.1	9
21	36	28.2	23
22	33	29.0	36
23	32	29.5	32
30	66	21.2	14
31	67	21.0	18
32	67	21.0	25

5. CONCLUSIONS

Extensive data were taken for upward flow of water in a vertical heated tube, with the range of interest from 20 to 67 psia, and flooding rates of from 1 to 6 in/sec. Heat was applied to the test section and heat transfer coefficients and quality as functions of axial position were calculated. These experimental heat transfer coefficients were compared with several theories and the results presented in Chapter 4. Several conclusions may be inferred from the accumulation of data and the comparison with the theories. These are the following:

a. Within the range of interest, a liquid carry over point can be observed at flooding rates of 1 in/sec or less. At higher flooding rates a distinct carry over point cannot be seen.

b. The heat transfer coefficients of the range of parameters investigated generally fall between the theories for turbulent tube flow.

c. Increased pressure decreases the velocity required to carry over the liquid droplets.

d. An increase in wall temperature (or in heat flux) increases the apparent vapor velocity at the carry over point. This is probably due to the higher vapor acceleration and greater slip of the droplets with increased heat flux.

e. At flooding rates of 1 in/sec, the data indicates the possibility of laminar tube flow (see Fig. 26) near the carry over point. A reasonable conclusion is that at low flooding rates a transition from turbulent film to laminar tube flow is possible before the transition to turbulent tube flow and dispersed flow film boiling.

f. The results of Sec. 4.3 and Fig. 25 indicate that the carry over velocities predicted by reference 3 are reasonable when compared with the data. However, the scatter in observed carry over velocities suggests that more research needs to be done in this area. Until then, it is recommended that Plummer's Critical Mass Velocity Criterion be adopted for predicting carry over velocity as a function of pressure.

NOMENCLATURE

A_{HT}	-	area for heat transfer of each copper block heat spike (0.0282 ft^2) (based on inside diameter of test section).
C_d	-	drag coefficient
c_p	-	specific heat at constant pressure
D	-	inside diameter of test section
D_d	-	diameter of FLECHT droplets
DP	-	data point
dt	-	time interval selected for duration of data point (12 minutes)
E	-	voltage potential across each cartridge heater
e	-	voltage potential across preheater
F	-	force
FR	-	flooding rate
G	-	mass flux (lb_m/ft^2-hr)
GPM	-	gallons per minute
g	-	gravitational acceleration
g_o	-	conversion factor
H	-	enthalpy
h	-	heat transfer coefficient
k	-	thermal conductivity
m	-	mass flow rate (lb_m/hr)
Nu	-	Nusselt Number
P	-	pressure
Pr	-	Prandtl Number
q	-	gross heat applied by each copper block heat spike

q_ℓ	-	heat lost to the ambient
q_L	-	heat lost (or gained) if wall temperature increased (decreased) over dt
q_{net}	-	net heat applied to test section by each copper block heat spike
q''	-	heat flux (q/A_{HT})
Re	-	Reynolds Number
T	-	temperature
t	-	time
V	-	velocity
W	-	power rating of each cartridge heater (nominally rated at 250 watts)
w	-	mass (of copper or of stainless steel in test section)
We	-	Weber Number
X	-	equilibrium quality
y	-	distance from wall of test section into vapor film (used in Turbulent Film Theory)
y^+	-	dimensionless distance, $\frac{y}{\nu_v}\sqrt{\frac{\tau_w g_o}{\rho_v}}$
z	-	axial distance from downstream end of preheater
Γ	-	mass flow rate per unit width
δ	-	vapor film thickness
δ^*	-	dimensionless vapor film thickness
ε	-	eddy diffusivity
μ	-	absolute viscosity
ν	-	kinematic viscosity (μ/ρ)
ρ	-	density

σ	-	surface tension
τ	-	shear stress

Subscripts

co	-	carry over
crit	-	critical
cu	-	copper
f	-	refers to liquid droplet properties
fg	-	refers to latent heat
g	-	refers to gravity
i	-	at the inlet to the preheater
ℓ	-	refers to saturated liquid (except for q_ℓ)
sat	-	saturation
ss	-	stainless steel
w	-	refers to tube wall
v	-	refers to vapor film
z	-	refers to the axial direction

REFERENCES

1. G. Yadigaroglu et.al., "Heat Transfer During the Reflooding Phase of the LOCA-State of the Art," EPRI Topical Report 248-1(September 1975).

2. F.F. Cadek et.al., "PWR FLECHT (Full Length Emergency Cooling Heat Transfer) - Final Report," WCAP-7665 (April 1971).

3. D.N. Plummer et.al., "Post Critical Heat Transfer to Flowing Liquid in a Vertical Tube," M.I.T. Report 72718-91 (September 1974).

4. D.C. Groeneveld, "Effect of a Heat Flux Spike on the Downstream Dry-out Behavior," Journal of Heat Transfer, Transactions of the ASME, Series C, Vol. 96, No. 2, May 1974, pp. 121-125.

5. H.R. Kunz and S. Yerazunis, "An Analysis of Film Condensation, Film Evaporation, and Single-Phase Heat Transfer for Liquid Prandtl Numbers from 10^{-3} to 10^{4}," Journal of Heat Tranafer, Transactions of the ASME, Series C, Vol. 91, No. 3, August 1969, pp. 413 - 420.

6. W. Rohsenow and H. Choi, Heat, Mass, and Momentum Transfer, Prentice-Hall, Inc., Englewood Cliffs, New Jersey, 1961.

7. R. Dougall and W. Rohsenow, "Film Boiling on the Inside of Vertical Tubes with Upward Flow of the Fluid at Low Qualities," M.I.T. Report, 9079-26 (September 1963).

8. C. Mantell, Engineering Materials Handbook, McGraw-Hill Book Company, Inc., New York, 1958.

APPENDIX A

FLSCHT Droplet Data

Run #	P(psia)	FR(in/sec)
0085	25	2.0
0487	18	0.8
0588	15	0.6
0690	15	0.6
3440	55	5.9
9983	19	1.0

Droplet # Run# - Drop#	D_d(in)	V_f(ft/sec)	V_v(ft/sec)	We
0085-1	0.126	10.4	42	5.0
-2	.146	13.1	47	6.7
-3	.097	10.8	38	3.0
-4	.146	12.5	46	6.7
-5	.116	12.0	42	4.3
-6	.152	11.2	46	7.4
-7	.097	12.8	40	3.0
-8	.136	11.2	44	5.9
-9	.165	7.9	44	8.7
-10	.146	8.9	42	6.7
0487-1	0.087	4.6	35	2.4
-2	.097	5.0	37	2.9
-3	.078	5.2	34	1.9
-4	.107	5.7	39	3.5
-5	.068	6.6	33	1.4
-6	.087	6.7	37	2.4
-7	.087	5.8	36	2.4
-8	.077	5.4	34	1.9
-9	.097	4.7	37	2.9
-10	.068	7.5	34	1.4

Droplet # Run# - Drop #	D_d(in)	V_f(ft/sec)	V_v(ft/sec)	We
0588-1	0.072	6.8	37	1.6
-2	.080	7.3	39	2.0
-3	.080	6.7	38	2.0
-4	.104	7.7	44	3.3
-5	.080	5.3	37	2.0
-6	.088	7.1	40	2.4
-7	.104	6.2	42	3.3
-8	.080	6.2	38	2.0
-9	.072	6.7	37	2.0
-10	.121	9.8	49	4.4
0690-1	0.072	5.3	35	1.6
-2	.080	7.8	39	2.0
-3	.104	7.0	43	3.3
-4	.064	7.4	36	1.3
-5	.072	8.8	39	1.6
-6	.113	8.0	46	3.9
-7	0.072	8.2	38	1.6
-8	.088	5.9	39	2.4
-9	.096	7.9	43	2.8
-10	.088	5.3	39	2.4
3440-1	0.096	11.8	30	3.2
-2	.080	15.2	32	2.2
-3	.072	16.3	32	1.8
-4	.104	8.0	27	3.8
-5	.080	8.3	25	2.2
-6	.088	14.0	32	2.7
-7	.080	9.0	26	2.2
-8	.096	13.2	32	3.2
-9	.080	8.2	25	2.2
-10	.080	9.4	27	2.7
9983-1	0.097	8.6	40	3.2
-2	.078	6.3	35	2.1
-3	.107	6.9	40	3.9
-4	.087	6.2	36	2.6
-5	.126	7.2	43	5.5
-6	.097	6.1	38	3.2
-7	.078	6.8	35	2.1
-8	.087	7.1	37	2.6
-9	.078	5.3	34	2.1
-10	.136	5.6	43	6.4

APPENDIX B: ORIGINAL EXPERIMENTAL DESIGN

The most important of this experiment's original objectives was to determine the carry over point, the location at which water droplets are entrained by the vapor and literally carried up the bundle. An accurate determination of this point is critical because it will be used as the criterion in determining which heat transfer correlation to use, the inverted annular film boiling theory or the dispersed flow theory.

The experimental apparatus itself, except for the probe (explained below) differed from the first version only in the method of applying heat to the test section. For a general description of the original test section, the reader is referred to Annex 1 to this Appendix.

As previously mentioned in Chapter 1, the test section was modeled after Groeneveld [4], who boiled Freon in a uniformly heated tube, achieving steady stable film boiling with a heat spike. However, it was found that for water, using only one heat spike, film boiling could be maintained only at that heat spike. Unless the DC generator current were increased, increasing the heat flux to the rest of the test section, the tube both upstream and downstream of the heat spike would quench. However, raising the current caused the tube temperature downstream of the heat spike to dangerously increase. No combination of heat fluxes in the heat spike and the rest of the test section was found that maintained stable film boiling (wall temperature at least 800°F above saturation) without overheating the downstream portion of the test section.

Several approaches were taken to try to solve this problem. A workable solution for maintaining steady state stable film boiling was found when six (6) copper block heat spikes were placed at intervals of several inches along the tube. This approach was rather unsophisticated in that the experimenter added an extra block where the test section seemed to preferentially quench, and repeated this trial and error procedure until the test section had six (6) heat spikes placed at somewhat random intervals along the tube. It should be remembered that unlike the final version, the entire test section was heated ohmically by DC current, to include the intervals between the heat spikes. Once the problem of maintaining steady state stable film boiling was solved, an "electrical resistance probe" was used to try to determine the carry over point. The remainder of this appendix discusses the probe, experimental results, and reasons for abandoning this approach in favor of using heat transfer coefficients derived from heat flux and wall temperature measurements.

B.1 The "Electrical Resistance Probe" Concept

It was originally determined that if stable film boiling could be maintained at steady state in some portion of the test section, all the regimes of boiling could be experienced at the same time at different locations of the tube (see Fig.1). We know by many experiments such as FLETCHER [2], that there is indeed a region of continuous liquid and one of liquid droplets dispersed in vapor for certain flow rates and pressures. If the carry-over point is in fact the point at which the liquid is no longer continuous, it was thought that finding this continuous liquid-vapor boundary would be equivalent to determining the carry-over point. Thus, the initial concept of this experiment was to use a "probe" to determine

the height of the liquid column, which was assumed to be stationary given that the coolant flow and wall temperature were steady.

The basic theory behind this probe was as follows: the electrical resistance of distilled water is very great, but much less than the resistance of steam. In an open circuit (see Fig. 27) consisting of a battery, voltmeter, the probe, tube wall, and water of the liquid column, no current can flow across the vapor gap and the meter reads zero volts. But, if the probe is pushed downward into the liquid, the circuit is closed, current flows, and the meter reads the battery's electric potential. The position of the probe's tip could be inferred and this location defined as the carry-over point. This simple theory was tested in a visual test section and appeared to give reliable results, even when air was forced into the section to generate slugs and bubbles to simulate boiling.

Several problems with the probe delayed experimentation. Two of these will be briefly mentioned in this report because they contributed to the ultimate dissatisfaction with this procedure. The entire probe, except for the tip, had to be electrically insulated because the tube could quench downstream of the heated section and the electric circuit completed through any part of the wall to the probe. Also, spacers had to be mounted on the probe near the tip to prevent contact with the tube wall. Extremely high temperatures inside the test section and requirements that the spacers and insulation be non-electrically conducting limited the choice of materials and design. The probe was insulated for the first two feet with flexible Pyrex glass tubing and the rest, where the temperatures were not as great, with Teflon tubing. Non-electrically conducting spacers, which met the demand of high temperature, could not be readily procured. So,

metal spacers were used and electrically insulated from the probe. The problems that developed were cracking of the Pyrex due to thermal stresses, melting of the Teflon, melting of the brass probe, and loss of the spacers. It was felt these problems could not be completely solved in a reasonable amount of time and this contributed to the decision to abandon this approach.

B.2 Initial Data

Although there were questions as to the reliability of the probe under operating conditions, on at least two occasions it worked well enough to enable the experimenter to record two data points. It was the results of these two points more than doubts of probe reliability that demanded the apparatus be redesigned and a new approach taken. The particulars of these two data points are reported in Table II at the end of this appendix.

As indicated earlier in this report, the method of determining the carry-over velocity as a function of length was the following: calculate enthalpy, H(z) from an energy balance

$$\int_{z_1}^{z_2} q'' \pi D dz = \int_{H_1}^{H_2} \dot{m}\, dH \qquad \text{(B-1)}$$

where $z_1 = 0$, the bottom of the test section, z_2 is the height at any level (e.g., the carry-over point) and H_1 and H_2 are the enthalpies at these locations. Next, calculate the quality,

$$X(z) = \frac{H(z) - H_f}{H_{fg}} \qquad \text{(B-2)}$$

Then relate quality to vapor flow rate by

$$V_v = \frac{G_v}{\rho_v} \qquad \text{(B-3)}$$

$$\text{where} \quad G_v = XG \qquad \text{(B-4)}$$

The FLECHT movie summary in Chapter I indicated that a critical U_g of less than 7.5 should probably be used in determining the critical mass flow rate, thus leading to a lower critical vapor velocity for carry-over. In Plummer's Critical mass Criterion [3], however, critical vapor flow rate is a function of $(We)^{1/4}$, but even a We as low as 2 could not by itself account for V_{co} of data point 1 being so low compared to the prediction.

The method for calculating the "experimental" vapor velocities was seen to depend solely on how much of the test section the energy balance included, i.e., on where the carry-over point was determined to be. Representations of the boiling regimes such as Fig. 1 were again studied and it was speculated that entrainment could take place at the top of the liquid column, at the top of the slug flow, or at any place in between (see Fig. 1). Since the determination of the carry-over point was dependent on the probe's completion of the electric circuit, it was again decided to use the probe to take another data point, but to be more aware of the probe indications while trying to find the continuous liquid.

For data point 2, two sets of figures are presented for each quantity. These represent the high and low readings of the height of the liquid column. As the probe was pushed into the tube, slugs of water, which probably filled much of the inside area hit the probe tip causing slight deflections of the voltmeter needle. However, a maximum deflection of the needle (indicating the full potential of the battery) did not occur until the probe reached a particular depth. As the probe was pushed further down-

ward, the needle fluctuated between the maximum and lower readings. Then the voltmeter needle pegged at maximum and did not return to lower values. The probe was withdrawn and reinserted several times and the locations of the "first maximum deflection" and the "continuous maximum deflection" were relatively constant.

4.3 Conclusions from Probe Experiments

These results have led the experimenter to infer that Fig. 28 is representative of what the probe encountered. The "first maximum deflection" indicates the top of the slug flow. The fluctuations between maximum and lower values occur as the probe is pushed downward, the tip passing through large slugs causing maximum deflection of the needle, then large gaps of vapor where the lower values are read. Finally, as the probe is pushed into the liquid column, the voltmeter continuously reads the full potential of the battery.

Data Point 2 has been reduced using both the top of the slug flow and the top of the liquid column as the carry-over point, hence the double entries for V_{co}, X_{co}, q_{co}, and Z_{co}. V_{co} for Data Point 2 was compared with predicted carry-over velocity [3] (see Fig. 29). For the lower carry-over point, the carry-over velocity again falls below that predicted, while the higher carry-over point, the top of the slug flow, yields a carry-over velocity greater than that predicted. It is felt that the results of this method brackated the area of interest, but the error and uncertainty were much too great and could not be accepted. Since the objective of the experimental program, the definition of the carry-over point, could not reliably be accomplished, it was decided to abandon this approach and to try to infer the carry-over point by experimental heat transfer data.

TABLE II

Data Point	1	2
Pressure (Psia)	18	18
Flooding Rate (in/sec)	1	1
Inlet Temperature (°F)	84	172
Height of Liquid to Carry-over Point, Z_{co} (in)	32	51 and 60*
Net heat added to Carry-over Point, q_{co} (Btu/hr)	6400	7500 and 10,500*
Carry-over Quality, X_{co} (%)	13	22 and 32*
Carry-over Velocity, V_{co} (ft/sec)	18	36 and 54*

*Dual entries for Data Point 2 reflect the effects of the high and low carry-over lengths (Z_{co}) inferred from probe measurements.

Annex 1: General Description of Original Experimental Apparatus

The original experimental apparatus differed from the final version only in the manner in which the test section was heated. The reader is referred to Fig. 6, the schematic of the apparatus, which is also applicable to the original design.

There was no preheater used in the initial version. However, the main generators were used to heat the test section. The water-jacketed power cables were clamped to the test section at a distance of 68 inches apart, and the entire test section was heated by resistance induction. In addition to the heat provided by the main generators, six (6) copper block heat spikes were clamped to the test section wall to provide significantly greater local heat fluxes.

The final version differed from the initial design in that the test section of the latter had a uniform heat flux applied, with local heat spikes superimposed at random locations (wherever the tube wall seemed to preferentially quench). The upstream ends of these copper block heat spikes were placed 36, 47, 52.5, 56.5, 60.5, and 65 inches, respectively, from the upstream power clamp. The heat flux applied by these heat spikes was whatever was necessary to maintain the local wall temperatures constant with time.

APPENDIX C EXPERIMENTAL DATA

This appendix contains all experimental data for Data Points 3 through 39, inclusive (DP 1 and 2 are summarized in Table II, Appendix B). The enclosed computer printout of the data is complete except for the heat flux to the 4 ft. preheater and the inlet coolant temperature. These, as well as a general summary of Data Point parameters, are provided in Sec. C.2 below. Sec. C.1 contains the definitions for the column headings used in the data printouts.

C.1 Column Heading Definitions

a. Z - the axial location of the downstream end (top) of each copper block heat spike, i.e., the distance in feet from the downstream end of the preheater.

b. TW- the average wall temperature (°F) of each copper block heat spike.

c. QNET-the net amount of heat (BTU/hr) applied to the tube by each copper block heat spike as computed by eqn. (3-2).

d. HEX-the experimental heat transfer coefficient (BTU/hr-ft^2-°F) as computed by eqn. (3-1).

e. REX-the experimental equilibrium quality (dimensionless) as computed by eqn. (3-6).

f. REX-the experimental vapor film or tube Reynolds Number (Re, dimensionless) as computed by eqn. (2-1) or eqn. (2-3).

g. H/K-EX-the experimental heat transfer coefficient divided by the vapor film thermal conductivity (ft^{-1}). Film properties evaluated as in Sec. 2.2.2.c.

h. H/K-MT-the Modified Turbulent Tube Theory prediction of Sec. 2.3.3 (ft^{-1}). Does not apply to Data Points with low flooding rates (1 in/sec or less).

i. H/K-TT-the Turbulent Tube Theory prediction of Sec. 2.3.2.

j. H/K-LF-the Laminar Film Theory Prediction of Sec. 2.4.1.

k.H/K-TF-the Turbulent Film Theory Prediction of Sec. 2.4.2.

C.2 General Summary of Data Points

DP	Pressure (psia)	Flooding Rate (in/sec)	Inlet Coolant Temperature (°F)	Preheater Heat Flux (BTU/hr)
3	20	1	140	3430
4	21	2	150	5690
5	22	3	172	8540
6	22	3	162	5070
7	21	4	140	7920
8	21	4	148	27,640
9	22	4	155	44,840
10	24	5	162	40,760
11	23	5	158	7950
12	24	6	160	7940
13	25	6	164	22,820
14	27	6	172	41,730
15	26	6	176	7610
16	25	5	175	7980
17	28	5	176	28,050
18	26	5	180	51,730
19	26	4	188	52,340
20	31	1	75	4110
21	36	1	80	9280
22	33	1	125	2850
23	32	1	120	9970
24	39	3	155	10,990
25	26	3	144	610
26	26	3	144	3610
27	41	6	130	6520
28	42	6	147	6490
29	42	6	152	35,840

DP	Pressure (psia)	Flooding Rate (in/sec)	Inlet Coolant Temperature (°F)	Preheater Heat Flux (BTU/hr)
30	66	1	155	560
31	67	1	160	1680
32	67	1	160	5890
33	67	1	160	17,690
34	67	3	145	5150
35	67	3	145	11,790
36	67	3	165	28,570
37	67	6	172	29,110
38	67	6	172	54,490
39	64	6	172	6450

DATA POINT 3 AT 20 PSIA & 1 IN/SEC

Z	Th	QNET	HEX	XEX	REX	H/K-EX	H/K-MT	H/K-TT	H/K-LF	H/K-TF
0.21	858	2774	158.8	0.17	2782.5	6576.4		318.9	354.5	9337.3
0.43	1040	2416	186.8	0.27	3953.4	3879.5		410.8	284.8	5573.1
0.65	995	1172	55.8	0.32	4783.9	2074.4		479.6	272.1	5619.4
0.86	948	1245	62.8	0.37	5713.5	2426.1		553.1	264.4	6453.1
1.08	1065	1456	66.8	0.43	6398.5	2472.5		605.8	245.8	4803.1
1.30	1058	1142	49.8	0.48	6996.3	1781.6		648.2	233.7	4402.8
1.52	1065	865	34.8	0.51	7383.2	1224.2		676.2	228.8	4229.2
1.74	1288	776	32.8	0.55	7929.9	1140.8		713.9	221.4	4036.2
1.96	1278	594	28.8	0.57	7427.4	631.7		676.7	206.8	3437.8
2.18	1388	427	14.8	0.59	7596.8	434.4		688.8	202.8	3314.6

DATA POINT 4 AT 21 PSIA & 2 IN/SEC

Z	Th	QNET	HEX	XEX	REX	H/K-EX	H/K-MT	H/K-TT	H/K-LF	H/K-TF
0.21	858	2748	157.8	0.09	2942.4	6522.7	2231.8	328.1	358.8	9189.7
0.43	1015	2396	128.8	0.14	4142.2	4011.6	2058.3	427.8	286.1	6898.3
0.65	1063	1486	63.8	0.17	4920.8	2267.5	2017.5	488.9	263.6	5275.3
0.86	1048	1552	67.8	0.21	6142.4	2447.9	2036.8	584.4	247.7	4831.6
1.08	1065	1514	65.8	0.24	6948.7	2336.4	2015.9	648.6	234.9	4433.8
1.30	933	1637	77.8	0.27	8303.7	3821.5	2138.6	758.3	237.1	4718.9
1.52	1055	1438	64.8	0.30	8715.2	2315.5	2024.2	772.6	218.8	4029.5
1.74	955	1713	88.8	0.34	10153.3	3212.8	2075.9	875.8	214.5	4015.7
1.96	1218	2284	75.8	0.38	10252.8	2453.3	1896.1	874.3	193.7	3245.7
2.18	1268	1878	64.8	0.42	10953.8	2038.4	1853.5	926.8	184.2	2985.8

DATA POINT 5 AT 22 PSIA & 3 IN/SEC

Z	TW	GNET	HEX	XEX	REX	H/K-EX	H/K-MT	H/K-TT	H/K-LF	H/K-TF
0.21	880	3111	170.0	0.10	4812.9	6904.3	3038.2	481.5	294.1	6544.5
0.43	1080	2693	110.0	0.14	6249.3	4120.6	2862.1	593.7	251.0	4986.7
0.65	1155	1868	66.0	0.16	6525.0	2875.8	2637.8	658.9	236.7	4080.0
0.86	1185	1826	68.0	0.19	7796.6	2256.9	2650.2	781.5	214.8	3765.4
1.08	1180	1836	68.0	0.21	8644.2	2263.0	2656.4	762.2	208.1	3608.9
1.30	1092	2008	83.0	0.24	10279.0	2925.2	2754.5	870.4	203.6	3602.2
1.52	1130	1761	69.0	0.27	11375.3	2371.3	2712.3	951.5	194.8	3332.2
1.74	1185	2139	87.0	0.30	12777.9	3039.5	2739.9	1045.7	188.4	3213.9
1.96	1320	2461	60.0	0.33	12623.8	2086.8	2504.9	1031.8	171.4	2640.6
2.18	1322	2144	70.0	0.36	13760.9	2187.6	2503.2	1105.4	166.4	2527.6

DATA POINT 6 AT 22 PSIA & 3 IN/SEC

Z	TW	GNET	HEX	XEX	REX	H/K-EX	H/K-MT	H/K-TT	H/K-LF	H/K-TF
0.21	880	3396	187.0	0.05	2486.4	7594.7	3038.2	276.6	370.4	10659.4
0.43	1190	2588	96.0	0.08	3272.6	3174.8	2644.0	352.5	286.0	5961.9
0.65	1160	2232	65.0	0.11	4578.3	2865.0	2680.1	468.4	259.8	5038.0
0.86	1245	1943	68.0	0.14	5538.1	2173.7	2578.1	534.0	232.9	4171.3
1.08	1145	3069	120.0	0.18	7538.7	4083.9	2696.1	683.8	221.3	3971.9
1.30	1122	2023	81.0	0.21	8882.4	2798.3	2721.1	780.8	211.3	3752.1
1.52	1115	2235	86.0	0.24	10175.1	2984.7	2728.8	871.2	202.5	3548.4
1.74	1230	2070	74.0	0.27	10777.6	2387.2	2595.7	910.6	188.1	3097.8
1.96	1163	2833	113.0	0.31	13163.7	3501.2	2724.0	1065.7	195.6	3126.9
2.18	1285	2567	87.0	0.35	13578.0	2715.1	2636.3	1095.1	169.6	2625.6

DATA POINT 7 AT 21 PSIA & 4 IN/SEC

Z	Th	QNET	HEX	XEX	REX	H/K=EX	H/K=MT	H/K=TT	H/K=LF	H/K=TF
0.21	1183	4037	165.0	0.03	1787.8	5781.8	3455.3	289.8	369.1	10500.3
0.43	1245	2478	87.0	0.06	3469.4	2785.3	3249.0	342.2	281.0	5764.3
0.65	1255	2345	81.0	0.08	4208.6	2577.5	3234.4	428.8	254.5	4797.4
0.86	1238	1811	64.0	0.10	5304.6	2057.7	3259.3	516.6	237.6	4309.9
1.08	1200	1813	66.0	0.12	6514.9	2172.4	3316.6	608.2	226.6	4850.3
1.30	1267	2049	70.0	0.14	7898.7	2211.4	3217.1	667.4	210.4	3574.1
1.52	1150	2117	78.0	0.16	8740.6	2583.6	3332.1	769.2	206.6	3564.3
1.74	1275	2095	71.0	0.18	9352.3	3232.3	3207.1	813.5	193.0	3163.8
1.96	1173	3207	121.0	0.22	12146.6	4051.2	3358.8	1000.3	186.9	3119.3
2.18	1250	2412	81.0	0.24	12394.9	2524.1	3189.8	1018.4	174.7	2740.6

DATA POINT 8 AT 21 PSIA & 4 IN/SEC

Z	Th	QNET	HEX	XEX	REX	H/K=EX	H/K=MT	H/K=TT	H/K=LF	H/K=TF
0.21	1183	4854	165.0	0.25	14224.9	5781.8	3455.3	1139.8	182.2	3064.9
0.43	1245	2488	87.0	0.27	14262.2	2785.3	3249.0	1139.8	170.3	2671.8
0.65	1258	2416	84.0	0.30	15799.4	2681.1	3241.6	1237.3	164.1	2530.8
0.86	1278	1768	62.0	0.32	16603.4	1882.1	3203.7	1287.6	159.2	2405.0
1.08	1216	1836	66.0	0.34	18278.4	2152.3	3292.2	1388.9	159.3	2448.1
1.30	1275	2110	76.0	0.36	18780.6	2263.7	3207.1	1416.3	153.2	2280.1
1.52	1202	2093	77.2	0.38	20630.6	2534.5	3316.6	1529.4	154.3	2353.6
1.74	1312	2112	74.0	0.40	20499.9	2155.8	3167.1	1521.7	146.6	2128.3
1.96	1187	2822	103.0	0.43	23534.1	3484.5	3336.8	1698.6	148.8	2246.4
2.18	1298	2445	81.0	0.46	23683.7	2512.2	3180.7	1709.0	140.4	2004.6

DATA POINT 9 AT 22 PSIA & 4 IN/SEC

Z	TW	QNET	HEX	XEX	REX	H/K-EX	H/K-MT	H/K-TT	H/K-LF	H/K-TF
0.21	1085	4035	168.0	0.43	24629.1	5948.3	3477.3	1778.2	152.6	2481.8
0.43	1235	2585	89.0	0.46	24488.5	2862.3	3260.0	1751.5	142.9	2092.8
0.65	1237	2441	86.0	0.48	25439.0	2762.5	3257.0	1810.6	140.8	2049.6
0.86	1255	1843	64.0	0.50	26214.5	2033.5	3230.7	1855.6	138.1	1984.6
1.08	1215	1836	66.0	0.52	27929.4	2148.9	3289.9	1949.8	138.1	2010.8
1.30	1273	2122	72.0	0.55	28564.8	2263.0	3206.5	1987.6	133.0	1876.2
1.52	1192	2101	77.0	0.57	31851.2	2543.2	3325.1	2120.8	135.1	1965.0
1.74	1255	2121	71.0	0.59	30382.7	2202.7	3181.3	2085.8	129.2	1790.9
1.96	1160	2773	106.0	0.62	34486.8	3572.8	3373.7	2301.5	132.7	1940.0
2.18	1323	2512	82.0	0.65	33115.5	2502.6	3149.8	2231.6	124.2	1682.9

DATA POINT 10 AT 24 PSIA & 5 IN/SEC

Z	TW	QNET	HEX	XEX	REX	H/K-EX	H/K-MT	H/K-TT	H/K-LF	H/K-TF
0.21	785	3508	266.0	0.29	25817.8	12242.3	5004.4	1858.9	196.6	4094.9
0.43	1330	3099	101.0	0.32	20288.1	3061.7	3752.7	1588.2	154.1	2336.6
0.65	1380	2291	76.0	0.34	21804.1	2344.3	3792.6	1600.8	152.2	2318.3
0.86	1367	2322	73.0	0.36	22508.3	2166.4	3704.7	1636.0	146.8	2159.5
1.08	1328	2289	75.0	0.38	24118.4	2276.1	3755.3	1731.7	145.6	2162.0
1.30	1360	2330	75.0	0.40	25264.3	2260.5	3739.6	1796.7	142.7	2095.3
1.52	1298	2559	88.0	0.42	27238.2	2730.5	3806.1	1901.4	142.3	2120.0
1.74	1365	2616	81.0	0.44	27326.2	2378.4	3681.2	1908.8	136.7	1947.4
1.96	1216	3357	124.0	0.47	31559.8	4038.0	3934.2	2151.6	140.5	2139.2

DATA POINT 11 AT 23 PSIA & 5 IN/SEC

Z	Tw	QNET	HEX	XEX	REX	H/K-EX	H/K-MT	H/K-TT	H/K-LF	H/K-TF
-	--	----	---	---	---	------	------	------	------	------
										23640.1
0.21	768	3329	226.0	0.01	855.2	10005.0	4850.6	121.8		7040.0
0.43	1370	3036	95.0	0.04	2502.3	2818.2	3703.8	282.0		5302.0
0.65	1335	2424	78.0	0.06	3800.2	2360.9	3749.2	394.9	269.0	4355.7
0.86	1355	2344	72.0	0.08	4954.4	2104.7	3671.3	486.7	240.7	3983.5
1.08	1357	2330	74.0	0.10	6281.4	2211.8	3720.7	589.7	225.6	3613.9
1.30	1372	2335	73.0	0.12	7493.4	2163.0	3701.2	678.7	211.5	3508.3
1.52	1308	2657	88.0	0.14	8958.8	2705.6	3785.0	785.2	204.3	3058.0
1.74	1425	2670	79.0	0.16	9799.9	2269.5	3633.3	838.7	189.6	2969.2
1.96	1348	3419	109.0	0.19	11975.1	3274.7	3732.3	988.5	182.6	

DATA POINT 12 AT 24 PSIA & 6 IN/SEC

Z	Tw	QNET	HEX	XEX	REX	H/K-EX	H/K-MT	H/K-TT	H/K-LF	H/K-TF
-	--	----	---	---	---	------	------	------	------	------
					1.0	7888.8	0.5	0.5	8294.5	-138933.7
0.21	860	3361	192.0	0.00	1473.0	2968.6	4212.0	184.2	357.1	9466.9
0.43	1417	3424	103.0	0.02	2953.6	2438.8	4222.2	321.5	284.8	5876.6
0.65	1410	2793	64.0	0.04	4368.4	2137.0	4150.6	437.2	245.0	4425.9
0.86	1460	2611	76.0	0.06	5168.8	2257.2	4222.2	583.1	235.7	4197.8
1.08	1410	2594	78.0	0.07	6577.9	2192.7	4181.8	689.2	215.3	3636.8
1.30	1438	2681	77.0	0.09	8268.5	2708.6	4294.0	734.5	205.3	3471.2
1.52	1362	2898	91.0	0.11	10169.3	2425.5	4157.6	862.5	185.0	2928.0
1.74	1455	2948	86.0	0.14	12058.5	3526.2	4304.4	993.6	181.5	2934.0
1.96	1355	3724	118.0	0.16						

DATA POINT 13 AT 25 PSIA & 6 IN/SEC

Z	TW	QNET	HEX	XEX	REX	H/K-EX	H/K-MT	H/K-TT	H/K-LF	H/K-TF
0.21	900	3401	183.0	0.10	9445.1	7296.5	5218.9	827.2	244.6	5145.5
0.43	1417	3420	103.0	0.12	8830.9	2964.8	4208.8	771.8	196.4	3210.8
0.65	1483	2761	84.0	0.14	10385.9	2437.6	4229.2	877.3	187.3	3021.5
0.86	1468	2652	77.0	0.16	11540.9	2153.2	4133.9	954.2	176.2	2724.5
1.08	1422	2625	79.0	0.18	13222.1	2267.5	4201.5	1065.7	171.4	2646.9
1.30	1458	2643	77.0	0.20	14542.2	2175.1	4161.6	1148.4	164.4	2470.8
1.52	1375	2542	92.0	0.22	16443.3	2713.8	4270.9	1271.9	162.3	2477.2
1.74	1465	2963	86.0	0.24	17339.8	2408.9	4139.0	1321.5	154.1	2242.8
1.96	1330	3751	122.0	0.26	19764.2	3693.5	4338.6	1476.8	155.3	2359.1

DATA POINT 14 AT 27 PSIA & 6 IN/SEC

Z	TW	QNET	HEX	XEX	REX	H/K-EX	H/K-MT	H/K-TT	H/K-LF	H/K-TF
0.21	985	3401	182.0	0.24	22522.6	7211.1	5193.2	1658.1	181.9	3380.3
0.43	1410	3439	105.0	0.26	19152.6	3027.1	4212.7	1434.0	151.8	2228.6
0.65	1452	2818	87.0	0.28	19888.7	2394.9	4086.5	1476.0	144.8	2039.1
0.86	1455	2651	78.0	0.30	21742.0	2191.8	4148.5	1583.4	143.2	2025.8
1.08	1415	2634	80.0	0.32	23529.2	2299.7	4205.5	1698.2	141.5	2018.0
1.30	1432	2668	80.0	0.33	24114.3	2277.5	4181.0	1722.2	139.5	1967.9
1.52	1365	2549	53.0	0.35	26215.4	2752.6	4279.5	1847.8	139.1	2002.6
1.74	1462	2963	86.0	0.37	26742.5	2408.9	4140.1	1868.9	133.3	1834.3
1.96	1345	3734	120.0	0.46	36185.8	3533.1	4309.6	2070.5	133.8	1911.2

DATA POINT 15 AT 26 PSIA & 6 IN/SEC

Z	Th	QNET	HEX	AEX	REX	H/K-EX	H/K-MT	H/K-TT	H/K-LF	H/K-TF
0.21	880	3481	186.0	0.01	949.7	7455.4	5240.7	131.6	528.0	19284.3
0.43	1400	3449	106.0	0.03	2219.8	3077.4	4230.4	258.3	312.8	7944.4
0.65	1393	2691	86.0	0.05	3709.2	2506.9	4240.7	386.0	264.3	6093.2
0.86	1452	2652	77.0	0.07	5082.0	2169.9	4155.6	495.1	232.8	4975.6
1.08	1410	2627	80.0	0.09	6634.8	2309.1	4215.7	614.1	216.4	3685.9
1.30	1448	2626	78.0	0.10	7291.6	2213.1	4172.6	661.3	207.4	3438.5
1.52	1350	2942	94.0	0.12	9045.8	2809.9	4305.2	789.5	199.6	3346.9
1.74	1458	2971	87.0	0.14	10141.5	2443.5	4147.1	860.3	184.6	2910.3
1.96	1385	3731	116.0	0.17	12648.6	3397.3	4252.6	1030.4	176.2	2781.4

DATA POINT 16 AT 25 PSIA & 5 IN/SEC

Z	Th	QNET	HEX	XEX	HEX	H/K-EX	H/K-MT	H/K-TT	H/K-LF	H/K-TF
0.21	880	3481	188.0	0.03	2394.6	7598.8	4559.3	276.8	391.2	11933.0
0.43	1385	3459	107.0	0.06	3723.2	3137.8	3678.3	387.4	268.1	8127.8
0.65	1375	2810	88.0	0.08	4982.8	2595.8	3691.3	489.4	241.8	4391.5
0.88	1442	2662	78.0	0.10	6076.9	2213.3	3606.5	571.6	220.4	3759.9
1.08	1410	2627	80.0	0.12	7378.8	2312.1	3646.4	668.7	209.1	3511.5
1.30	1460	2633	77.0	0.15	9088.9	2175.1	3596.7	788.5	192.2	3085.7
1.52	1342	2960	95.0	0.17	10720.2	2856.4	3734.1	904.8	189.5	3128.9
1.74	1455	2963	86.2	0.20	12056.5	2422.5	3590.7	990.8	174.4	2692.7
1.96	1365	3724	117.0	0.23	14373.1	3471.7	3704.4	1143.1	170.3	2663.6

DATA POINT 17 AT 28 PSIA & 5 IN/SEC

Z	Th	QNET	HEX	XEX	REX	H/K-EX	H/K-MT	H/K-TT	H/K-LF	H/K-TF
0.21	895	3401	186.0	-	15832.5	7409.1	4617.0	1222.8	227.2	4762.2
0.43	1375	3442	108.0	[illegible]	14197.8	3173.8	3739.2	1113.4	186.2	3074.6
0.65	1363	2793	89.6	0.25	16156.6	2630.9	3782.6	1237.9	177.9	2909.8
0.86	1435	2644	79.2	0.27	17030.2	2242.5	3661.1	1284.4	178.3	2679.4
1.08	1415	2617	88.2	0.29	18430.8	2297.2	3686.7	1369.5	167.2	2623.8
1.30	1445	2633	78.8	0.31	19479.7	2201.6	3648.5	1429.6	162.2	2493.8
1.52	1335	2982	96.2	0.34	22371.2	2887.5	3798.6	1602.5	162.1	2571.6
1.74	1457	2955	86.2	0.36	22528.1	2411.1	3633.5	1604.6	153.9	2308.0
1.96	1330	3734	122.2	0.40	26398.1	3680.2	3806.3	1829.2	153.8	2395.6

DATA POINT 18 AT 26 PSIA & 5 IN/SEC

Z	Th	QNET	HEX	XEX	REX	H/K-EX	H/K-MT	H/K-TT	H/K-LF	H/K-TF
0.21	880	3401	189.0	0.40	31878.1	7627.6	4553.9	2187.9	164.9	2991.2
0.43	1378	3459	109.0	0.43	26810.3	3226.5	3694.9	1881.0	138.0	1979.0
0.65	1368	2821	88.2	0.45	28078.3	2603.2	3697.5	1952.0	136.0	1941.5
0.86	1438	2679	79.2	0.48	29187.8	2241.0	3608.7	2006.1	130.8	1808.6
1.08	1415	2627	88.2	0.50	30660.4	2302.5	3637.3	2089.1	129.7	1794.3
1.30	1447	2641	78.2	0.52	31516.9	2204.3	3597.7	2132.2	127.8	1727.0
1.52	1332	2968	96.2	0.55	34785.2	2899.3	3744.2	2320.9	128.4	1818.7
1.74	1460	2963	86.2	0.57	34372.8	2412.7	3581.3	2284.2	122.8	1643.8
1.96	1345	3734	126.2	0.60	37761.8	3597.3	3727.4	2477.8	124.3	1735.1

DATA POINT 19 AT 26 PSIA & 4 IN/SEC

Z	Th	QNET	HEX	XEX	REX	H/K-EX	H/K-MT	H/K-TT	H/K-LF	H/K-TF
0.21	885	3401	188.0	0.53	33672.2	7561.3	3799.1	2286.1	161.4	2921.7
0.43	1355	3469	110.0	0.87	28591.3	3278.9	3107.2	1981.5	135.8	1946.9
0.65	1355	2828	90.0	0.60	30096.1	2682.7	3107.2	2064.9	133.5	1582.7
0.86	1425	2654	82.0	0.63	30792.7	2289.3	3032.2	2095.2	129.1	1776.6
1.08	1418	2627	79.0	0.66	32377.3	2273.7	3042.4	2182.2	127.4	1771.7
1.30	1432	2668	79.0	0.68	33151.8	2251.7	3024.9	2221.9	125.6	1739.3
1.52	1315	2979	98.0	0.72	30665.3	2988.9	3150.8	2422.6	127.0	1802.8
1.74	1457	2971	87.0	0.75	35234.3	2444.8	2999.3	2382.7	120.8	1610.2
1.96	1355	3714	118.0	0.79	39626.6	3517.4	3107.2	2573.2	121.8	1684.6

DATA POINT 20 AT 31 PSIA & 1 IN/SEC

Z	Th	QNET	HEX	XEX	REX	H/K-EX	H/K-MT	H/K-TT	H/K-LF	H/K-TF
0.21	1315	1181	39.0	0.04	530.9	1182.6		80.3	567.1	20010.8
0.43	1559	722	20.0	0.07	843.6	531.9		115.6	442.2	12939.4
0.65	1607	511	13.0	0.09	1031.1	345.2		138.7	397.1	10936.1
0.86	1572	304	8.0	0.10	1181.4	212.6		152.6	389.0	10672.9
1.08	1587	582	16.0	0.13	1556.7	420.4		189.2	358.7	9541.1
1.30	1410	1431	44.0	0.19	2414.3	1262.7		269.4	328.5	8173.4
1.52	1162	1944	76.0	0.27	3872.6	2527.4		394.1	314.8	7147.5
1.74	1245	1880	67.0	0.35	4847.4	2117.1		469.9	382.0	5850.6
1.96	1317	2111	78.0	0.44	5832.8	2120.2		546.4	255.0	4930.6
2.18	957	1758	86.0	0.52	8133.8	3186.6		716.7	267.0	5773.8

DATA POINT 21 AT 36 PSIA & 1 IN/SEC

Z	Th	QNET	HEX	XEX	REX	H/K-EX	H/K-MT	H/K-TT	H/K-LF	H/K-TF
0.21	1327	1101	37.0	0.25	3277.0	1108.7		344.8	321.5	7411.1
0.43	1455	452	13.0	0.27	3362.2	361.9		358.5	302.9	6554.9
0.65	1560	388	11.2	0.23	3436.1	292.9		358.4	287.2	5917.9
0.86	1575	346	9.2	0.30	3507.6	239.1		366.4	288.2	5747.8
1.08	1592	306	8.2	0.32	3686.2	212.5		383.6	274.3	5475.2
1.30	1620	323	8.2	0.33	3711.1	212.3		389.7	268.4	5298.5
1.52	1625	332	5.2	0.34	3872.9	238.5		401.8	247.4	5245.2
1.74	1675	343	9.2	0.36	3913.3	229.7		406.3	256.1	4844.2
1.96	1585	388	18.2	0.38	4004.2	265.6		441.2	259.7	4975.7
2.18	1037	2814	92.2	0.46	6960.7	3301.8		634.4	286.9	6492.7

DATA POINT 22 AT 33 PSIA & 1 IN/SEC

Z	Th	QNET	HEX	XEX	REX	H/K-EX	H/K-MT	H/K-TT	H/K-LF	H/K-TF
0.21	942	2739	142.0	0.10	1621.0	5448.2		197.5	496.2	18553.4
0.43	972	2628	130.0	0.21	3334.1	4887.0		351.8	383.0	18580.9
0.65	1335	2879	55.0	0.33	4318.3	2842.1		430.6	293.1	6257.9
0.86	1365	1695	54.0	0.41	5293.1	1587.4		505.8	278.3	5460.8
1.08	1408	528	29.2	0.45	5732.0	835.3		538.4	259.7	5093.9
1.30	1455	632	18.0	0.47	5777.7	491.6		539.8	249.9	4782.6
1.52	1488	455	13.2	0.49	6057.0	358.2		560.9	247.4	4646.7
1.74	1565	283	6.2	0.56	6124.0	163.2		565.3	244.2	4531.0
1.96	1522	417	12.0	0.52	6329.6	323.2		580.2	240.8	4398.4
2.18	1458	796	23.2	0.55	6773.6	629.8		613.1	237.5	4362.1

DATA POINT 23 AT 28 PSIA & 1 IN/SEC

Z	Th	QNET	HEX	XEX	REX	H/K-EX	H/K-MT	H/K-TT	H/K-LF	H/K-TF
0.21	1285	1316	45.8	0.34	4690.7	1387.1		458.6	280.7	5764.5
0.43	1382	973	24.8	0.37	4748.8	699.3		463.3	264.8	5158.8
0.65	1595	897	24.8	0.41	4739.8	637.5		468.8	248.6	4309.5
0.86	1587	333	9.8	0.42	4888.7	239.1		478.4	239.5	4273.1
1.08	1582	306	8.8	0.44	5144.1	212.6		497.3	236.3	4181.1
1.30	1550	303	8.8	0.45	5413.7	212.7		511.8	237.7	4207.2
1.52	1510	257	7.8	0.46	5627.5	189.8		527.8	238.5	4258.3
1.74	1532	185	3.8	0.47	5783.9	80.4		533.1	235.5	4157.4
1.95	1517	362	10.8	0.48	5857.2	270.1		544.8	234.7	4149.8
2.18	1225	1346	49.2	0.64	7535.6	1565.4		669.2	246.3	4756.5

DATA POINT 24 AT 29 PSIA & 3 IN/SEC

Z	Th	QNET	HEX	XEX	REX	H/K-EX	H/K-MT	H/K-TT	H/K-LF	H/K-TF
0.21	1198	3662	138.8	0.11	4684.6	4520.2	2679.9	458.4	252.6	6286.3
0.43	1178	2819	108.8	0.15	6442.7	3582.1	2700.8	592.1	265.4	5432.6
0.65	1347	3471	112.8	0.20	7830.1	3342.0	2509.0	692.4	228.1	4164.2
0.86	1417	2664	81.8	0.24	9138.0	2320.4	2446.5	781.1	218.8	3652.6
1.08	1322	2356	78.8	0.27	10729.9	2360.9	2836.5	889.9	208.2	3695.2
1.30	1352	2398	77.8	0.30	11711.4	2291.1	2503.7	955.6	199.8	3439.4
1.52	1300	2398	80.8	0.34	13693.4	2452.5	2561.3	1080.5	194.2	3355.6
1.74	1262	1981	69.8	0.36	14843.4	2163.2	2605.5	1150.6	193.1	3356.3
1.96	1152	2344	92.2	0.49	17314.1	3086.4	3719.9	1306.8	192.4	3450.4
2.14	1262	2191	77.2	0.43	17729.7	2414.2	2605.5	1326.4	182.8	3082.2

DATA POINT 25 AT 25 PSIA & 3 IN/SEC

Z	TW	QNET	HEX	XEX	REX	H/K-EX	H/K-MT	H/K-TT	H/K-LF	H/K-TF
0.21	980	3035	146.0	2.00	1.0	5509.3	0.5	0.5	4913.8	-118483.2
0.43	1022	2303	106.0	0.00	1.0	3889.0	0.5	0.5	4819.2	-117233.4
0.65	1285	3122	106.0	0.02	772.7	3290.1	2529.8	110.6	464.5	14282.4
0.86	1385	2368	73.0	0.06	2232.1	2137.9	2442.5	257.2	313.9	8020.6
1.08	1420	2611	80.0	0.10	3699.6	2322.5	2429.7	385.1	263.8	5072.5
1.30	1385	2654	82.0	0.13	4836.2	2401.5	2442.5	477.5	242.7	4414.1
1.52	1337	2657	86.0	0.17	5438.9	2589.9	2483.9	601.8	224.7	3970.2
1.74	1290	2013	68.0	0.20	7712.0	2104.4	2525.3	696.9	215.5	3787.9
1.96	1172	2495	95.0	0.23	9460.5	3159.2	2656.9	819.9	213.7	3879.7
2.18	1147	1856	73.0	0.26	10838.7	2466.6	2686.0	914.3	206.3	3744.1

DATA POINT 26 AT 26 PSIA & 3 IN/SEC

Z	TW	QNET	HEX	XEX	REX	H/K-EX	H/K-MT	H/K-TT	H/K-LF	H/K-TF
0.21	1000	3041	142.0	0.00	1.0	5286.5	0.5	0.5	4868.3	-117922.6
0.43	1052	2533	111.0	0.02	868.1	3993.3	2790.5	122.0	499.5	16878.5
0.65	1330	3434	112.0	0.08	3038.1	3386.5	2489.9	330.1	289.3	6193.3
0.86	1452	2594	76.0	0.14	3993.0	2141.7	2386.8	408.2	252.3	4602.3
1.08	1482	2656	82.0	0.15	5362.2	2272.4	2358.6	517.0	225.5	3858.7
1.30	1457	2912	85.0	0.19	6884.5	2383.6	2382.7	631.1	210.0	3487.0
1.52	1392	2872	88.0	0.23	8534.2	2566.7	2436.5	751.9	200.3	3320.5
1.74	1255	2168	73.0	0.26	10026.4	2252.5	2520.8	858.1	197.2	3347.6
1.96	1242	2726	101.0	0.30	12113.1	3296.2	2620.0	1000.0	193.5	3351.4
2.18	1150	1589	78.0	0.33	13739.6	2630.4	2682.9	1105.1	190.9	3328.4

DATA POINT 27 AT 41 PSIA & 6 IN/SEC

Z	TH	QNET	HEX	XEX	REX	H/K-EX	H/K-MT	H/K-TT	H/K-LF	H/K-TF
0.21	845	4487	276.0	0.00	1.0	11158.8	0.5	0.5	6328.6-243655.7	
0.43	980	4162	207.0	0.00	1.0	7644.7	0.5	0.5	5879.2-215981.8	
0.65	1265	3697	129.0	0.00	1.0	3930.4	0.5	0.5	5066.8-169985.9	
0.86	1372	2654	85.0	0.00	1.0	2462.7	0.5	0.5	4865.1-156573.9	
1.08	1325	2361	79.0	0.02	1867.6	2352.8	4369.9	191.1	428.0	13643.8
1.30	1362	2489	78.0	0.03	2314.9	2273.0	4318.4	260.7	370.2	10677.9
1.52	1385	2647	91.0	0.05	3966.0	2740.8	4408.1	401.3	317.5	7279.3
1.74	1275	2958	104.0	0.07	5654.5	3187.1	4466.0	532.0	286.0	6193.2
1.96	1337	2934	97.0	0.10	7791.4	2868.5	4369.1	689.0	249.5	4973.4
2.18	1270	2858	91.0	0.11	8913.0	2796.9	4476.8	765.7	247.1	4996.1

DATA POINT 28 AT 42 PSIA & 6 IN/SEC

Z	TH	QNET	HEX	XEX	REX	H/K-EX	H/K-MT	H/K-TT	H/K-LF	H/K-TF
0.21	810	4502	296.0	0.00	1.0	12249.8	0.5	0.5	6458.7-263468.4	
0.43	1265	3264	116.0	0.00	1.0	3572.6	0.5	0.5	5116.9-174504.4	
0.65	1380	3011	104.0	0.00	1.0	3138.8	0.5	0.5	5028.8-165796.8	
0.86	1405	2614	82.0	0.01	758.7	2329.3	4243.7	186.6	527.5	18147.3
1.08	1425	2609	80.0	0.03	2258.9	2246.9	4214.5	254.9	364.8	10533.4
1.30	1455	2641	79.0	0.04	2978.4	2182.1	4171.7	317.7	328.2	7716.6
1.52	1457	2559	88.0	0.06	4464.3	2426.0	4168.9	439.1	286.6	5971.6
1.74	1350	3089	98.0	0.09	6867.0	2807.7	4265.9	621.4	254.7	5047.2
1.96	1417	3011	93.0	0.11	8307.7	2623.8	4226.1	722.9	236.6	4598.8
2.18	1350	2968	94.0	0.13	9919.0	2693.1	4265.9	834.0	225.4	4247.9

DATA POINT 29 AT 42 PSIA & 6 IN/SEC

Z	Th	QNET	HEX	XEX	REX	H/K-EX	H/K-MT	H/K-TT	H/K-LF	H/K-TF
0.21	812	4511	295.0	0.16	16564.4	12191.2	5502.2	1278.1	253.7	6884.9
0.43	1315	3345	113.0	0.18	14180.0	3381.3	4086.1	1112.5	206.4	3820.2
0.65	1357	3095	101.0	0.20	15453.9	2949.4	4315.8	1198.9	196.9	3528.2
0.86	1435	2666	81.0	0.22	16503.6	2262.3	4200.2	1258.8	187.8	3285.8
1.08	1432	2612	80.0	0.24	18024.2	2238.1	4284.5	1342.4	181.8	3088.8
1.30	1452	2549	76.0	0.26	19381.1	2102.7	4176.8	1421.5	176.1	2929.1
1.52	1620	3143	89.0	0.28	20357.7	2373.1	4082.6	1474.6	169.8	2711.7
1.74	1425	3581	110.0	0.30	22589.4	3089.6	4214.5	1606.6	169.1	2787.7
1.96	1475	3611	103.0	0.33	24390.7	2813.5	4143.8	1706.9	161.8	2584.8
2.18	1487	3817	94.0	0.35	26533.6	2667.1	4240.8	1831.8	161.4	2627.8

DATA POINT 30 AT 66 PSIA & 1 IN/SEC

Z	Th	QNET	HEX	XEX	REX	H/K-EX	H/K-MT	H/K-TT	H/K-LF	H/K-TF
0.21	935	3953	228.0	0.04	632.3	8174.7		93.8	814.9	42379.8
0.43	882	1548	109.0	0.11	1873.3	4433.9		223.3	618.8	29083.3
0.65	1450	2320	71.0	0.21	2583.3	1930.4		283.2	401.1	11811.6
0.86	1567	1687	47.0	0.28	3189.3	1199.4		338.3	358.1	8815.9
1.08	1760	856	21.0	0.32	3310.2	485.7		358.5	317.1	7264.5
1.30	1762	541	13.0	0.35	3618.2	300.4		376.3	307.7	6853.8
1.52	1697	346	9.0	0.36	3800.4	214.7		392.3	309.2	6959.5
1.74	1725	337	8.0	0.38	3973.8	188.2		406.2	321.8	6645.1
1.96	1737	1242	31.0	0.43	4479.9	725.0		446.9	288.8	6169.3
2.18	1352	2367	58.0	0.54	6891.1	1297.5		623.7	302.3	7023.6

DATA POINT 31 AT 67 PSIA & 1 IN/SEC

Z	TH	QNET	HEX	XEX	REX	H/K-EX	H/K-MT	H/K-TT	H/K-LF	H/K-TF
0.21	955	3878	269.8	0.09	1482.3	7658.4		176.8	616.9	27845.8
0.43	1038	1998	94.8	0.18	2657.4	3241.3		293.1	474.8	16528.9
0.65	1437	2448	76.8	0.29	3583.8	2879.9		368.2	361.3	9319.4
0.86	1377	1988	62.3	0.37	4675.3	1764.4		456.8	338.2	8338.4
1.08	1642	1638	48.8	0.44	4768.7	980.8		469.9	293.5	6412.7
1.30	1692	688	17.8	0.47	4971.2	486.4		480.3	283.2	6009.6
1.52	1690	488	12.8	0.49	5187.7	287.1		503.2	279.4	5886.4
1.74	1757	458	11.8	0.51	5278.8	254.6		509.1	271.6	5561.6
1.96	1742	2458	58.8	0.60	6239.3	1166.8		582.3	258.1	5164.1
2.18	1842	2258	64.8	0.70	8148.9	1654.5		713.1	260.6	5463.4

DATA POINT 32 AT 67 PSIA & 1 IN/SEC

Z	TH	QNET	HEX	XEX	REX	H/K-EX	H/K-MT	H/K-TT	H/K-LF	H/K-TF
0.21	988	3878	282.8	0.28	4288.4	7281.8		439.6	418.7	12850.2
0.43	1142	2428	182.8	0.38	5386.1	3318.1		513.4	369.7	9781.6
0.65	1437	2488	77.8	0.49	6854.4	2107.3		660.2	283.4	6979.2
0.86	1377	1888	62.8	0.58	7328.9	1764.4		654.5	291.2	6671.7
1.08	1642	1388	36.8	0.64	6936.2	882.7		634.1	259.1	5386.1
1.30	1685	678	17.2	0.67	7110.6	487.8		647.4	252.1	5053.4
1.52	1642	858	14.8	0.69	7405.1	339.8		668.5	251.3	5054.8
1.74	1687	832	13.8	0.72	7633.8	311.5		685.3	246.8	4877.4
1.96	1557	2268	62.8	0.82	9057.7	1056.3		786.7	241.7	4803.7
2.18	1775	1442	35.2	0.88	9058.1	883.2		783.6	225.6	4238.1

DATA POINT 33 AT 67 PSIA & 1 IN/SEC

Z	TW	QNET	HEX	XEX	REX	H/K-EX	H/K-MT	H/K-TT	H/K-LF	H/K-TF
								809.2	256.8	5413.3
0.21	1479	3670	110.0	0.79	9612.8	2942.7		734.4	224.4	4181.4
0.43	1574	1870	24.0	0.84	8330.7	525.7		826.9	225.3	4291.4
0.65	1712	1600	40.0	0.92	9657.1	946.7		808.9	217.2	3943.8
0.86	1858	780	18.0	0.94	9457.4	398.7		824.9	214.1	3847.0
1.08	1878	540	12.0	0.97	9700.8	263.3		845.2	215.9	3948.8
1.30	1812	380	9.0	0.98	9973.8	202.9		868.0	218.2	4071.9
1.52	1747	340	8.0	0.99	10278.9	186.1		870.5	218.7	4094.5
1.74	1737	350	8.2	0.99	10310.9	187.0				

DATA POINT 34 AT 67 PSIA & 3 IN/SEC

Z	TW	QNET	HEX	XEX	REX	H/K-EX	H/K-MT	H/K-TT	H/K-LF	H/K-TF
0.21	972	3860	171.0	0.00	1.0	6196.5	0.5	0.5	6816.1	-284343.1
0.43	1327	2610	92.0	0.00	1.0	2679.1	0.5	0.5	5749.1	-216617.0
0.65	1352	2930	82.0	0.03	1148.1	2363.6	2468.2	148.7	545.0	20794.7
0.86	1325	2300	93.0	0.07	2706.7	2711.3	2481.8	295.7	413.9	13489.6
1.08	1315	2650	104.0	0.11	4269.9	3049.8	2490.7	426.0	357.0	9272.0
1.30	1315	2960	93.0	0.15	5822.6	2727.2	2490.7	546.0	322.0	7862.9
1.52	1342	2680	78.0	0.18	6914.9	2251.7	2466.9	625.7	300.9	7061.5
1.74	1327	2440	103.0	0.23	8955.7	3034.7	2497.8	778.8	279.9	6435.5
1.96	1252	2680	97.0	0.26	10448.4	2949.4	2558.1	870.7	273.5	6339.2
2.18	1160	3340	126.0	0.31	13082.0	4051.4	2661.7	1042.9	265.6	6234.9

DATA POINT 35 AT 67 PSIA & 3 IN/SEC

Z	Th	QNET	HEX	XEX	REX	H/K-IX	H/K-MT	H/K-TT	H/K-LF	H/K-TF
0.21	987	3590	185.0	0.06	2743.8	6638.8	2860.6	301.3	483.7	17120.7
0.43	1370	2940	97.0	0.10	3830.8	2755.7	2442.9	387.2	363.3	9483.6
0.65	1485	2620	84.0	0.14	5251.5	2339.8	2413.5	800.7	321.9	7701.4
0.86	1377	2980	98.0	0.18	6823.4	2773.0	2436.9	618.1	298.2	6905.9
1.08	1380	3250	106.0	0.23	8708.9	2994.3	2434.4	951.2	274.6	6138.6
1.30	1380	2520	96.0	0.27	10223.5	2711.8	2434.4	854.1	260.3	5701.2
1.52	1412	2650	81.0	0.31	11598.1	2247.5	2407.7	943.4	246.6	5238.6
1.74	1355	3340	112.0	0.36	13761.2	3209.1	2455.7	1084.5	238.1	5043.6
1.96	1315	2560	103.0	0.40	15526.9	3020.5	2490.7	1196.6	232.3	4919.2
2.18	1175	3610	146.0	0.46	19290.2	4649.6	2645.8	1421.5	231.9	5101.9

DATA POINT 36 AT 67 PSIA & 3 IN/SEC

Z	Th	QNET	HEX	XEX	REX	H/K-EX	H/K-MT	H/K-TT	H/K-LF	H/K-TF
0.21	1032	3570	173.0	0.32	14291.2	6032.8	2803.8	1126.9	272.9	6747.3
0.43	1352	2860	93.0	0.37	13946.9	2609.4	2424.4	1094.4	233.7	4868.3
0.65	1438	2560	88.0	0.40	14865.5	2197.8	2392.9	1149.6	225.3	4567.8
0.86	1256	1820	67.0	0.43	17248.4	2033.7	2554.6	1300.5	231.1	4981.2
1.08	1477	2520	76.0	0.47	17168.0	2035.3	2354.8	1287.1	211.2	4103.6
1.30	1462	2340	75.0	0.50	18776.6	2092.6	2416.1	1387.7	210.9	4179.6
1.52	1382	2550	84.0	0.54	20431.7	2378.2	2432.7	1486.8	206.6	4083.6
1.74	1417	2730	86.0	0.58	21639.2	2379.6	2403.5	1574.5	199.9	3861.3
1.96	1385	2550	96.0	0.62	23432.1	2704.2	2430.2	1657.9	197.1	3822.6
2.18	1242	3360	124.0	0.67	27085.7	3792.2	2569.7	1865.3	200.3	4077.3

DATA POINT 37 AT 67 PSIA & 6 IN/SEC

Z	TH	QNET	HEX	XEX	REX	H/K-EX	H/K-MT	H/K-TT	H/K-LF	H/K-TF
-	--	----	---	--	---	------	------	------	------	------
0.21	1087	4280	193.0	0.10	8789.5	6505.7	4774.8	756.6	313.9	8887.5
0.43	1437	2940	92.0	0.12	8858.2	2517.8	4156.0	762.1	266.9	5800.7
0.65	1475	2640	88.0	0.14	10235.2	2144.7	4182.7	851.1	281.1	5277.4
0.86	1385	1890	67.0	0.15	11698.4	1976.4	4352.1	954.0	256.3	5791.9
1.08	1565	2580	76.0	0.17	12260.3	2005.0	4057.4	983.1	233.5	4719.3
1.30	1428	2410	76.0	0.19	14174.7	2099.4	4180.4	1107.2	230.8	4712.7
1.52	1410	2590	83.0	0.21	15725.2	2335.5	4194.9	1203.6	223.0	4518.3
1.74	1415	2770	88.0	0.23	17198.8	2437.8	4187.6	1292.3	216.1	4311.8
1.96	1408	2950	96.0	0.25	18790.6	2681.5	4209.6	1388.6	211.0	4185.1
2.18	1262	3350	123.0	0.27	21569.0	3718.4	4433.9	1555.5	213.7	4434.4

DATA POINT 38 AT 67 PSIA & 6 IN/SEC

Z	TH	QNET	HEX	XEX	REX	H/K-EX	H/K-MT	H/K-TT	H/K-LF	H/K-TF
-	--	----	---	--	---	------	------	------	------	------
0.21	985	4310	222.0	0.28	25643.7	7976.9	4985.9	1800.8	230.1	5388.7
0.43	1482	8640	88.0	0.30	22531.9	2371.6	4206.4	1605.6	198.4	3838.4
0.65	1585	3230	89.0	0.32	21518.0	2248.3	3889.7	1663.3	183.9	3280.6
0.86	1482	1810	54.0	0.34	24793.7	1442.3	4093.0	1726.7	186.6	3441.5
1.08	1575	2580	75.0	0.36	24414.1	1304.7	3909.7	1726.6	176.7	3138.7
1.30	1435	2650	83.0	0.37	27458.3	2273.9	4158.8	1877.3	183.5	3412.3
1.52	1432	2570	81.0	0.39	28966.2	2222.8	4163.1	1960.1	180.8	3338.2
1.74	1432	2710	85.0	0.41	30451.6	2332.6	4163.1	2040.1	177.5	3263.7
1.96	1352	2932	55.0	0.43	32417.1	2665.5	4221.1	2148.8	176.5	3279.7
2.18	1255	3360	125.0	0.46	36923.6	3794.2	4447.9	2389.8	179.4	3502.1

DATA POINT 39 AT 64 PSIA & 6 IN/SEC

Z	TH	QNET	HEX	XEX	REX	H/K-EX	H/K-MT	H/K-TT	H/K-LF	H/K-TF
0.21	982	2340	254.0	0.00	1.0	9664.2	0.5	0.5	7127.4	-218730.1
0.43	1382	2730	89.0	0.00	1.0	2515.6	0.5	0.5	5638.3	-212589.6
0.60	1460	3000	91.0	0.00	1.0	2463.5	0.5	0.5	5475.3	-206688.1
0.86	1380	1820	59.0	0.00	1.0	1669.5	0.5	0.5	5642.6	-212757.4
1.08	1452	2550	78.0	0.01	738.1	2128.7	4139.8	184.0	689.0	24056.7
1.30	1437	2640	82.0	0.03	2226.6	2247.8	4160.3	251.7	424.9	14375.9
1.52	1410	2592	82.0	0.05	3748.4	2281.6	4199.4	382.3	368.1	9294.3
1.74	1367	2742	91.0	0.07	5333.4	2594.1	4262.2	587.8	325.5	7507.2
1.96	1915	2932	93.0	0.09	5328.6	2001.6	3502.7	510.3	258.0	4996.4
2.18	1235	3378	128.0	0.11	8958.2	3937.5	4494.6	768.8	291.4	6955.5

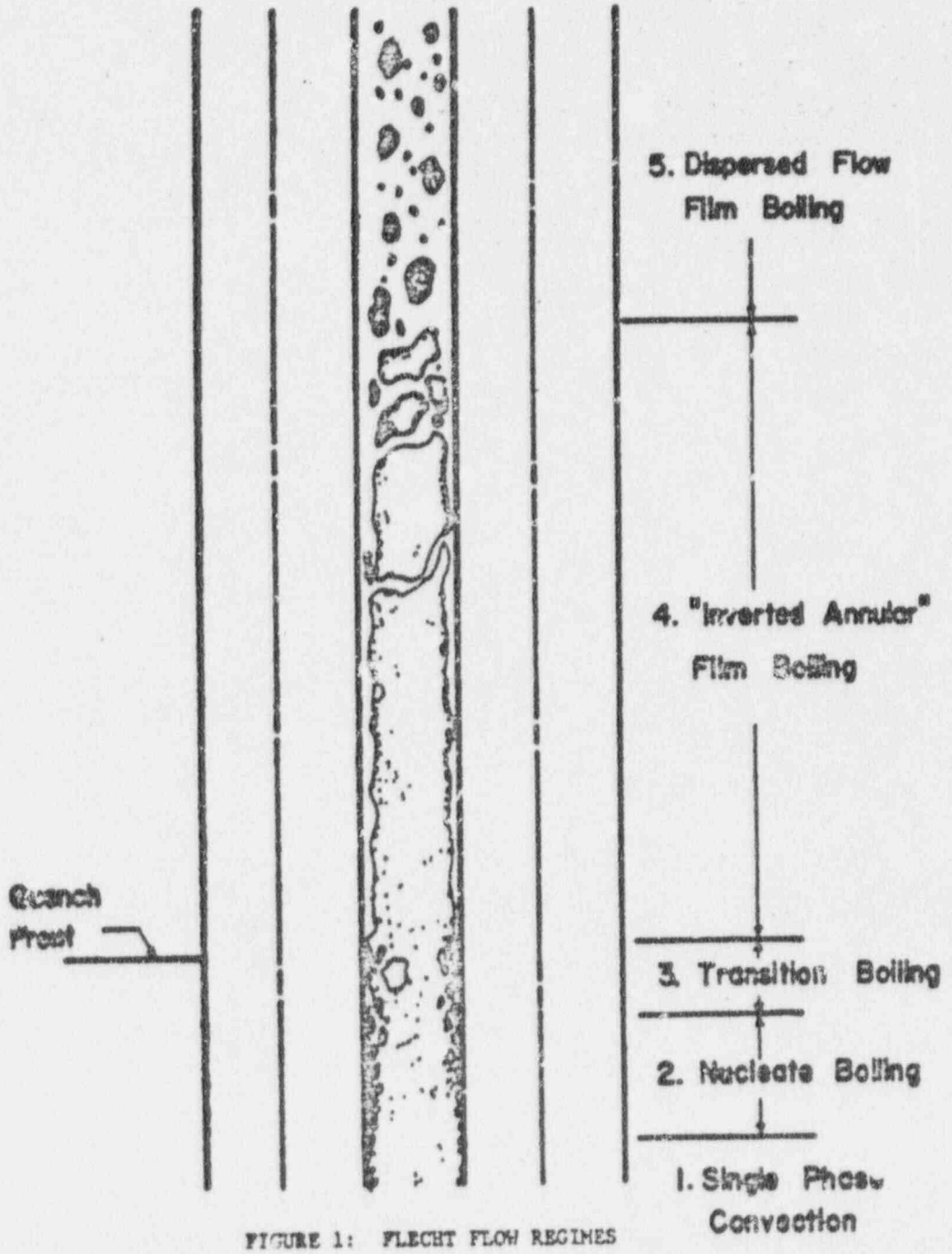

FIGURE 1: FLECHT FLOW REGIMES

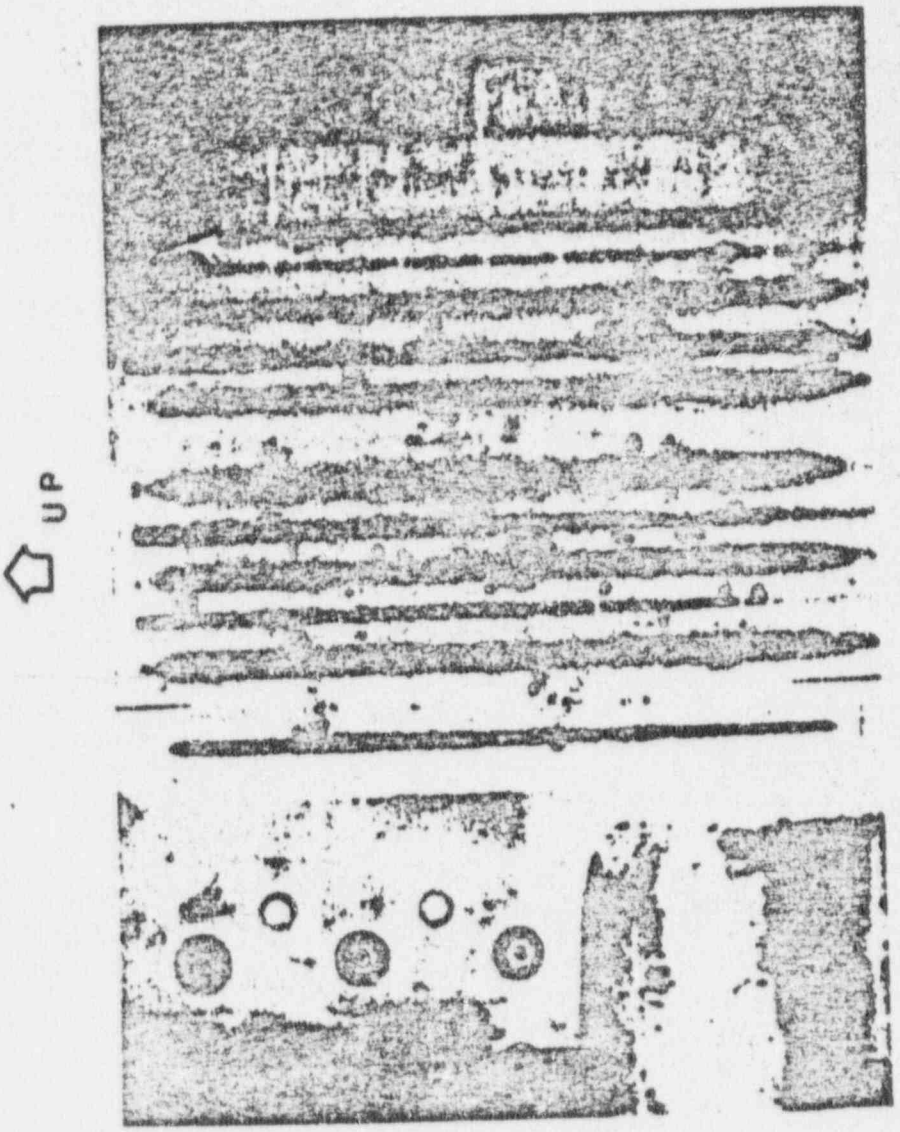

FIGURE 2: PHOTOGRAPH OF FLECHT DROPLETS, LOW PRESSURE, LOW FLOODING RATE (Run #9983)

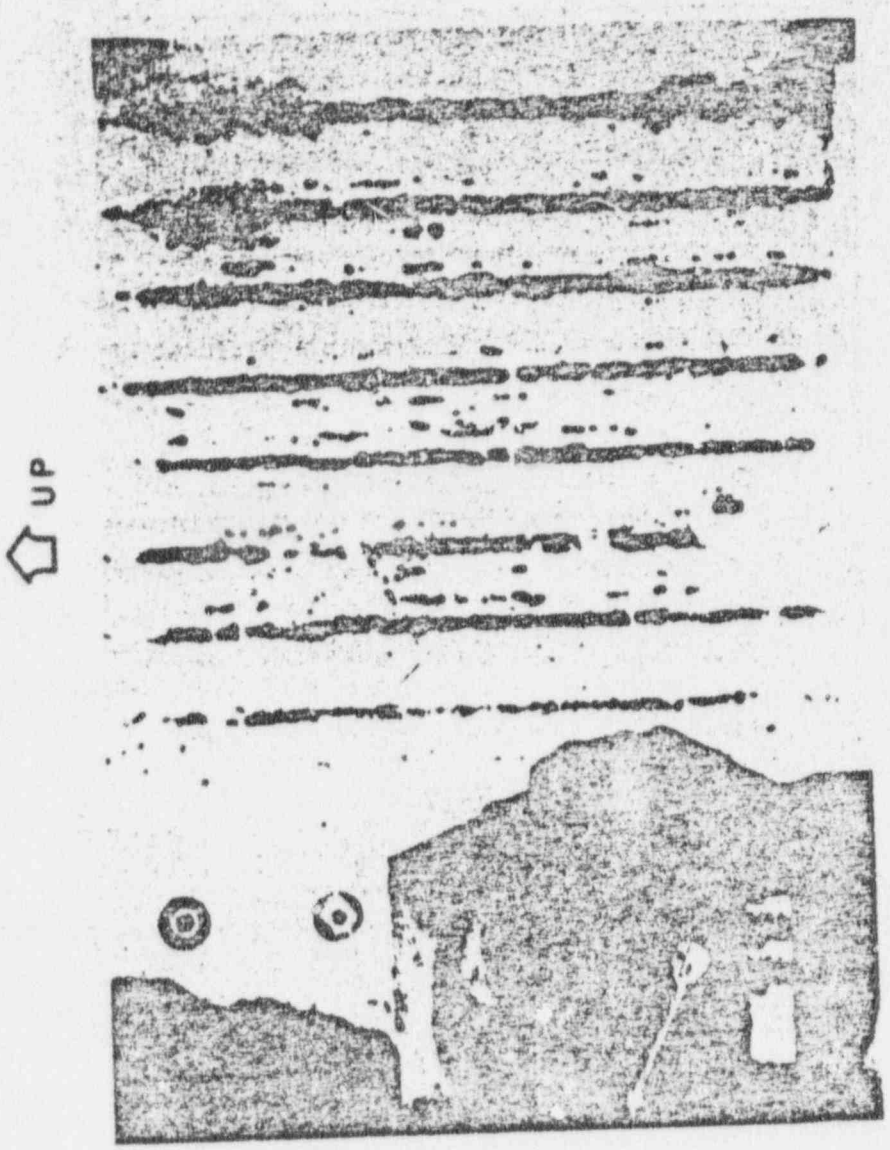

FIGURE 3: PHOTOGRAPH OF FLECHT DROPLETS, HIGH PRESSURE, HIGH FLOODING RATE (Run #3440)

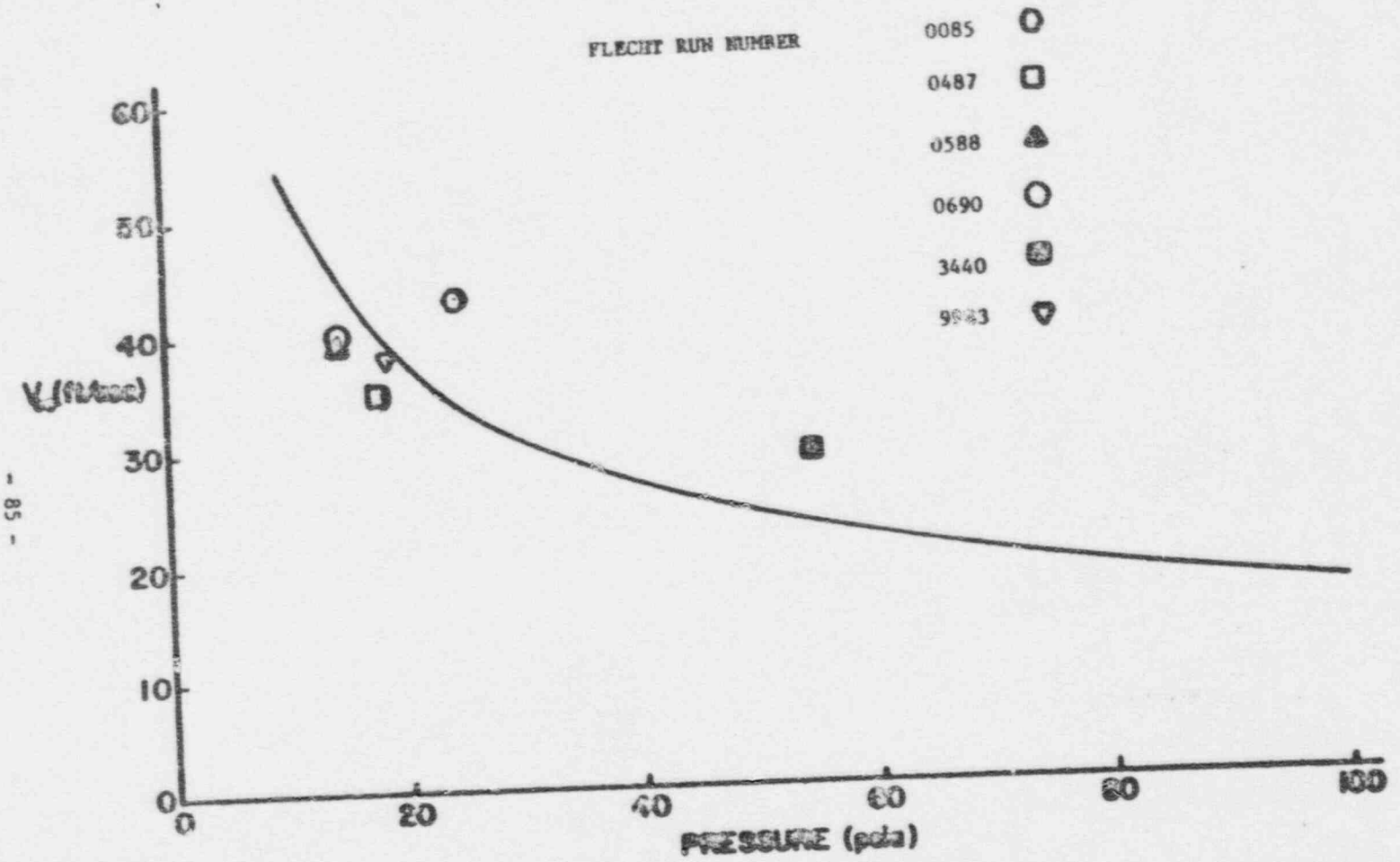

FIGURE 4: FLECHT VAPOR VELOCITIES COMPARED WITH PLUMMER'S CRITICAL MASS CRITERION

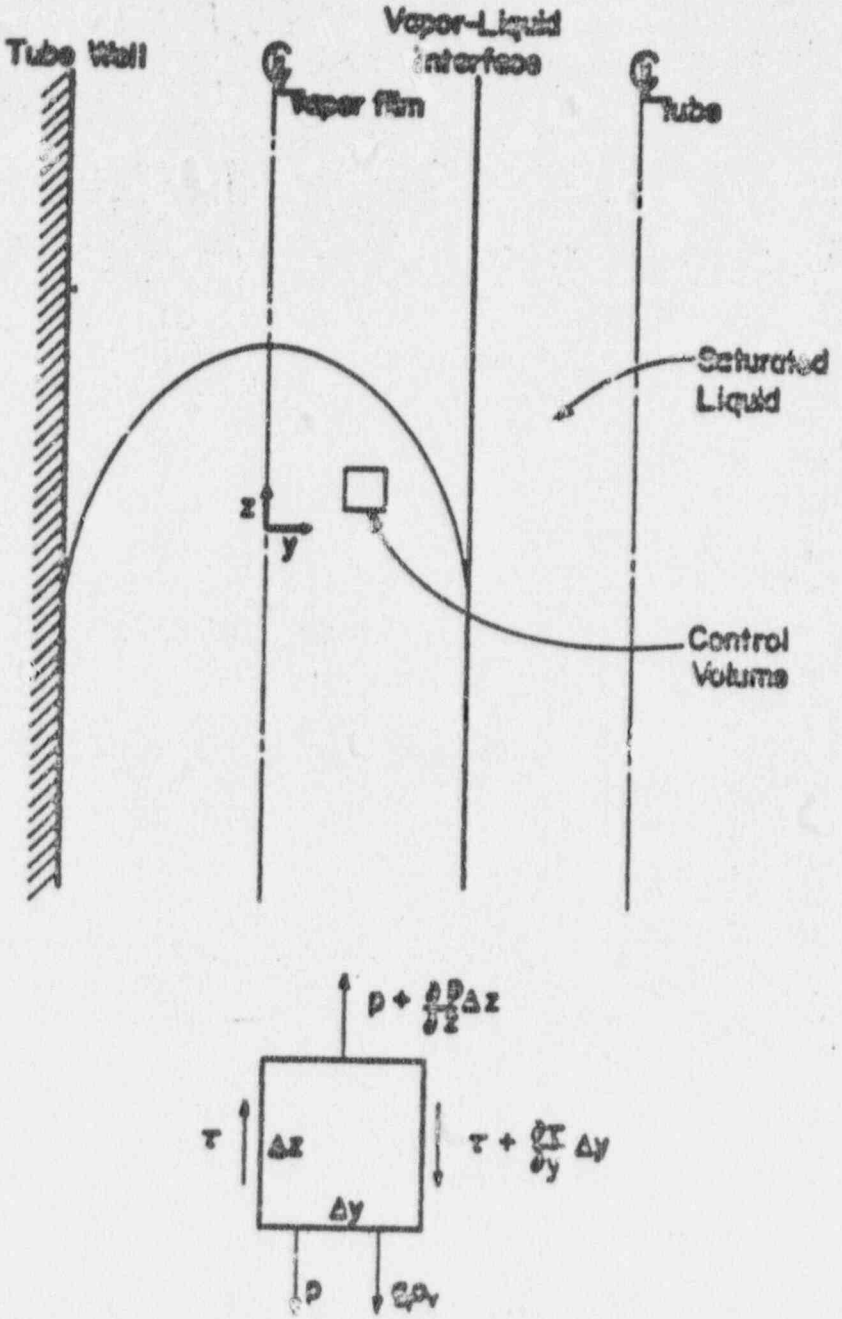

FIGURE 5: CONTROL VOLUME FOR VAPOR FILM FORCE BALANCE

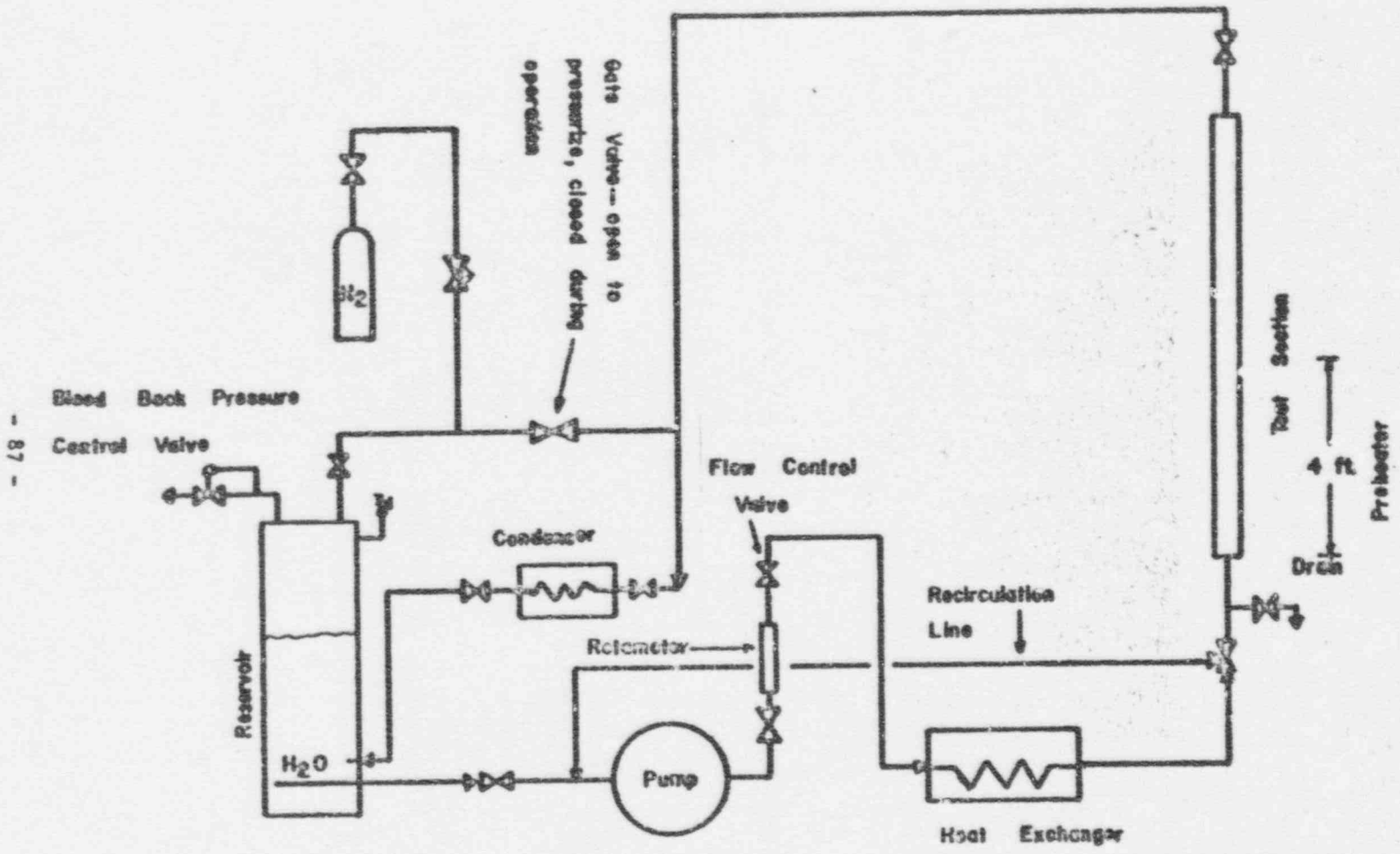

FIGURE 6: SCHEMATIC DIAGRAM OF THE EXPERIMENTAL APPARATUS

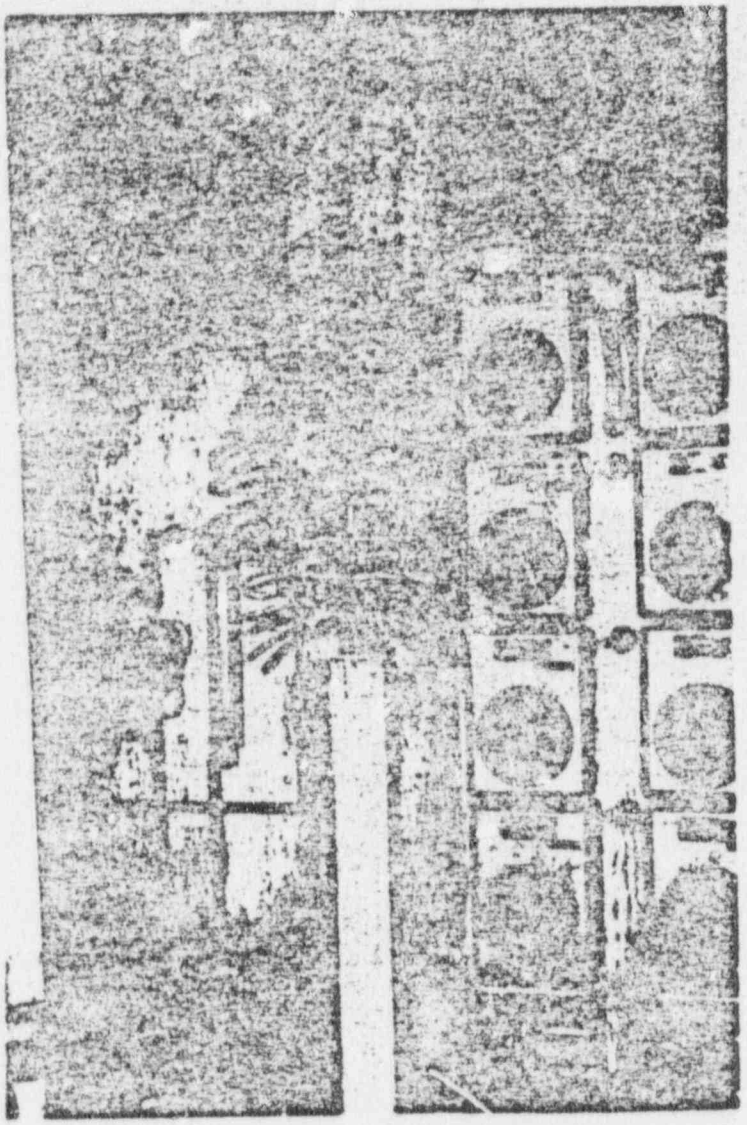

FIGURE 7: PHOTOGRAPH OF EXPERIMENTAL APPARATUS

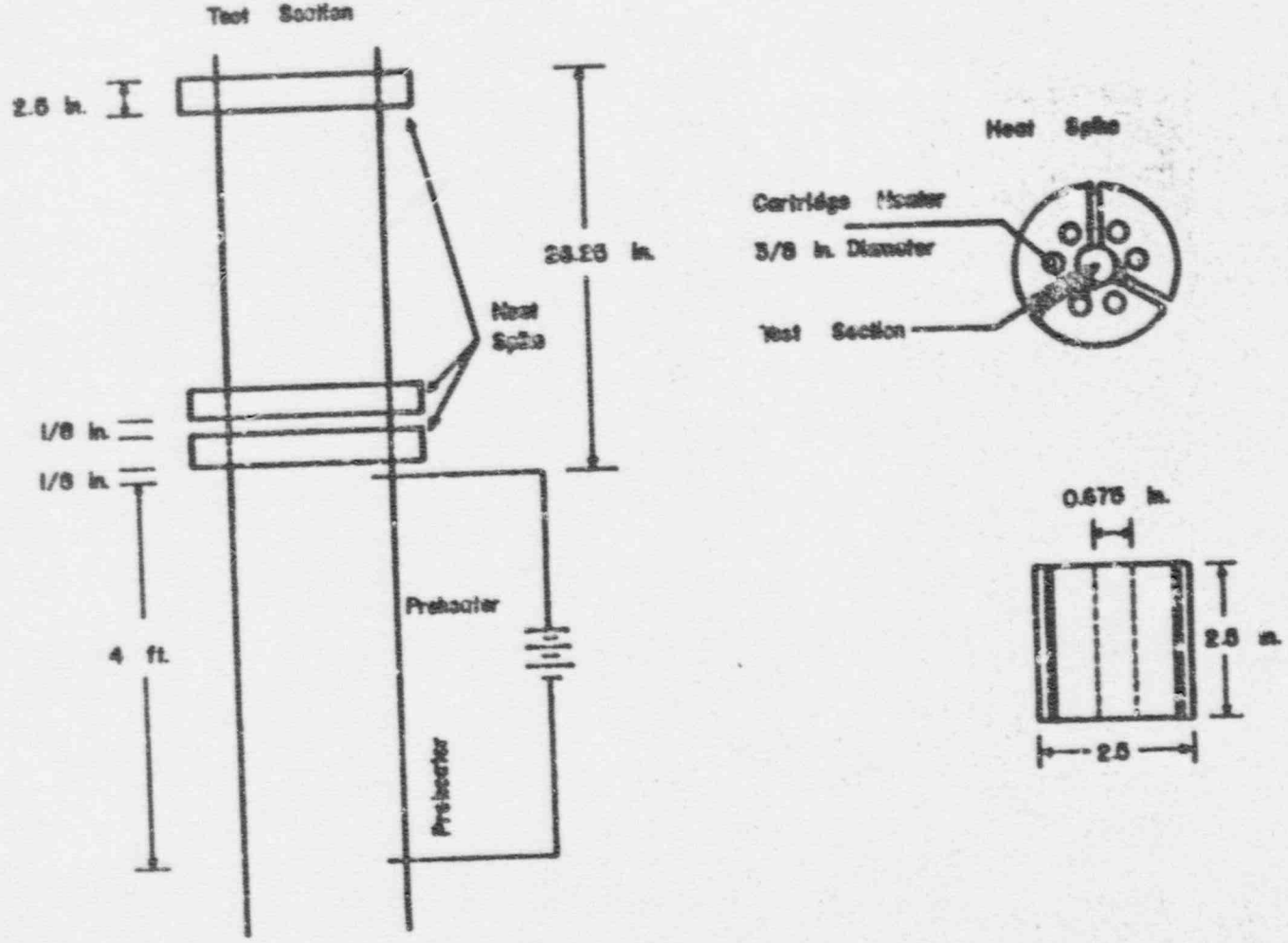

FIGURE 8: SCHEMATIC OF TEST SECTION WITH COPPER BLOCK/CARTRIDGE HEATER HEAT SPIKES

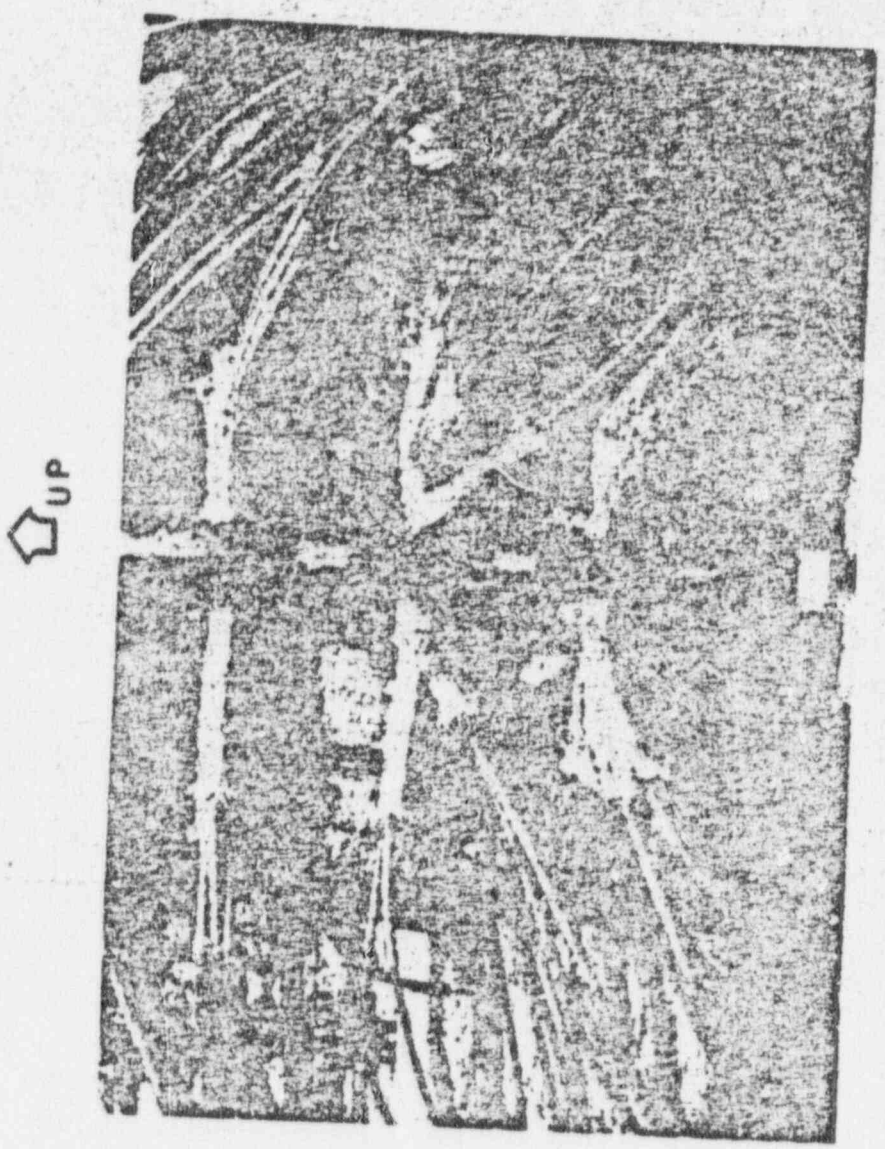

FIGURE 9: PHOTOGRAPH OF COPPER BLOCK HEAT SPIKES MOUNTED ON TEST SECTION

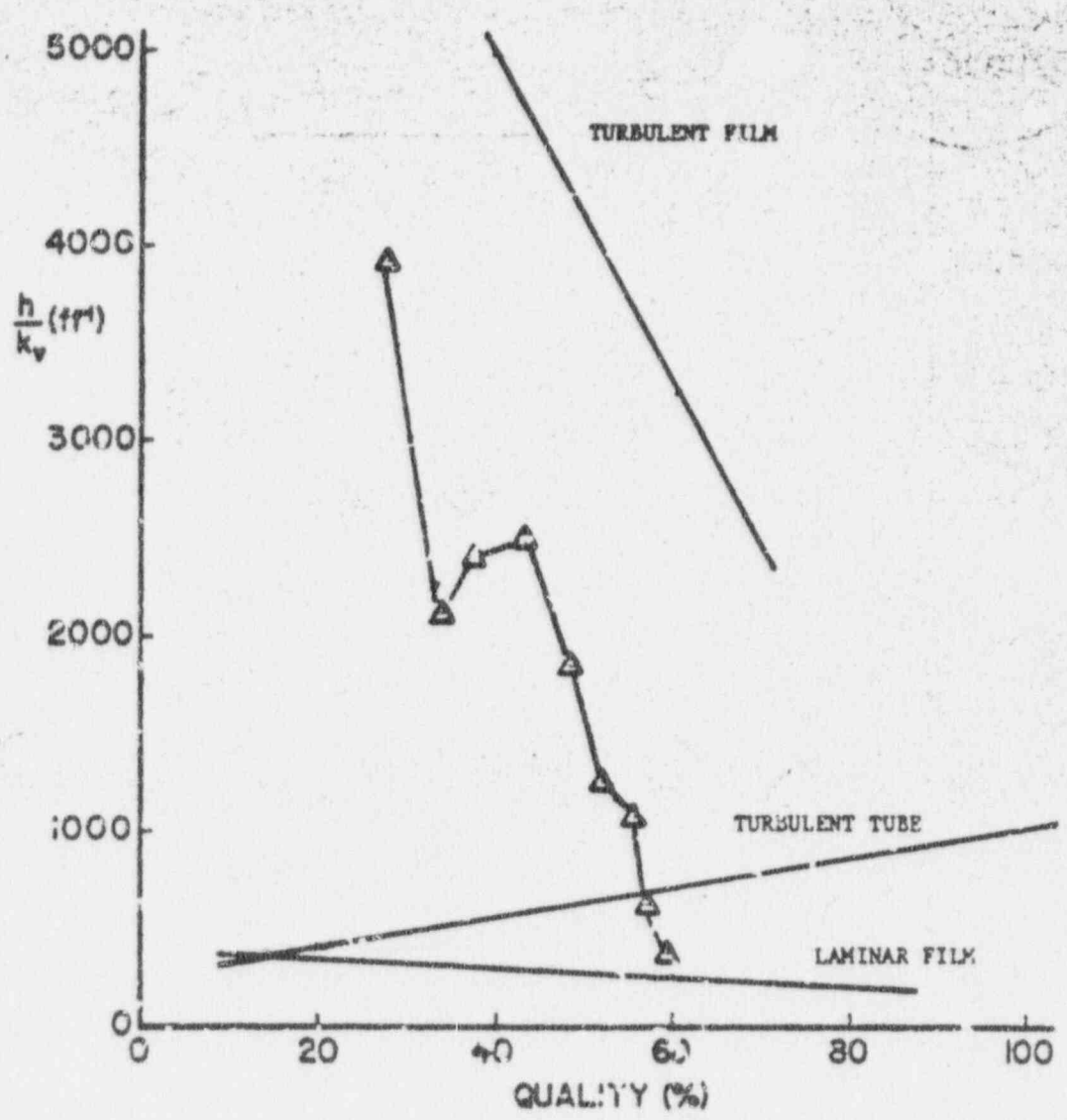

FIGURE 10: COMPARISON OF LOW PRESSURE, LOW FLOODING RATE DATA (DF 3) WITH THEORY

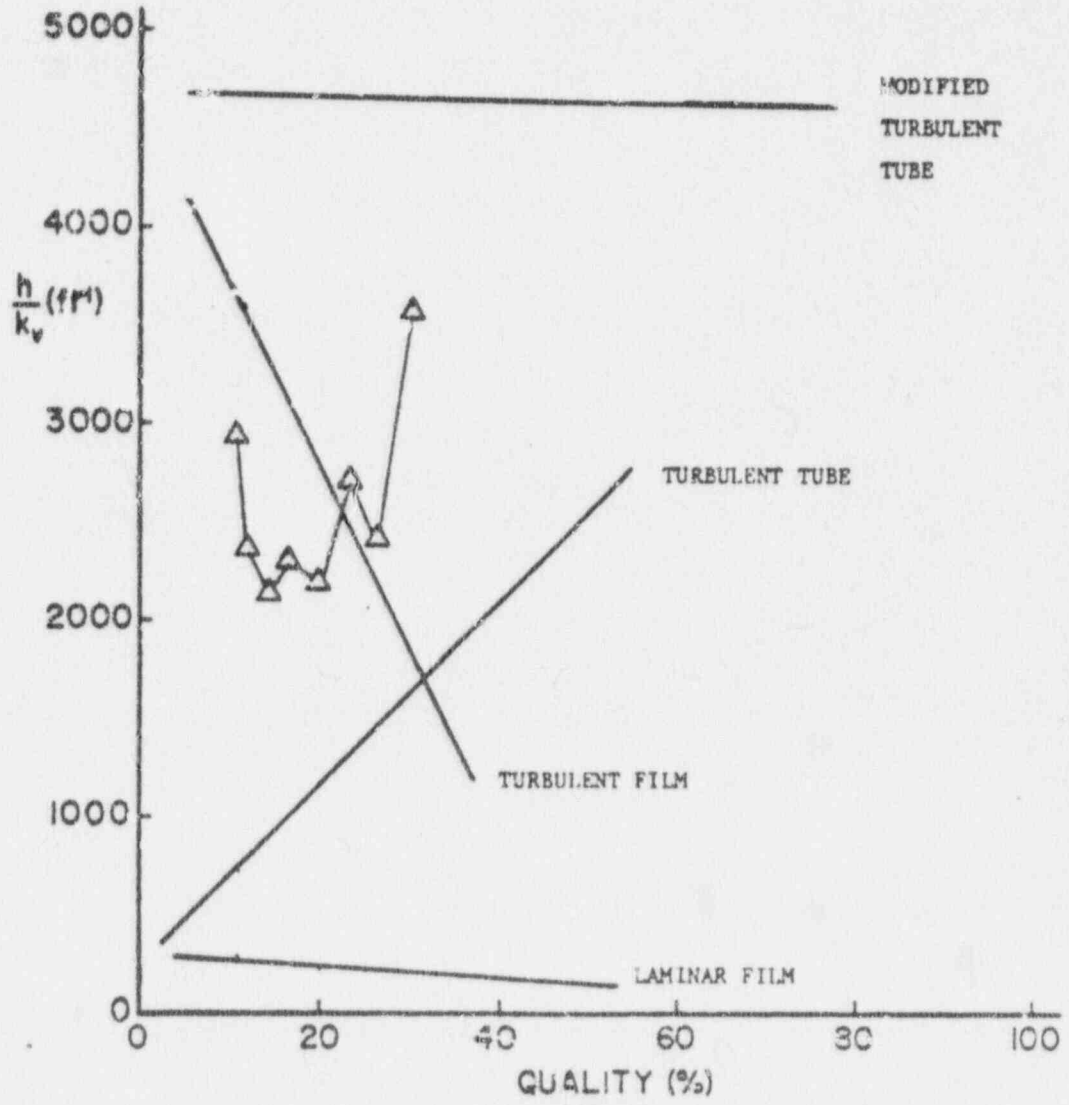

FIGURE 11: COMPARISON OF LOW PRESSURE, HIGH FLOODING RATE DATA (DP 13)

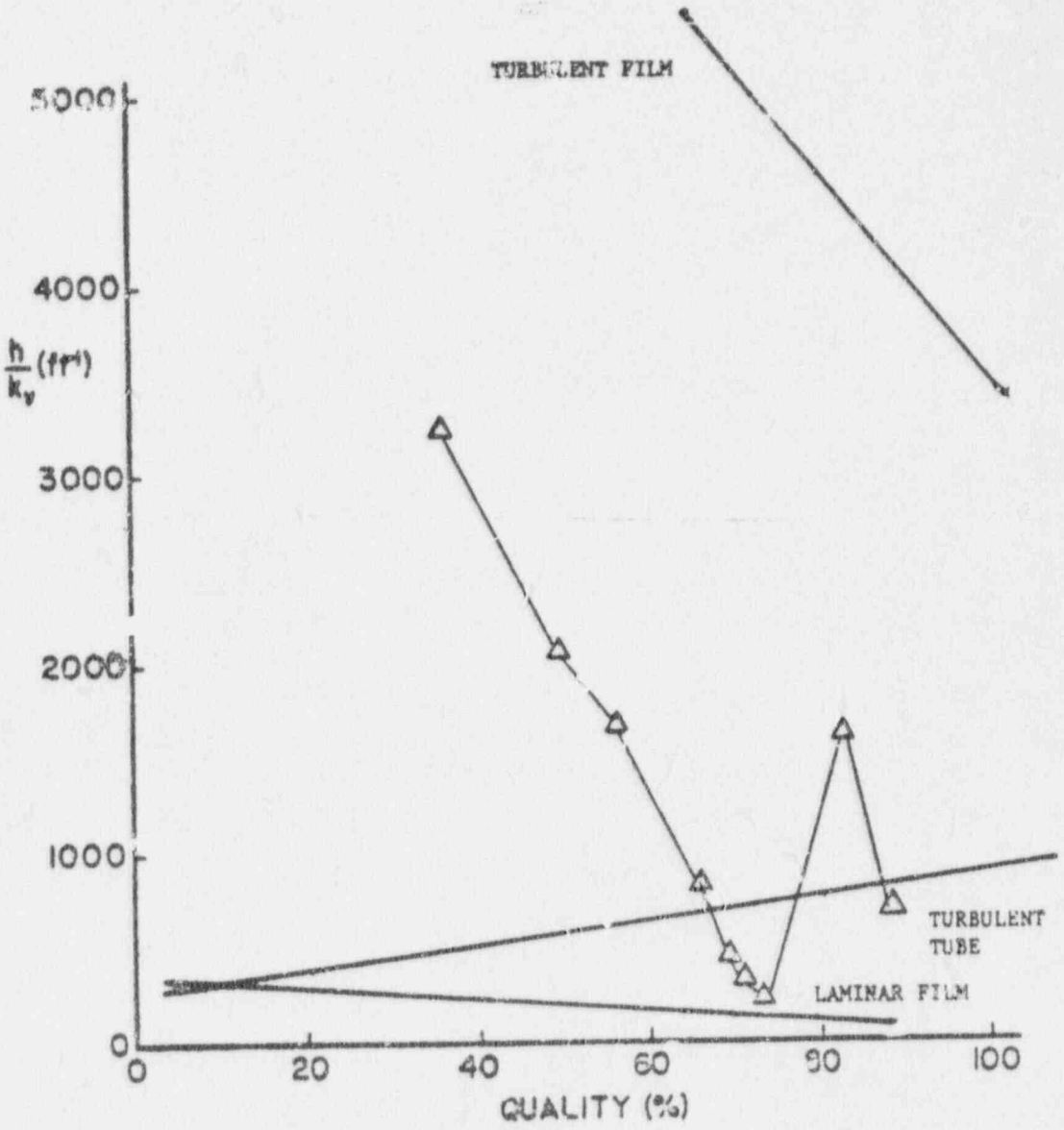

FIGURE 12: COMPARISON OF HIGH PRESSURE, LOW FLOODING RATE DATA (DP 32) WITH THEORY

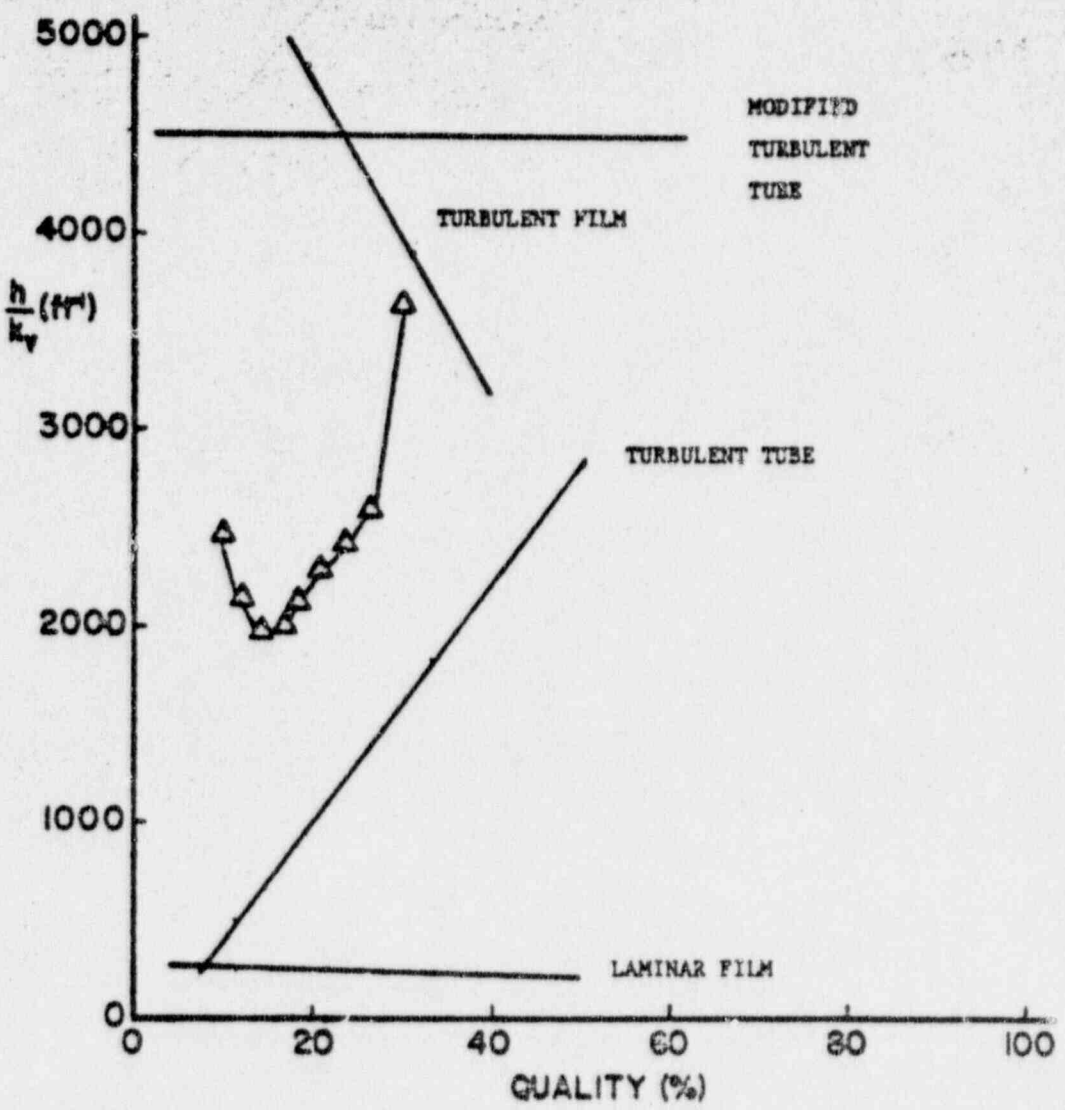

FIGURE 13: COMPARISON OF HIGH PRESSURE, HIGH FLOODING RATE DATA (DP 37) WITH THEORY

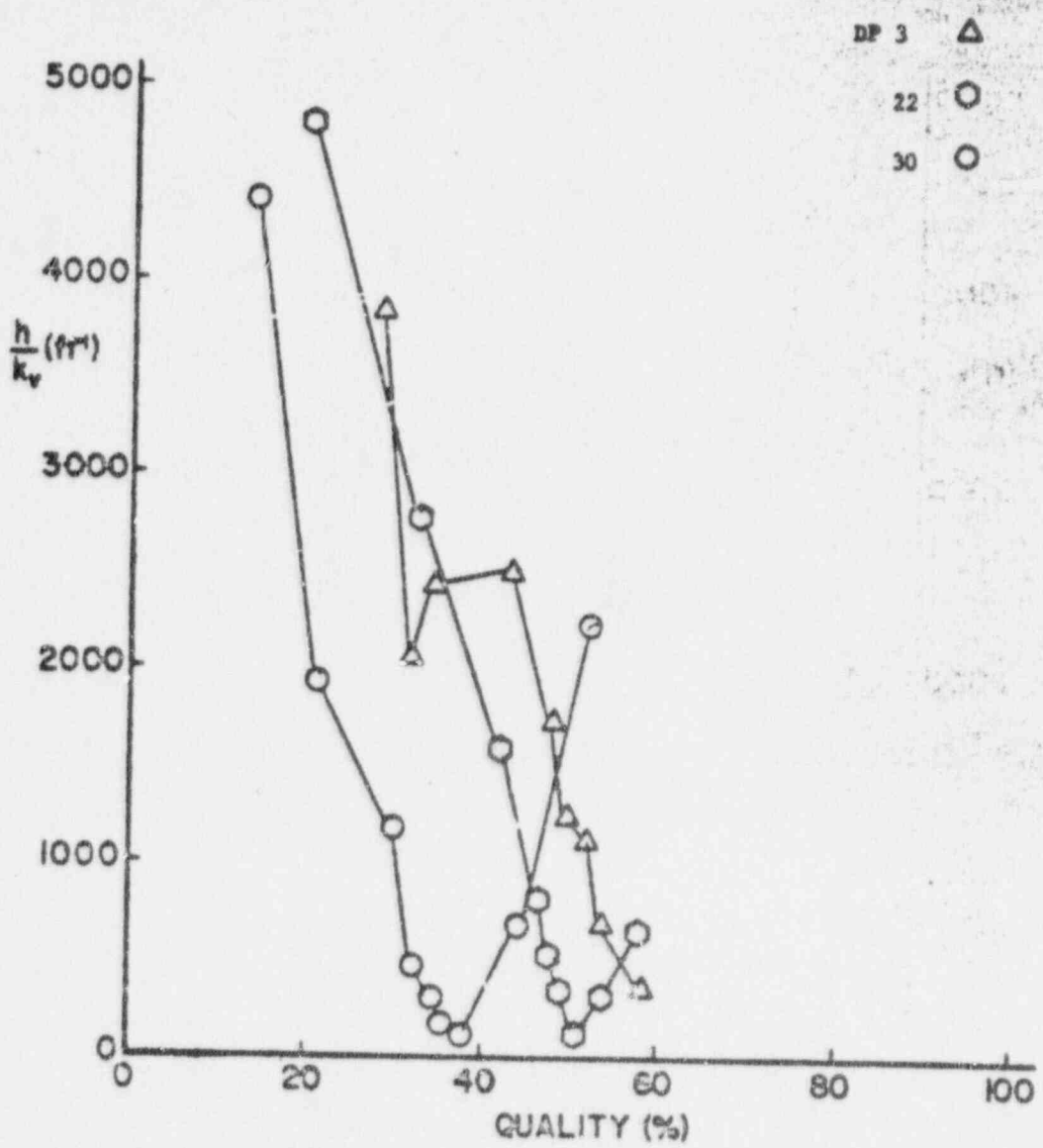

FIGURE 14: EFFECT OF PRESSURE ON CARRY OVER

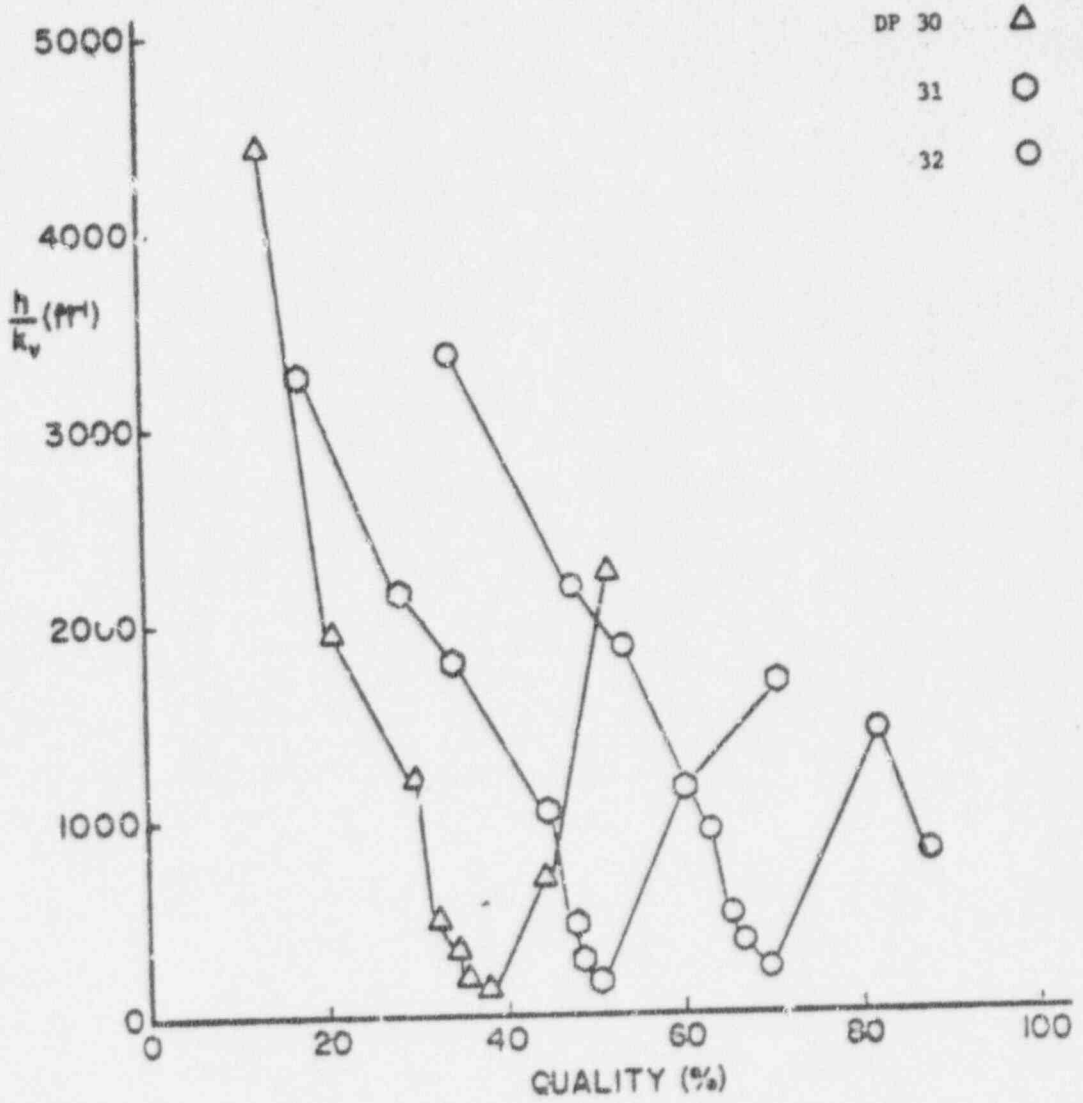

FIGURE 15: EFFECT OF WALL TEMPERATURE ON CARRY OVER

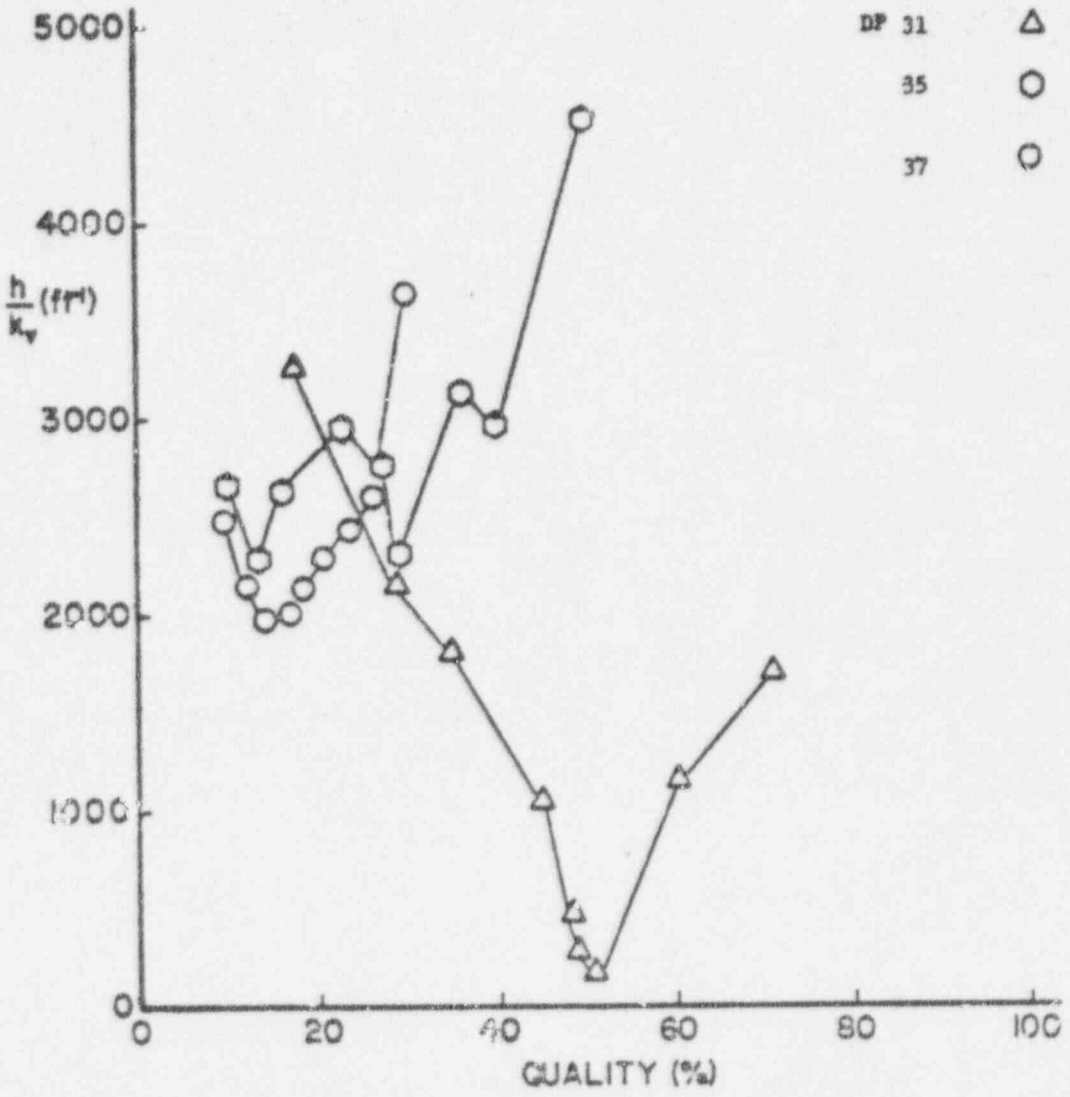

FIGURE 16: EFFECT OF FLOODING RATE ON CARRY OVER

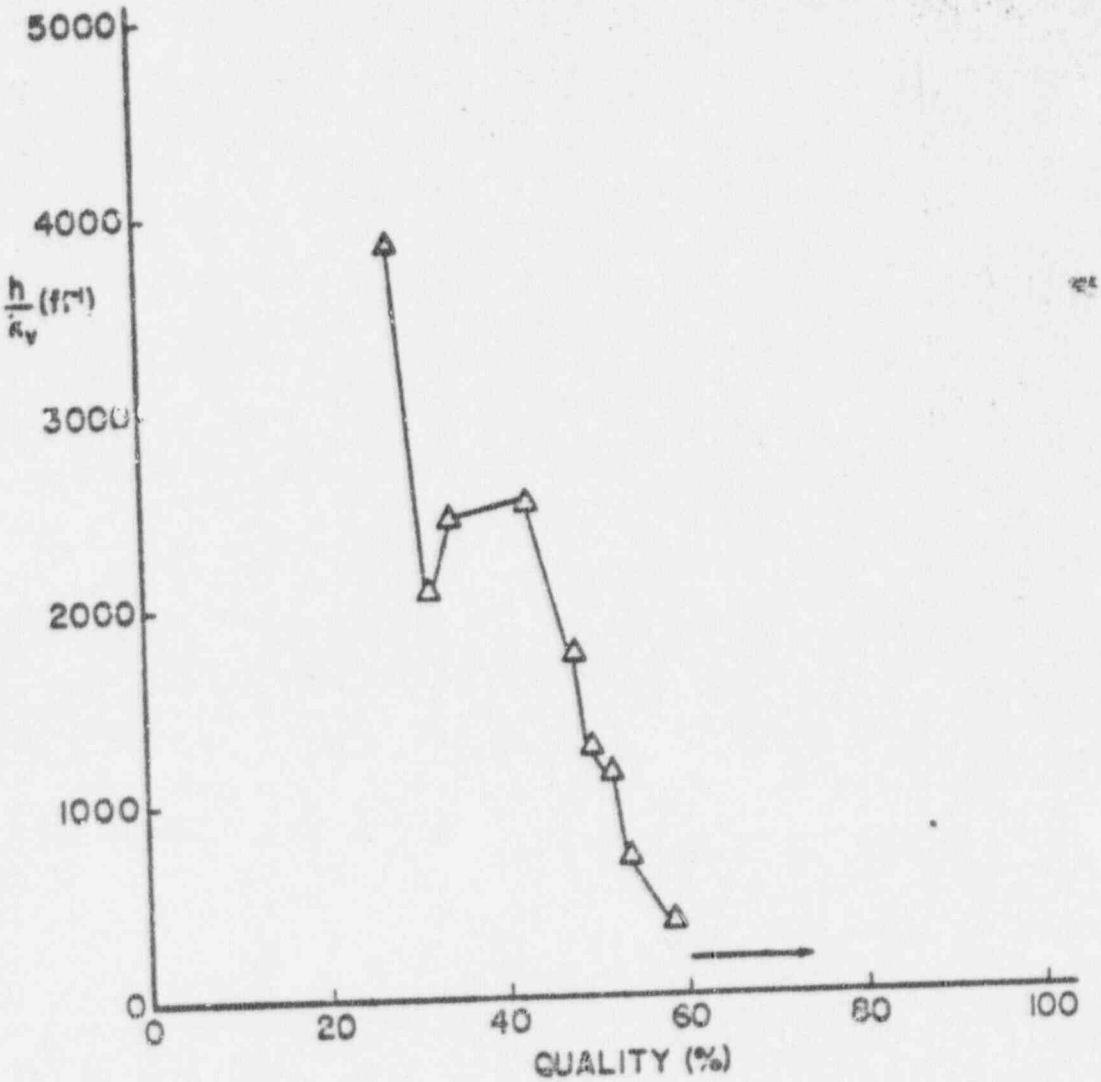

FIGURE 17: CARRY OVER FOR DP 3

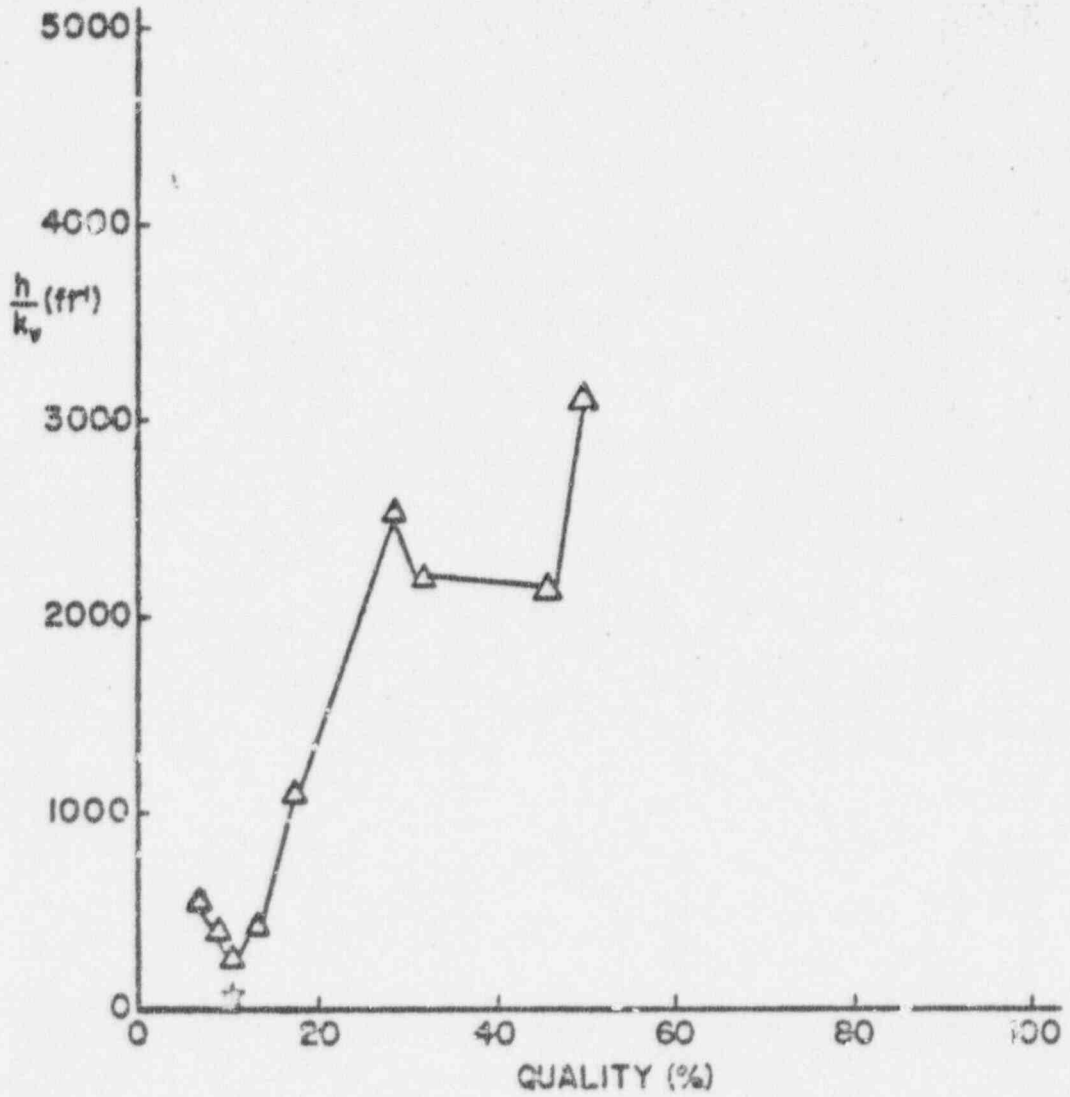

FIGURE 18: CARRY OVER FOR DP 30

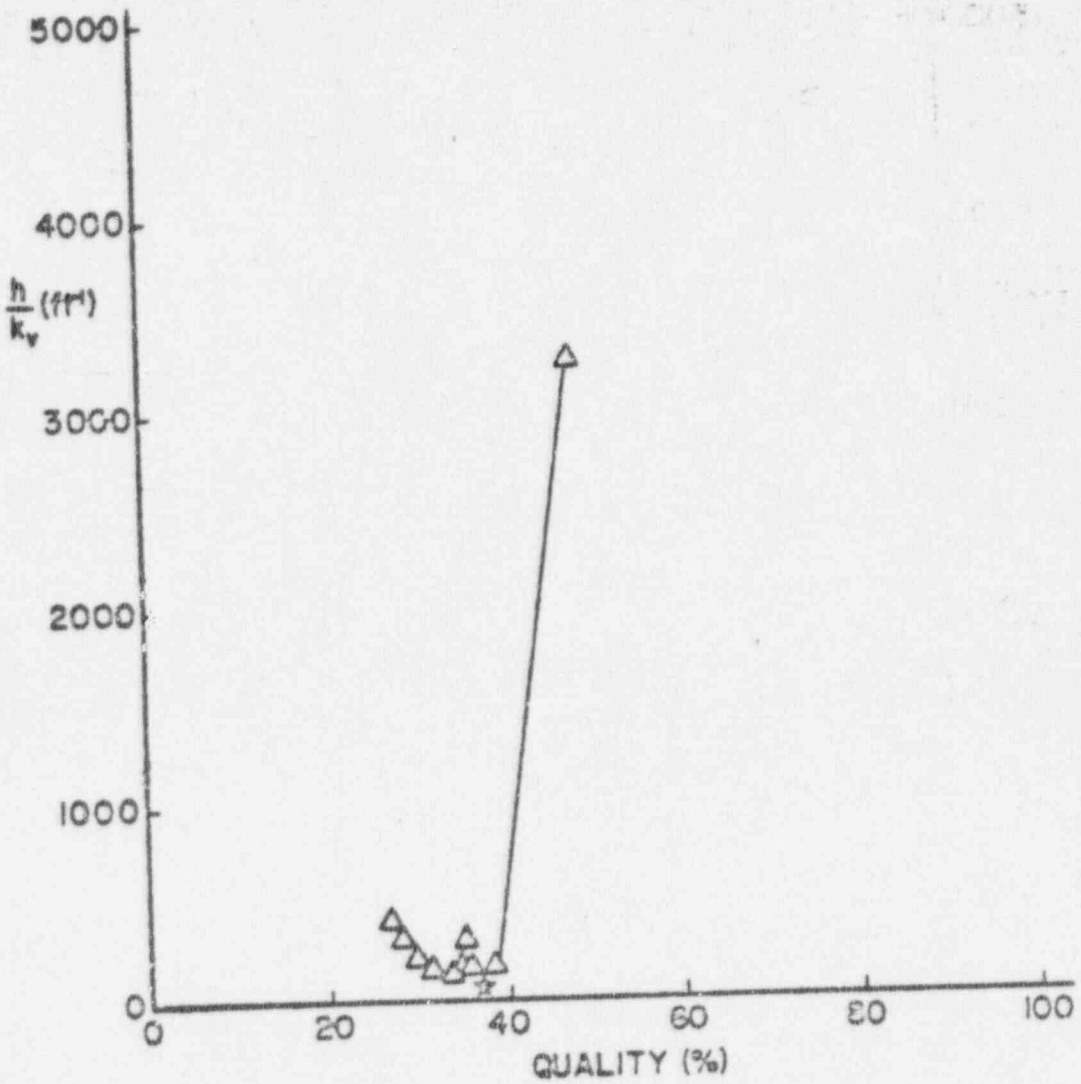

FIGURE 19: CARRY OVER FOR DP [illegible]

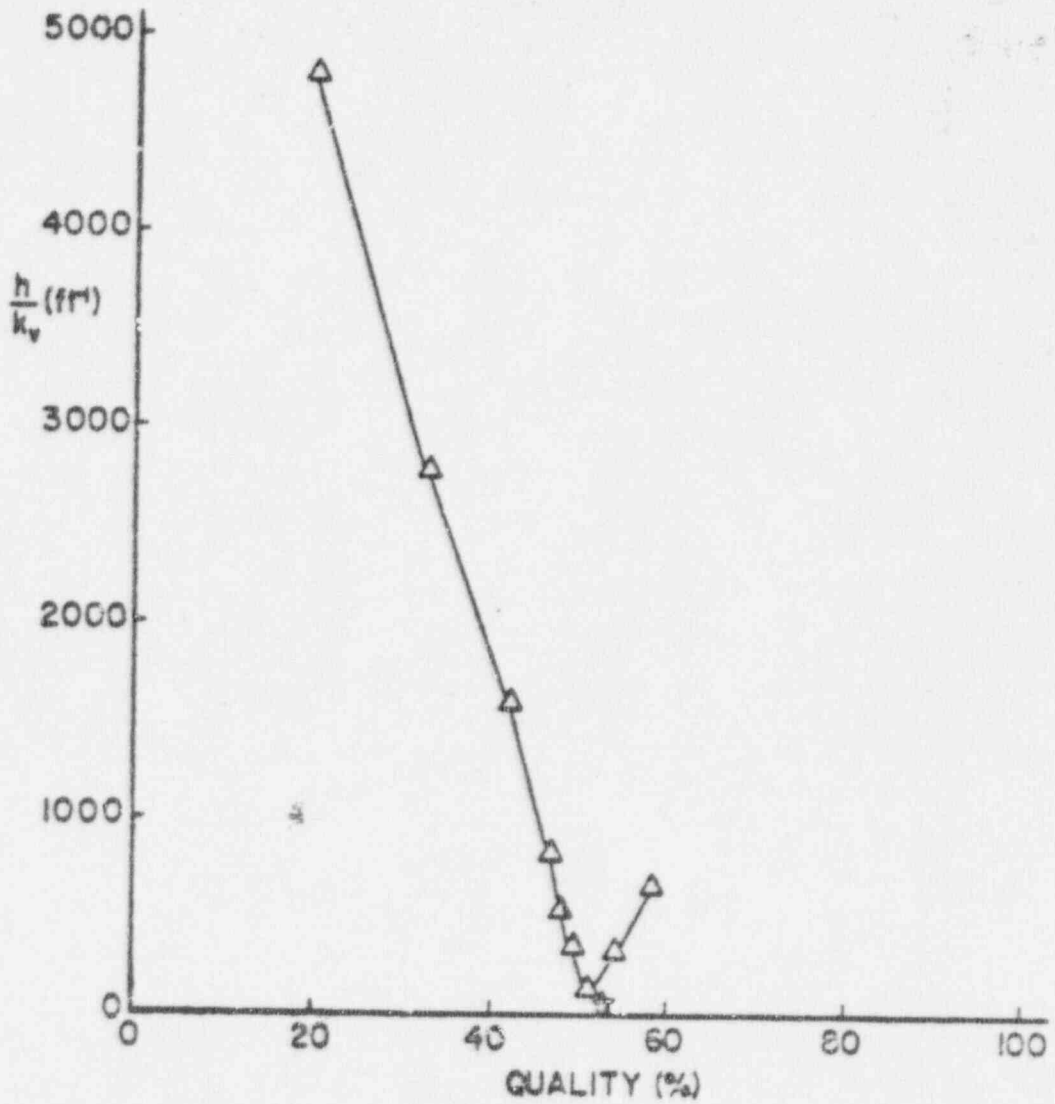

FIGURE 20: CARRY OVER FOR DP 22

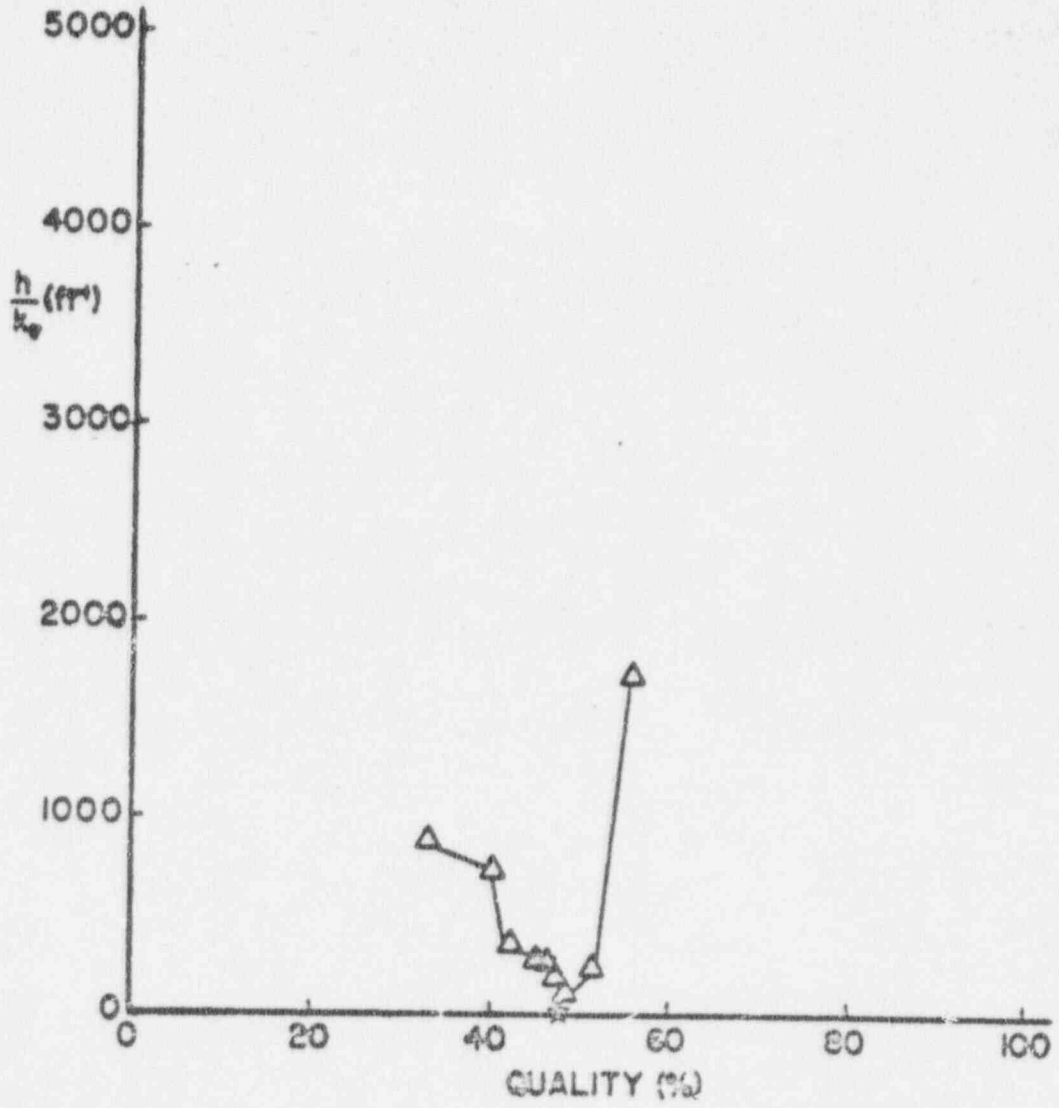

FIGURE 21: CARRY OVER FOR DP 23

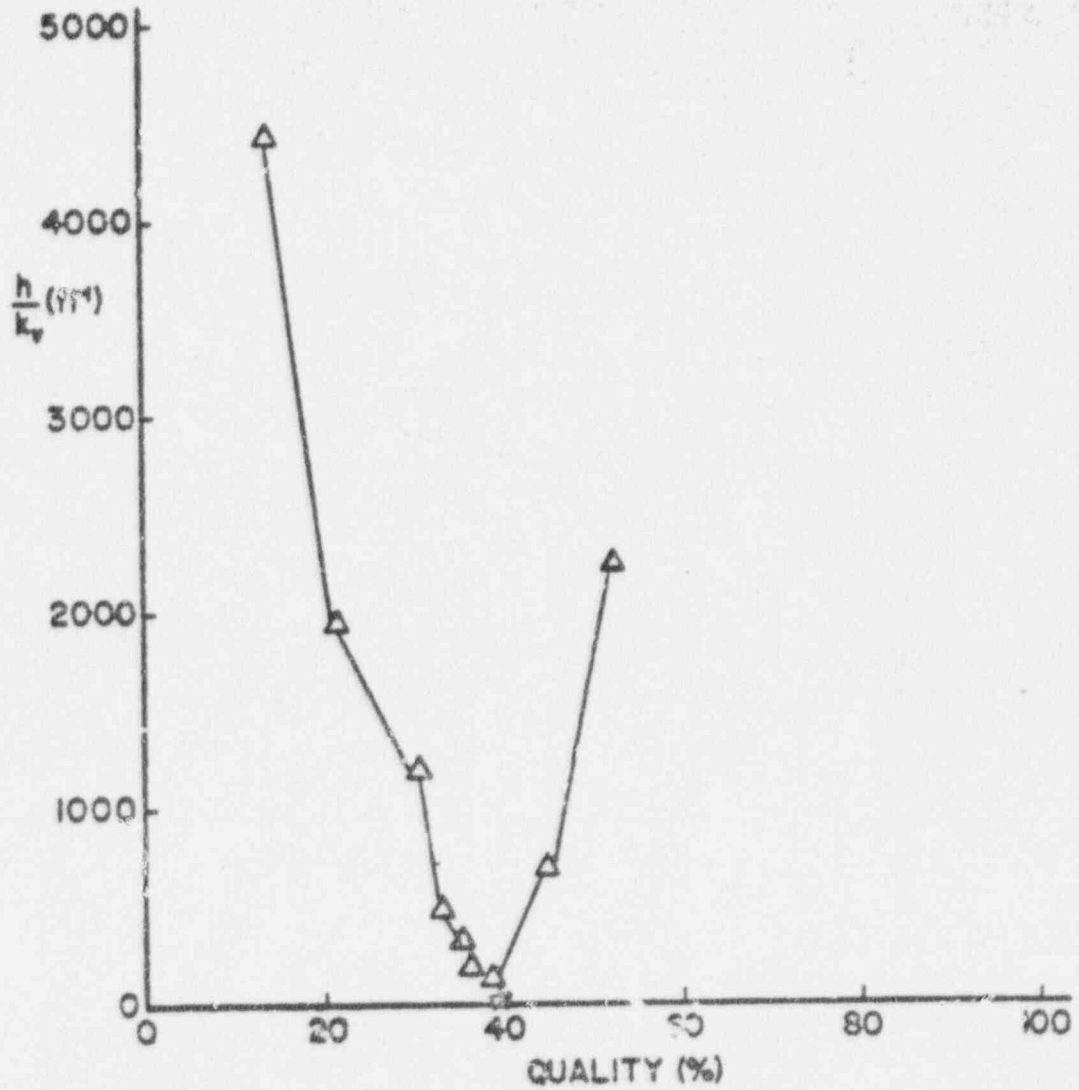

FIGURE 22: CARRY OVER FOR DP 30

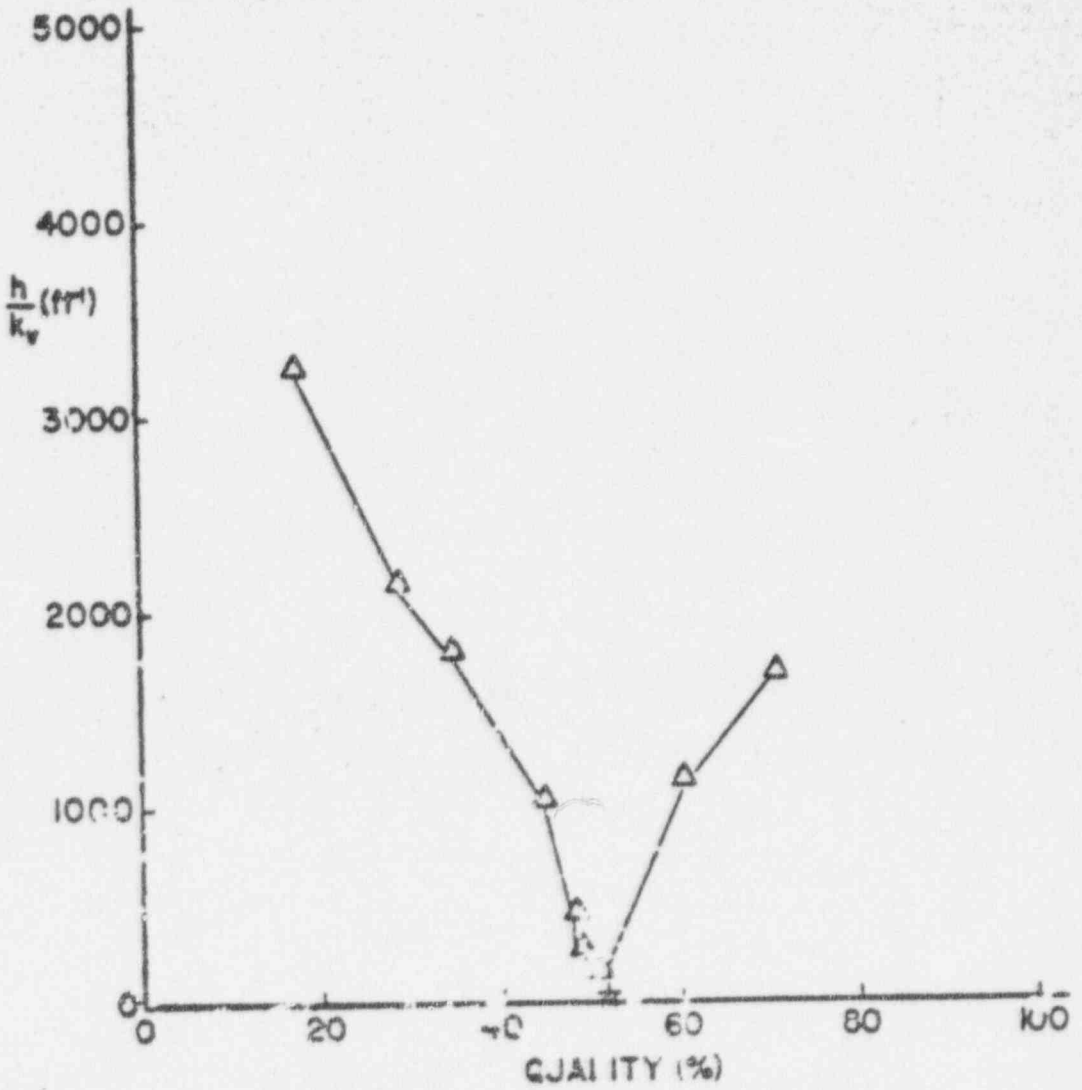

FIGURE 23: CARRY OVER FOR DP 31

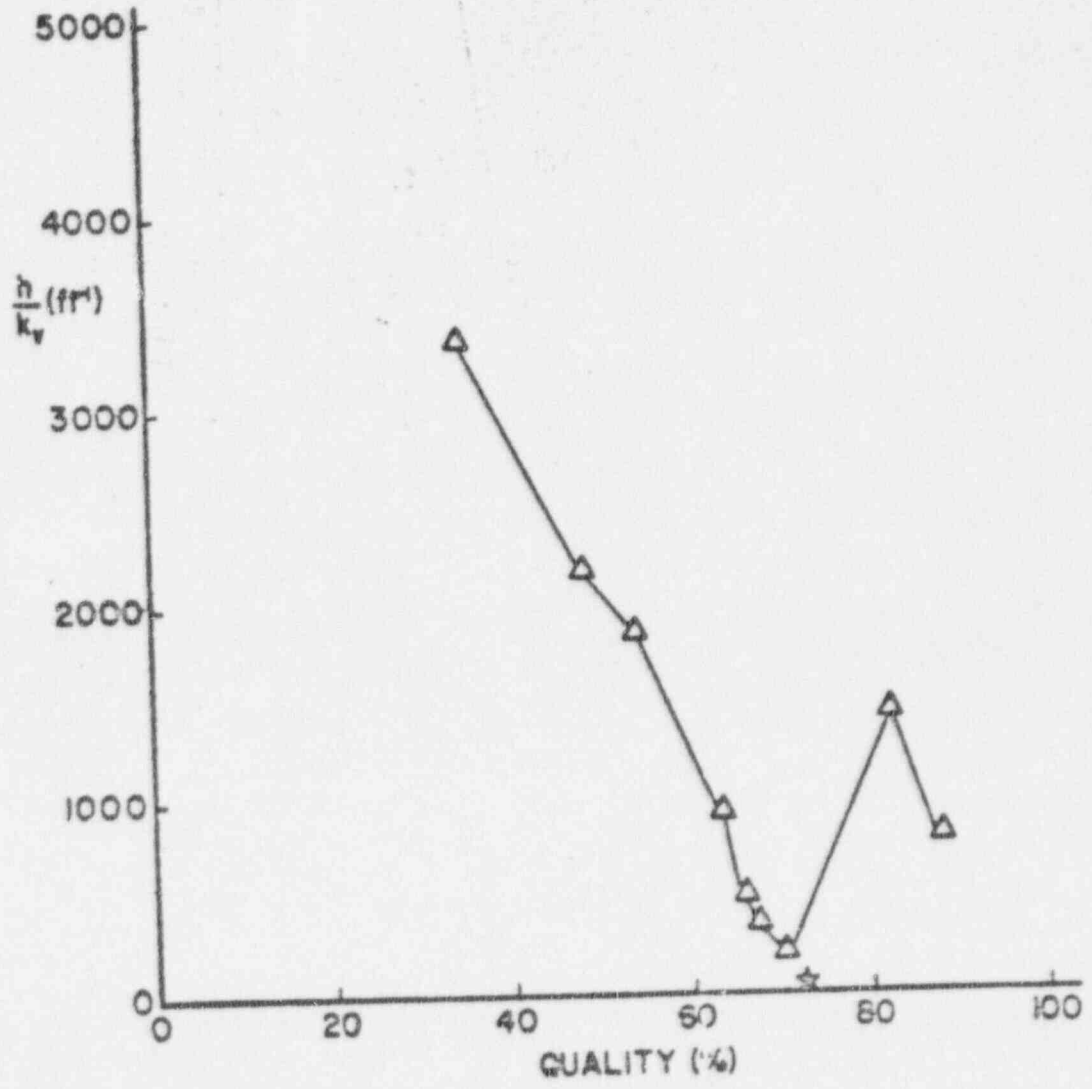

FIGURE 24: CARRY OVER FOR DP 32

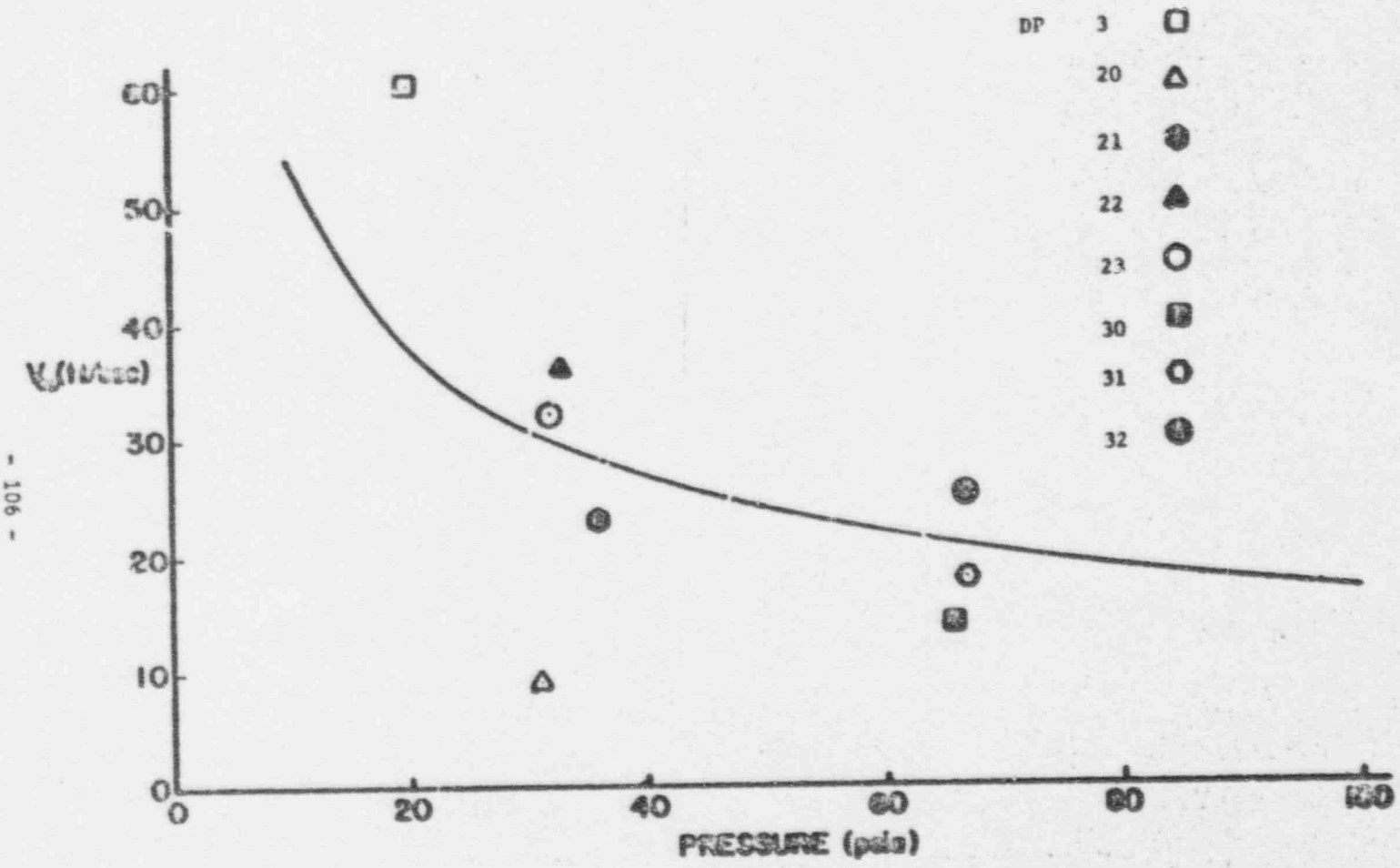

FIGURE 25: COMPARISON OF EXPERIMENTAL CARRY OVER VELOCITIES WITH PLUMMER'S CRITICAL MASS CRITERION

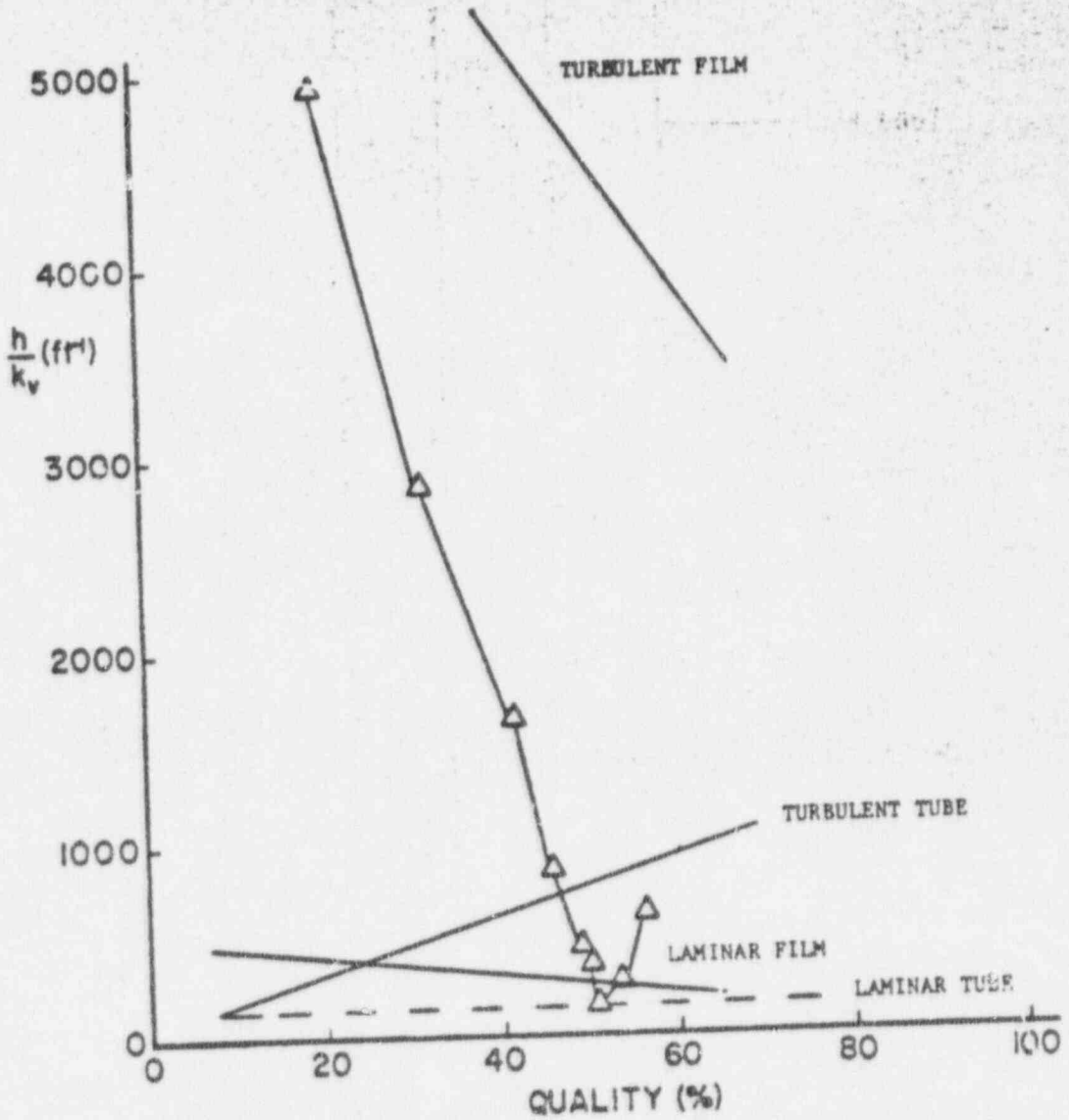

FIGURE 26: TRANSITION FROM TURBULENT FILM TO LAMINAR TUBE FLOW (DP 22)

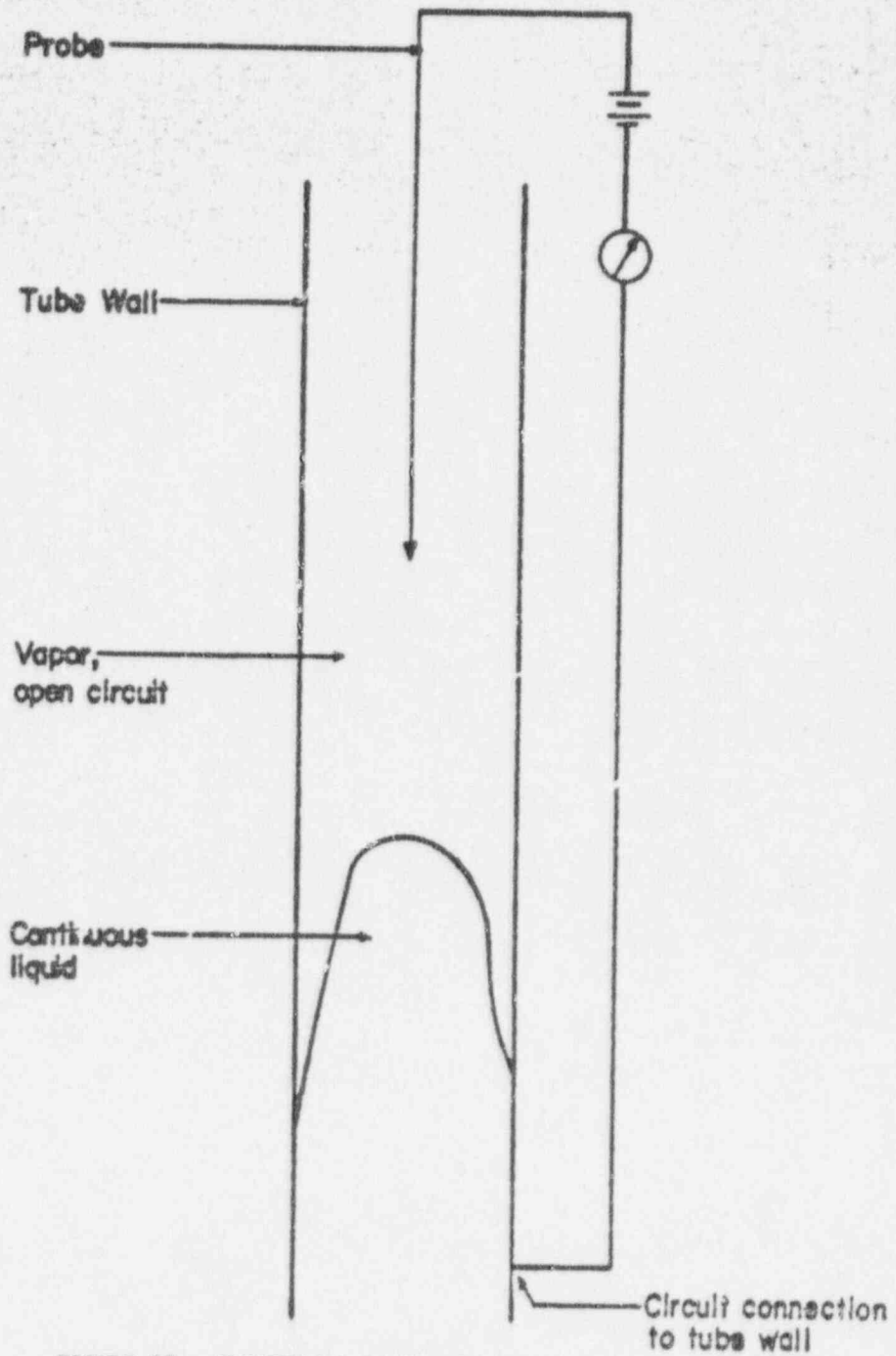

FIGURE 27: ELECTRICAL RESITANCE PROBE CIRCUIT

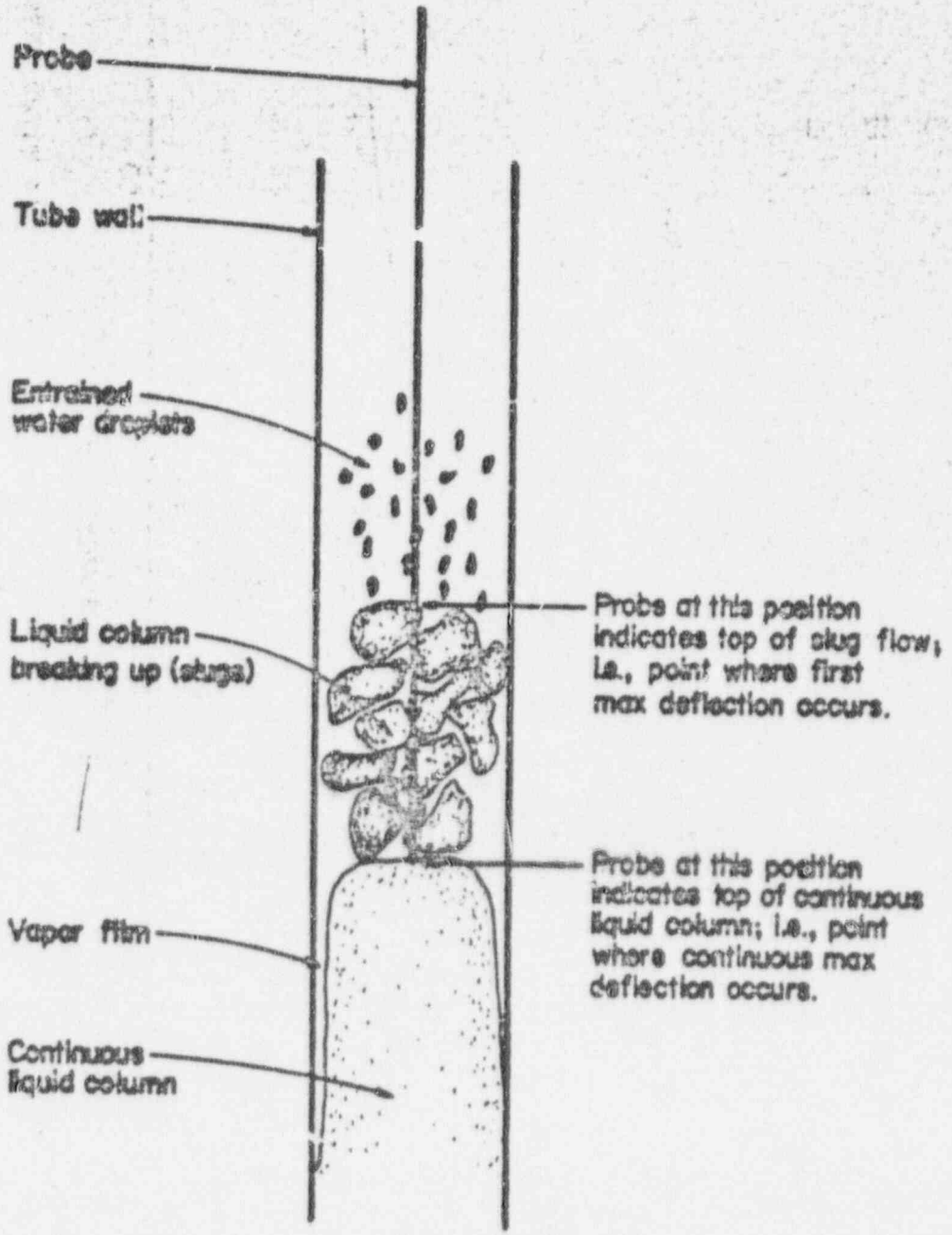

FIGURE 28: DETERMINING THE CARRY OVER POINT
(Probe Configuration)

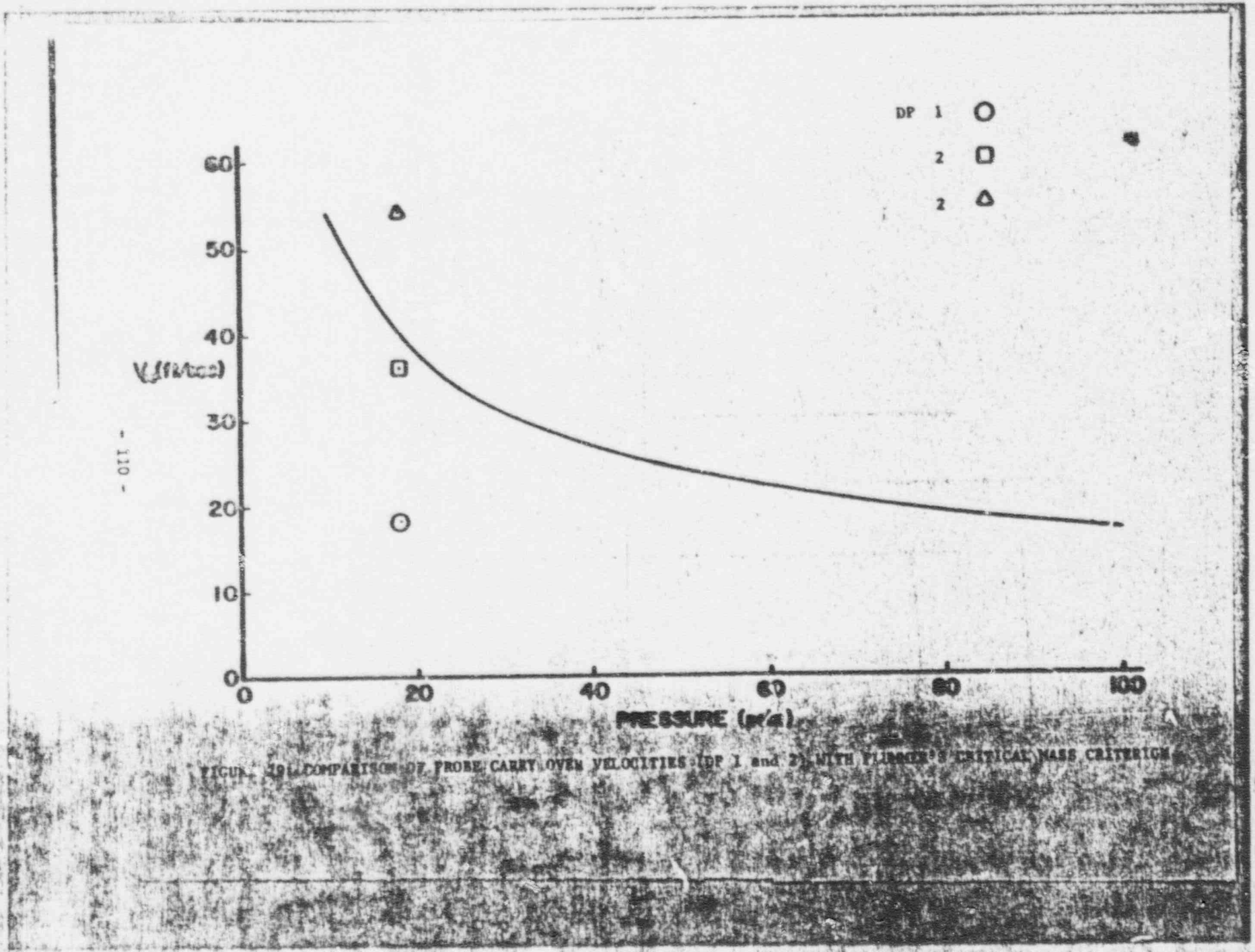

FIGURE 29 COMPARISON OF PROBE CARRY OVER VELOCITIES (DP 1 and 2) WITH FLIPPEN'S CRITICAL MASS CRITERION

END

DATE

FILMED

9-24-76

NTIS